University of Nottingham

UK | CHINA | MALAYSIA

THE ENHANCEMENT OF MECHANICAL DAMPING AND STIFFNESS TRADE-OFF USING UNIDIRECTIONAL CARBON FIBER REINFORCED POLYMER COMPOSITE INTERLEAVED WITH RECYCLED CARBON FIBER AND SHORT VIRGIN ARAMID FIBER NON-WOVEN MATS

A thesis submitted to The University of Nottingham for the degree of Doctor of Philosophy

Submitted by Cephas Yaw Attahu,

BSc. (Aerospace Engineering), MEng. (Aerospace Manufacturing Engineering)

2022-03-08

The University of Nottingham

CONTENTS

LIST OF FIGURES

LIST OF TABLES

NOMENCLATURE

ANF: aramid non-woven fabric 22

ASTM: American Society for Testing and Materials 53

DAC: data acquisition card 61

DOF: degree of freedom 59

F.W.: Filament winding 41

FRFs: frequency response functions 60

LVDT: Linear Vertical Displacement Transducer 50

PTFE: polytetrafluoroethylene 44

RFI: Resin film infusion 41

RTM: Resin transfer molding 41

TCA: titanate coupling agent 32

UD: unidirectional 17

VACM: vacuum-assisted compression molding 16

vAFs: virgin aramid fibers 17

VARI: Vacuum-aided resin injection 41

wt.: weight 32

ABSTRACT

It is possible to suppress unwanted mechanical vibrations without sacrificing stiffness; however, it is difficult when recycled carbon fibers (rCFs) are utilized. The characteristics of these rCFs have slightly deteriorated. Carbon fiber reinforced polymer composites (CFRPs) are increasingly used in various applications. This builds up in waste generated during the manufacture of raw carbon fibers and prepregs and during the end-of-life of their products. Fibers from these wastes are recovered primarily due to environmental and regulatory regulations. The strength of the recovered fibers was only slightly degraded compared to their new counterparts, according to many authors. To manufacture composite laminates that include the rCFs for structural applications, the developed composite laminate should meet a trade-off between mechanical damping and stiffness. To determine whether a material meets this trade-off, it must be able to escape what is known as the Ashby limit for mechanical damping/stiffness trade-off. To manufacture the composite laminates, a papermaking method was utilized to convert all involving fibers into 60 g/m^2 non-woven mats and the non-woven mats (mats) were either sized with titanate coupling agent-L12 or not, depending on the investigating factors. Before being used for interleaving, the mats were sandwiched between two layers of 125 g/m^2 resin films. The composite laminates were then made using a vacuum-assisted compression molding technique. To get around the Ashby limit, the author looked at the impacts of titanate coupling agent-L12 on the mats; the number of interleaved rCFs mats; their placements; and the influence of rCF lengths and combinations, kinds, and micro-hybridization with short virgin aramid fibers (vAFs). The limit (Ashby limit for mechanical damping/stiffness trade-off) was eluded by escaping to the curve's far right-hand corner (the best route for mechanical

damping/stiffness trade-off). In the figure of merit, the best laminate [Unidirectional CFRP with a 100% (T700 + M46J) (3 mm + 6 mm) (in the percentage ratios of 75:25 due to manufacturing limitations) recycled carbon fiber non-woven mat] (herein referred to as **Laminate T**) was 54.2 percent better than the control sample (herein referred to as **Laminate A**). A reproducibility test was conducted for the best laminate because manufacturing processes could influence the results. There were no significant differences in the mean flexural modulus values measured for the composite laminates and only minor variances in the standard deviation values for the individual laminates. These findings were not surprising given the challenges of producing consistent, homogenous non-woven mats. Also, the test samples were cut from various portions of the laminates; thus, the results were not unexpected. Additionally, a composite made of non-woven mats was designed to analyze the dynamic behavior utilizing free and forced vibrations (modal and harmonic analyses, respectively). This allowed for a direct evaluation of the non-woven mats' dynamic performance. There was excellent agreement between the numerical (FEA) and the theoretical natural frequencies when the natural frequencies were analyzed using both theoretical and FEA approaches. The effects of rCFs and short virgin aramid fibers (vAFs) hybridization as well as the influence of fiber volume fraction and combination of fiber lengths (using only rCFs), were investigated. The damping capacities of the composite laminates were evaluated using the amplitude-frequency plot for the two simulated modes. The specific stiffness values of the various composites were utilized to comprehend the effects of the parameters more clearly under investigation, and it was determined that increasing the specific stiffness of the non-woven mat composites might enhance their dynamic performance.

ACKNOWLEDGMENT

First and foremost, I thank the almighty Jehovah God for the gift of life, grace, and mercies. In addition, I would like to express my gratitude to my mother, Millicent Otu Attahu, for her continuous support and prayers.

Dr. Jian Yang, my principal supervisor, deserves my sincerest and heartfelt gratitude. I owe him (Dr. Jian Yang) a huge debt of gratitude for recruiting and nurturing me. I also appreciate his leadership and assistance in the face of unforeseen challenges and scenarios.

Thank you also to Dr. Kok-Hoong Wong and Dr. Chung Ket Thein for their guidance. Dr. Robert Pierce, who has served as an internal assessor for the past three (3) years, deserves my heartfelt gratitude for his invaluable and objective analyses of my work.

In addition, I would like to express my gratitude to my sponsors (the University of Nottingham and Dr. Jian Yang) for their financial assistance, which I greatly appreciate.

Prof. Xiaosu Yi (head of the Composites Group, University of Nottingham Ningbo China) and Dr. Xiaoling Liu (deputy head of the Composites Group, University of Nottingham Ningbo China) deserve a special mention too. Also, I want to express my gratitude to the Graduate School of the University of Nottingham in Ningbo, China, for providing me with suitable training during my Ph.D. studies (the pieces of training and seminars were very insightful and helpful).

Finally, I thank the faculty of Science and Engineering (FoSE) technical employees at Nottingham New Material Institute (NMI) and all my family and friends.

"If you want to find the universe's secrets, think about energy, frequency, and vibration."

Nikola Tesla, 1856-1943.

This page is intentionally blank

1 INTRODUCTION

1.1 BACKGROUND

Because of their high specific strength and high specific stiffness, CFRP composites are being used in numerous industries, especially the aerospace and wind industries [1-7]. As a result, the amount of CFRP waste has increased, and it is estimated that by 2050, the aerospace and wind industries will generate around 500,000 and 483,000 tonnes, respectively [8]. Most waste composites are currently disposed of in landfills or burned, which are both unsustainable waste management methods and outlawed by most governments. Therefore, optimizing a process for recycling CFRP composites is essential for preserving the environment, increasing material use, and improving energy efficiency [9]. The argument in favor of recycled carbon fiber is nuanced. The industry is based on finding solutions to issues, including the need to prevent carbon fiber waste from ending up in landfills and close any potential supply-demand gaps. There are difficulties in recycling these CFRPs; many of the CFRP materials used contain thermoset resins. These thermoset resins are hardened after curing, making it difficult to separate from the fibers, making the recovered fibers unclean in some recycling methodologies. Regardless, comparing the recycling of composite materials to conventional manufacturing, cost savings of up to 70% could be reached, and a 90–95% decrease in CO_2 emissions as well [10]. Although it is possible to recycle carbon fiber composites and produce products with mechanical properties that are very similar to those of virgin material, the composites recycling industry is still relatively new. It is still in the process of creating markets for the materials it produces from the recyclate. The case for employing rCF goes beyond sustainability and issues of the environment. Another advantage is a lower

price and the ability of the reclaimed and repurposed materials to close a possible supply and demand gap. For instance, rCF from ELG Carbon Fiber is about 40% less expensive than industrial-grade virgin carbon fiber. Other industrial providers assert that their product is between 20% and 40% less costly than virgin carbon fiber [11]. Additionally, the requirement for discontinuous fiber forms exists for many applications, suggesting a chance for rCF to provide a more cost-effective and environmentally friendly alternative to virgin material.

Also, it has been demonstrated that in some situations, the quality of the rCF generated is on par with virgin fiber. According to ELG Carbon Fibre, which uses pyrolysis to recover carbon fibers, its fiber typically keeps at least 90% of its tensile strength with no loss in the modulus [11]. Commercial suppliers have started to refocus their attention away from downcycling rCF into lower-performance products and more toward finding suitable applications that profit from the material's properties because of recent advancements over the past few years in rCF processing and fiber quality. The rCFs sector is a relatively new one, and it has a variety of issues to address. Technologies for recycling fiber are not new, in any case. It is also apparent that recycled fibers will never be a perfect substitute for new fibers, especially in the aerospace sector, where there are high strength and high stiffness requirements [12]. Reuse-related queries have gained attention as recyclers' confidence in the quality of fiber they generate grows.

Consequently, a technique for reusing these reclaimed carbon fibers for specific applications needs to be created. Previous research [8] has demonstrated that carbon fiber modulus and tensile strength can fall by up to 13 and 85 percent, respectively, after recycling, for optimum performance of these fibers, exploring different avenues through which one could enhance the mechanical properties of their

composites is prudent. Since natural or synthetic fibers are combined with a matrix (resin) to create composite materials, exploring the possibilities of adding extra fibers to enhance the rCF composites' performance is not far-fetched. As a result, the idea of hybrid composite materials was investigated. Hybridization is nothing more than the matrix's reinforcement of two or more different fiber types. Hybridization frequently results in the final composites' characteristics being improved [13].

1.2 HYBRID COMPOSITES

1.2.1 Introduction

More than one type of fiber is inserted in the matrix of hybrid composites. They (hybrid composites) were created as a structural material and as a natural follow-up to traditional composites, which only have one type of fiber. Hybrid composites offer distinct characteristics that can be used to suit a wide range of design needs at a lower cost than advanced or traditional composites. Some advantages of hybrid composites over conventional composites are improved fracture toughness and crack-arresting properties, balanced bending and membrane mechanical properties, balanced thermal distortion stability, reduced weight and cost, improved fatigue resistance, reduced notch sensitivity, and improved impact resistance [14]. It is feasible to achieve a viable balance between mechanical properties and cost by employing hybrids to suit specific design needs. In the fields of analysis, design applications, and fabrication techniques, much data has been collected for hybrid composites. These findings indicate that research in this field (hybrid composites) has progressed [14].

Depending on how the constituent materials are mixed, there are several types of hybrid composites [15]: (i) interply hybrids are made up of layers of two (or more) homogenous reinforcements placed on top of each other; (ii) intraply hybrids are made

out of tows of two (or more) constituent fiber types combined in the same layer; (iii) interply/intraply (intricately mixed) (intermingled) hybrids in which the constituent fibers are mixed as randomly as possible to ensure that there are no concentrations of either type in the material; (iv) over the basic reinforcing laminate layer, reinforcements are applied selectively where additional strength is required;(v) metal foils or metal composite plies placed in a specific orientation and sequence make up the super-hybrid composite.

1.2.2 Hybrid constituent materials and types of hybrid composites

Commonly used synthetic fibers were examined because only synthetic fibers were considered for this investigation. Carbon, glass, and aramid synthetic fibers are the frequently used fibers. As stated earlier, the construction of two or more fibers embedded in a single-base epoxy matrix (resin) can be classified as a hybrid polymer composite material: the resulting composite is often believed to have better qualities than the constituent materials. Carbon fibers (the most critical fiber in this research) have already received much attention. As for glass fibers, they are currently considered the most adaptable industrial fibers. They're simple to make out of raw materials, which come in an almost limitless quantity. Several types of glass fibers (A-glass, C-glass, D-glass, E-glass, AR-glass, R-glass, S-glass, and S-2-glass) are used to produce glass-reinforced polymer composites, depending on the application (GFRPs). Compared to carbon fibers, one of the critical disadvantages of GFRPs is their somewhat low modulus [16].

Aramid fiber (trademark by DuPont as Kevlar) was the first organic fiber with a tensile modulus and strength sufficient for use as insulation in specialized composites. They outperform steel and glass fibers in terms of mechanical qualities on a weight-for-weight basis. The word 'aramid' refers to fibers of the aromatic

polyamide form in which at least 85 percent of the amide bonds (CO–NH) are bonded directly to two aromatic rings, according to the US Federal Trade Commission [17]. The structure of these bonds is frequently used to classify polymers as para or meta. As the aliphatic carbon backbone is replaced with aromatic groups, the characteristics of the resultant fibers alter considerably. DuPont's Nomex, launched in the 1960s, was the first fiber of this type. This non-flammable yarn has a low tenacity and is often used for fireproof fabrics, electrical insulation, and other purposes. The mechanical qualities of these fibers are outstanding, and they are also thermally stable. The anisotropy of their stacked substructures, which have fibrillar, pleated, crystalline, and skin–core features, contributes to their extraordinary capabilities. Aramid fibers are polar due to the creation of hydrogen bonds. This characteristic improves the wettability of aramid fibers. The following are some of the most common aramid fiber features. Toughness and strength-to-weight ratios are high [17].

The main benefits of aramid are its high strength and lightweight. Aramid laminates can be made thermally stable in dimensions because it has a slightly negative axial coefficient of thermal expansion, like graphite. It is highly resistant to impact and abrasion damage, unlike graphite. It can be waterproof when mixed with other materials, such as epoxy. Its high tensile modulus and low breakage elongation, combined with excellent chemical resistance, make it a perfect choice for various composite structural parts in multiple applications. It's a para-aramid fiber with a tensile modulus of 124 GPa and a strength of 3620 MPa (Kevlar 49), and a relative density of 1.44 g/cm^3 (both Kevlar 49, and Kevlar 29). This density is lower than glass fiber, which has a density of 2.54 g/cm^3. Unlike glass and carbon fibers, aramid maintains its strength and durability at cryogenic temperatures (-196 °C). Furthermore, aramid fiber has a similar tensile strength to glass fiber but a modulus at

least twice as high. Aramid is a strong material that can absorb much energy within its molecular structure. It is abrasion and cutting resistant; it has no melting point and is resistant to heat deterioration and flammability.

Furthermore, it maintains fabric integrity at high temperatures [17]. Kevlar 49 and Kevlar 29 are two standard aramid fibers (has tensile modulus and strength of about 62 GPa and 2760 MPa, respectively). Kevlar 49 and Kevlar 29 have a diameter of 12 μm and elongation of 2.8 and 3.4 percent, respectively.

1.3 DRIVERS FOR CFRP RECYCLING

As shown in **Figure 1.1** and **Figure 1.2**, the current global composite materials market is large and likely to grow significantly in the coming years. Carbon and aramid fibers are in high demand, driving expansion in every industry. Pickering et al. [18] estimated that current carbon fiber production is about 100,000 tonnes per year, with annual growth expected to be between 10% and 20%. Inevitably, the increasing use of composites and the projected worldwide market size for composite products will result in increased waste from production/manufacturing or end-of-life. As a result of environmental concerns, governments, corporate sector companies, global universities, and researchers, in general, have partnered to address these issues (environmental hazards). This (increased use of composites and projected worldwide market size for composite products) resulted in a composite recycling revolution.

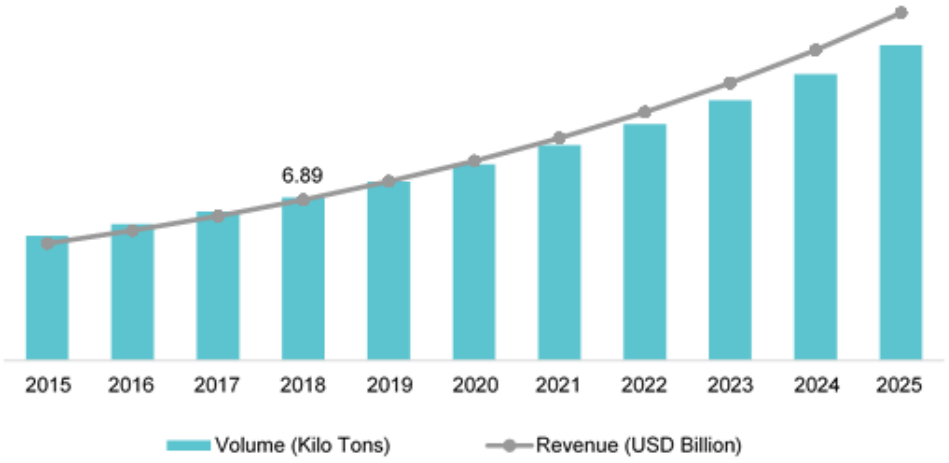

Figure 1.1. Global Advanced Carbon Materials Market Size, 2015-2025 (Kilo Tons USD Billion) (https://www.adroitmarketresearch.com/industry-reports/advanced-carbon-material-market).

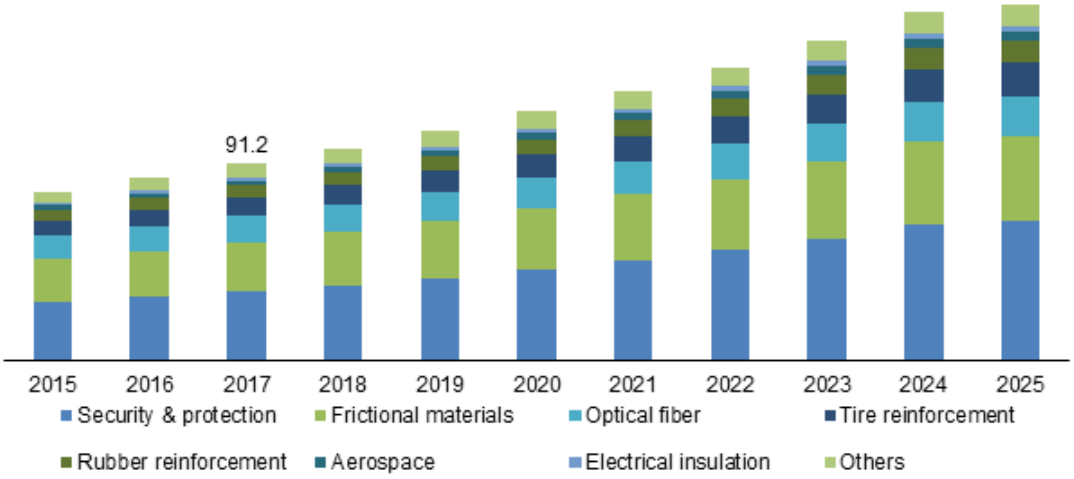

Figure 1.2. Global Aramid Fiber Market Share, By Application, 2015-2025 (Kilo Tons) (https://www.adroitmarketresearch.com/industry-reports/aramid-fibers-market).

As a result (of this composite recycling revolution), Oliveux et al. [19] conducted a comprehensive evaluation of the various recycling strategies for fiber-reinforced polymers (Mechanical recycling; Thermal processes: pyrolysis, fluidized bed pyrolysis, micro-waves assisted pyrolysis; and Solvolysis) (Fibers considered: glass,

carbon, and aramid). The review (Oliveux et al.'s work) also examined how recovered fibers have been repurposed in new materials or applications and the significant technological challenges encountered. And Oliveux et al. concluded that recycled fibers could replace modest amounts of virgin fibers in applications (that is, not at high enough percentages according to the review research). Furthermore, according to Oliveux et al., reclaimed carbon fibers (rCFs) from high-end technology applications cannot be reused in the same applications from which they were recovered, and new applications that are acceptable for the fibers must be developed. The reasons are: (1) the lower mechanical performance of the rCFs; (2) the inconsistency in quality in terms of fiber length distribution, orientation, and surface quality (adhesion to a new matrix); and (3) the origin of the rCFs (as different grades of fiber can be found in a batch of composite material waste collected from different sources).

1.4 CARBON FIBER REINFORCED POLYMER MATRIX COMPOSITES (CFRPS) RECYCLING TECHNOLOGIES

Broadly, technologies for recycling CFPs can be grouped into mechanical, thermal, and chemical [20]. **Figure 1.3** shows a classification of the effective CFRP recycling techniques. Since the rCFs utilized were recovered using the fluidized bed process, below is brief literature on the process.

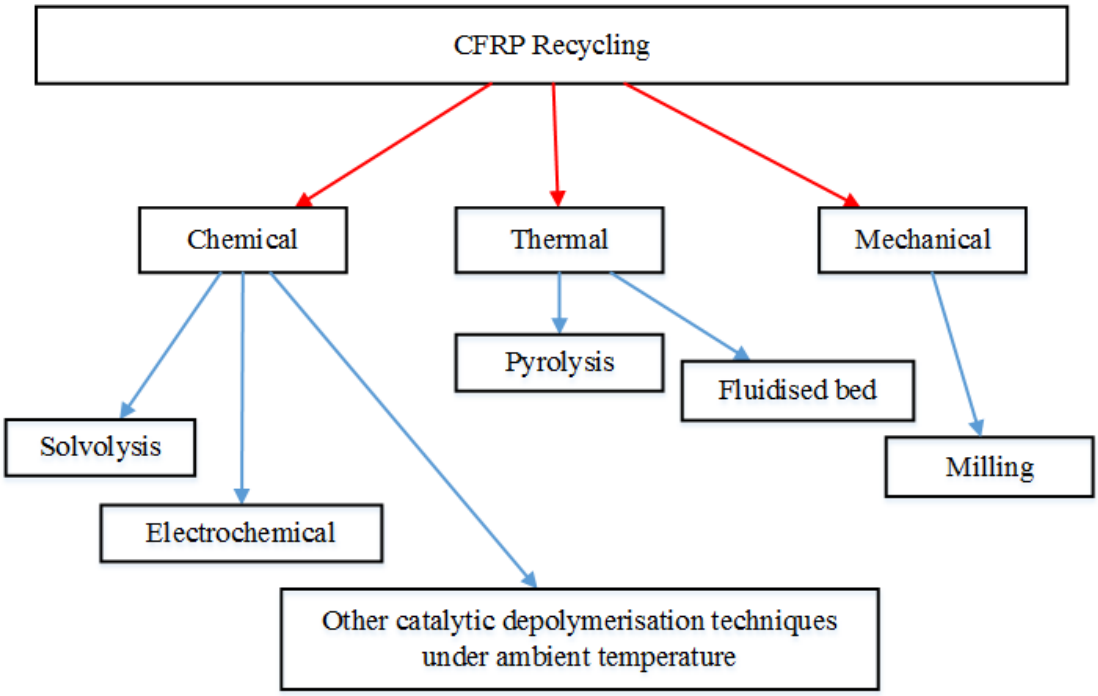

Figure 1.3. A classification of the effective CFRP recycling techniques [20].

The fluidized bed method is a thermal decomposition technology that the University of Nottingham has been developing and using for over 25 years. A bed of silica sand with average particle sizes of less than 1 mm is used in the process. A stream of hot air passing through a distributor plate at a superficial velocity of more than 0.4 m/s and a temperature typically above 500°C fluidizes the silica sand. Individual fibers break off and are elutriated away from the hot zone by the gas stream when the thermoset resin burns off, and the char degrades. When enough char has decayed, individual fibers further break off and are elutriated away from the hot zone by the gas stream. The fibers are subsequently separated from the outgoing gas stream using a cyclone. The fibers are collected inside a bin connected beneath the cyclone. At the same time, extremely efficient heat exchangers are employed for energy recovery to warm the incoming air [21-23], and the exhaust is sent to an afterburner for additional oxidization at 850°C.

The approach offers the following benefits: (1) reduced labor requirements; (2) a robust and continuous process; (3) the ability to cope with mixed and contaminated composite scrap; (4) the ability to separate metallic pieces from carbon fibers [21-23].

1.5 How to reuse Recycled Carbon Fibers

The growth prediction for carbon fibers, as indicated in **1.3**, leads to an increase in end-of-life (EoL) and the production associated wastes. Recycling these wastes can help mitigate their harmful environmental effects (the wastes). Recycling is mainly done for three reasons: 1. cost and energy efficiency, 2. environmental benefits, and 3. government requirements. Following recycling these fibers, suitable applications for their use must be identified.

Many applications have used recycled carbon fibers (rCFs) to reinforce composite laminates. There are numerous techniques for reusing rCFs in general [18]:

1. Direct rivalry with virgin materials (composite or metallic)

• Lower costs may compensate for lower mechanical performance.

• Should recycled materials be compared to other materials on a tow, mat, or compound scale?

2. The creation of new markets or the penetration of new markets

• New material forms (e.g., commingled with other fibers) may be acceptable for using rCFs as a replacement for glass and virgin carbon fibers.

3. Improved performance

• Discontinuous fibers can be employed in applications to improve drape properties for more straightforward manual or automated forming.

• Making use of the rCFs' conductivity in applications where reduced mechanical strength is a secondary concern.

• Producing materials with low fiber areal mass, in which discontinuous rCFs may be preferred.

1.6 AIMS AND OBJECTIVES

With the hindsight of the works done by Oliveux et al., this project seeks to incorporate the right amount/concentrations of recycled carbon fibers in the form of non-woven mats (mats) into conventional/virgin fiber materials for enhanced structural damping. “Enhancement” here means the developed composite laminates (the best) showing improvements by escaping the Ashby limit for mechanical vibration damping-stiffness trade-offs as much as possible compared with the control sample.

To attain the project's aim, the recycled carbon fibers (rCFs) must be converted into non-woven mats using the paper-making technique/process since they (rCFs) are fluffy and in the form of short fibers. These non-woven mats, in turn, can be incorporated into conventional/virgin fiber materials by interleaving unidirectional carbon fiber prepregs to produce composite laminates. The composite laminates can then be manufactured using vacuum-assisted compression molding (VACM).

Since composite laminates incorporating rCFs exhibit specific mechanical and damping properties because of the characteristics imparted by the constituent fibers, upon a thorough literature survey of most fibers by considering their merits and demerits, chopped virgin aramid fibers (they have high specific strength, creep resistance,

toughness, and inherent damping properties) can be used to hybrid the rCFs to achieve the project' objectives.

The project explored the factors:

1. the effects of titanate coupling agent-L12 on the mats;

2. the effects of the interleaved rCFs mat's numbers and their locations/positions;

3. the influence of the rCFs' lengths and their combinations;

4. the effects of the rCFs' types and their micro-hybridization with short virgin aramid fibers(vAFs).

1.7 CONTRIBUTION OF THE THESIS TO THE REUSE OF RECYCLED CARBON FIBERS

This research investigated incorporating recycled carbon fibers (rCFs) into carbon fiber reinforced polymer composites (CFRPs) for structural applications. The impacts of titanate coupling agent-L12 on the mats; the interleaved rCFs mat's numbers; their locations (the interleaved rCFs mat); the influence of the rCFs' lengths and their combinations (combining different rCF lengths); types (different rCF types); and their (rCFs) micro-hybridization with short virgin aramid fibers (vAFs) were all explored as part of the investigations.

Currently, the materials developed here: unidirectional (UD) CFRP composite interleaved with either 100 % rCFs' non-woven mats or non-woven mats in addition with short virgin aramid fibers (vAFs)'s non-woven mats (being it single, triple, or quintuple non-woven mats) being used for the mechanical damping/stiffness trade-offs are the first of a kind. The UD CFRP composite interleaved with only 100% vAFs' non-

woven mats without any additional 100 % rCFs' non-woven mats are completely for comparison purposes.

This project addressed and closed a significant gap in using rCFs for structural applications. The methodology used (the interleaving of UD fiber/epoxy prepreg with rCF non-woven mats) is the first of its kind. Furthermore, the final product (the best configuration, **Laminate T**) was very competitive: it was pegged against another novel composite material from an excellent source, and the results were very encouraging.

1.8 THESIS OUTLINE

This thesis is divided into **seven** (**7**) **chapters**.

The overarching theme of the thesis is introduced in **chapter 1**, which also includes a statement of the thesis's goal and aims.

Chapter 2 presents a comprehensive literature review of the project's background and considered factors.

In general, **chapter 3** discusses the materials and methods: the fabrication of non-woven mats, their sizing using a titanate coupling agent, and the fabrication of composite laminates.

The work characterizing the fiber-reinforced polymer laminates used for the project is captured in **chapter 4**. The characterizations are Dynamic mechanical analysis (DMA); bending (flexural moduli and flexural strength determinations) and shear (short beam shear strength determinations) tests; free vibration tests; surface electron microscopy (SEM); Fourier-transform infrared (FTIR) spectrometry; and density tests.

The results are described and discussed in **chapter 5**.

Chapter 6 discusses finite element analysis of designed composite laminates, including free vibrations (modal analysis) and forced vibrations (harmonic analysis).

The project's general conclusions and limitations are discussed in **chapter 7**. It also includes ways/methods that should be considered in the future.

2 LITERATURE REVIEW

2.1 INTRODUCTION

Carbon fiber reinforced polymers (CFRP) find their way into vital structural applications without adding significant weight due to their excellent strength-to-weight ratio [24-26]. As a result (increasing use of CFRPs), these wastes threaten the ecosystem. Many scholars investigated the potential recycling of these wastes. These investigations were motivated by environmental concerns and government regulations. Consequently, Pakdel et al. [27] and May et al. [28] compiled such publications and conducted detailed reviews. The authors of such comprehensive review studies, Pakdel et al. and May et al., noted that very energy-efficient and cost-effective recycling systems for CFRP composites had been developed on an industrial scale. Those same review articles (Pakdel et al. and May et al.) mentioned positive environmental and waste management effects. Furthermore, Pakdel et al. pointed out that, despite all the benefits of recycling these fibers, little research has been done on their reuse. That is, turning them (recycled fibers) into non-woven mats for composite laminate fabrication.

Oliveux et al. [19] also did a comprehensive study of the various recycling systems (mechanical recycling; thermal processes: pyrolysis, fluidized bed pyrolysis, micro-waves assisted pyrolysis; and solvolysis) established to recycle fiber reinforced polymer composites (fibers: glass, carbon, and aramid). Oliveux et al. found that the rCFs recovered from the fluidized bed method had a 25% lower tensile strength than their virgin counterparts. Oliveux et al. went on to say that reclaimed fibers could only replace small amounts of virgin fibers in structural applications. Carbon fibers recovered from high-end technology applications could not be reincorporated into the same high-end technology applications from which they were retrieved because 1. of

the lower quality of the rCFs; 2. the rCFs are not entirely controlled in terms of the length, length distribution, and surface quality (adhesion to a new matrix); and 3. of the origin of the rCFs (often different grades of fibers are found in a batch of recycled composites coming from different manufacturers).

According to the preceding remark, only a particular amount of recycled carbon fibers (rCFs) might be accepted in a material designed for structural uses, whether light-weight or not. Furthermore, for example, fibers recovered from an aircraft's fuselage cannot be used in any other fuselage component. On the other hand, such fibers (fibers retrieved from an aircraft's fuselage) could be used in various light-weight structural applications in the aircraft's cabin. Applications could range from the cockpit panels to the aircraft's interior trays. Regardless of the slight decrement in the mechanical properties of the rCFs, these rCFs could be used for other forms of structural applications (light-weight structural applications) if incorporated appropriately into conventional materials at low fiber loadings. In reusing rCFs, other authors usually convert the rCFs into non-woven mats (partially aligned or randomly) and stack them up in the desired number of layers to fabricate the composite [29-34]. However, from the works of Oliveux et al., for structural applications, this will not suffice; hence it was necessary to find other means of reusing the rCFs. Incorporating high stiffness and high strength short fibers into polymer matrices improves their composites' mechanical properties [35].

To maximize the properties of the rCFs to be used for structural applications, Shah et al. [36], Tse et al. [37], and Bachmann et al. [38] all observed that when the rCFs were mixed with another type of fiber, the mechanical properties of their composites improved (this concept is referred to as hybridization). Hybridization is the

process of combining two or more fibers to enhance the properties of their composites. However, it should be recognized that the method has its shortcomings: either a negative or positive effect [39]. Ideally, the final composite is expected to exhibit the merits of involving fibers (positive hybridization) in hybridization. However, such is always not the occurrence because a situation could arise where the final composite laminates exhibit the demerits of the involving fibers rather than the merits (negative hybridization). To explore the effects of hybridizing the interleaved rCFs' non-woven mats with another kind of fibers' nonwoven mats, reference was made to the works of Ni et al. [40], wherein a high damping and high stiffness CFRP composites with aramid non-woven fabric (ANF) interlayers were developed, it was noted that the ANF enhanced the mechanical properties and damping performance of the co-cured composite laminates. In addition, the authors, Wong et al. [41] and Cheng et al. [42], observed that aramid non-woven mats used as an interleaf to fabricate composites lead to improvements in the mechanical properties of the composites. From the works of Ni et al. [40], Wong et al. [41], and Cheng et al. [42], short virgin aramid fibers (vAFs) were selected to make aramid non-woven mats to study the hybrid effect when in combinations with interleaved rCF non-woven mats.

With regards to potentially further maximizing their properties (composite laminates made of rCFs) for possible structural applications, reference was once again made to the concept of hybridization (see **section 1.2**): the combination of high strength, standard modulus fiber, T700 rCFs with high modulus fiber, M46J rCFs, to form a non-woven mat for interleaving, the resultant composite laminate is expected to take up the merits of the properties of the T700 and the M46J rCFs. This is because the positive hybrid effect depends on the properties of the involving fibers (it should be noted that environmental factors could also have an impact); the two combined rCFs have different

favorable properties that are expected to blend to produce the intended positive hybrid effect.

2.2 STRUCTURAL DAMPING COMPOSITES (CONSIDERED FACTORS)

The project's objective requires a new category of materials with improved stiffness and damping characteristics. Structural damping composites are a new category of materials with both high stiffness and high damping. Structural damping composites, also known as composite laminates for structural purposes, must strike a balance between mechanical damping and stiffness [43, 44]. For structural damping applications, a maximum product of stiffness and mechanical damping (E tan δ), a figure of merit, is desirable [45-46]. Ashby's loss coefficient-modulus chart for various materials is necessary to fulfill this trade-off. This log/log plot of the loss coefficient, η (same as tan δ), against Young's modulus, E (at 30°C), with the guideline, ηE is equal to 0.04 GPa, which is referred to as the 'Ashby' limit for mechanical stiffness/damping trade-off [47, 48].

The figure of merit (the damping capacity), which is expressed as the product of the stiffness (storage modulus) and tan delta (loss factor): all from the dynamic mechanical analysis (DMA) test, is used to quantify the trade-off between mechanical damping and stiffness according to Chung [49]. The DMA is a technique that deforms a sample with a dynamic force to measure the storage and loss moduli as a function of temperature. By dividing the loss modulus by the storage modulus [50], the loss factor, tanδ or η, is derived. The storage modulus evaluates the material's ability to store energy, while the loss modulus measures the material's ability to dissipate energy; thus, a balance between the two parameters (storage and loss moduli) is desirable for an excellent damping/stiffness composite material.

Because materials with solely high damping (such as high loss elastomers) tend to be too soft, and materials with high stiffness tend to be overly rigid [51], simultaneously, high stiffness (defined as flexural moduli in bending) and high damping (described as loss factor) are needed for structural damping composite laminates. Additionally, Gibson et al. [52] asserted in the article, recent research on enhancement of damping in polymer composites that considerations must be made to the effects of the constituents' properties, fiber/matrix interphase, lamina hybridization, and stacking sequences. In a recent comprehensive review article, Treviso et al. [53] also ascribed the same factors laid down by Gibson et al. [52].

Bending, which is characterized as flexural modulus, is synonymous with stiffness. To improve the stiffness, Ma et al. [54] noted that the same factors that affected the loss factor above must be considered [54]. Additionally, Madhan et al. [55] investigated the influence of stacking sequence and thickness on the free vibrational behavior of carbon-reinforced epoxy laminates. They concluded that the stacking sequences and the thicknesses of the laminates influenced the vibrational behaviors. Moreover, the works of Rajesh et al. [56], Dong et al. [57], Bennet et al. [58], and Ary Subagia et al. [59] all noted the effect of stacking sequences on the mechanical properties of the various composite laminates under investigations. They also noted how the intra-ply, or the position of the different hybridized configurations' layers, affected the mechanical properties' performances. Also, Wang et al. [60] investigated the correlation between the performances and configurations of plain weave composites reinforced by T300 carbon and aramid fibers using various hybrid ratios and stacking sequences. Wang et al. noted that the properties of the outermost layers mainly determined the fiber hybrid composite's flexural modulus, and the carbon fiber's shear failure in the inner layer was also shown to manifest in a lower flexural strength. The

hybrid ratio and the stacking sequence affected the loss factor, and the mechanism of the damping performance was like that of the flexural modulus.

Additionally, in a study where fiber-enhanced viscoelastic damping polymers (a new composite damping material consisting of high elastic modulus fibers) were investigated [61], it was concluded that the high elastic modulus fibers enhanced the damping performance of the developed composite material. In a related study wherein the effects of elastic/Young's modulus and the damping of a viscoelastic layer interleaved in the middle plane of unidirectional laminate were analyzed, a correlation between the loss factor and the elastic/Young's modulus was established: the elastic/Young's modulus influenced the damping performance of the composite material [62].

Furthermore, Capela et al. [63] also looked at the impact of fiber length on the tensile and DMA properties of short fiber-reinforced composites with low content. They (Capela et al. [63]) found that increasing the fiber length from 2 to 4 mm boosted the stiffness and tensile strength by 25%, but the stiffness and tensile strength tended to decline for the 6 mm fiber length composites. Also, when fiber length rose from 2 mm to 4 mm, the DMA elastic modulus increased slightly and then increased slightly again when fiber length increased from 4 mm to 6 mm. Moreover, Sabrine et al. [64] also looked at the tensile characteristics of ten different carbon fiber non-woven composites. They (Sabrine et al. [64]) concluded that the fiber type and length significantly impact the composites' mechanical properties. In other literature about the effects of the fiber lengths, a reference was made to the works of Suarez et al. [65], wherein an investigation was conducted on the impact of fiber length and fiber orientation on polymer composite materials' damping and stiffness. They (Suarez et al. [65]) discovered that relatively low fiber aspect ratios (length of fiber/diameter of fiber) are

necessary to enhance damping dramatically. Furthermore, fibers considered candidates for high stiffness and high damping composite laminates must absorb energy initially and disperse it appropriately (damping).

Additionally, literature on the influence of aramid fibers on the mechanical properties of hybrid carbon-aramid composites was investigated to gain further insight into the performance of hybrid carbon-aramid composites [66]. This investigation conducted by Pincheira et al. [66] reported that the energy absorption values of the carbon–aramid composites were higher: the results showed that the aramid phase in the hybrid carbon–aramid composite significantly increased the impact (37.9 percent in energy absorption). The results also indicate that the inclusion of aramid fibers was responsible for the improvements observed.

Regarding the works of Madhan et al.[55], Rajesh et al. [56], Dong et al.[57], Bennet et al.[58], Ary Subagia et al.[59], and Wang et al.[60] it was necessary to evaluate the effect of the interleaved rCFs non-woven mat's numbers and position/locations because mechanical properties, including loss/damping properties, are influenced by the stacking sequences; and the position/location of the non-woven mats in the case of intra-ply stacking sequencing (i.e., the interleaving of the non-woven mats in-between the prepreg tapes).

Additionally, and according to the works of Alberts et al. [61], Berthelot et al. [62], Capela et al. [63], Sabrine et al. [64], and Suarez et al. [65], the fiber lengths and fiber types/elastic moduli influence the damping performances of composite materials hence it was imperative to investigate these factors when developing a high stiffness and high damping composite material using rCFs. Furthermore, from the works of

Pincheira et al. [66], coupled with the inherent damping properties of aramid fibers, the effect of hybridizing aramid fibers with rCFs was also investigated.

3 MATERIAL AND METHODS

3.1 NON-WOVEN MATS MANUFACTURING AND SIZING PROCESS

3.1.1 Introduction

Non-woven is a manufactured sheet, web, or batt of directionally or randomly orientated fibers bonded by friction, cohesion, or adhesion. The fibers may be of natural or manufactured origin [67]. One way of manufacturing non-wovens is the use of the papermaking process. The papermaking process is a mature technology that has been used at the University of Nottingham in many ways. Notably, Wong et al. [34] used a modified form of it (papermaking process) (wet hydrodynamic technique) to align recycled carbon fibers in the form of short individual filaments to get aligned mats. Additionally, Wong et al. [68] used it (a wet papermaking method) to convert virgin and recycled carbon fibers into circular discs of non-woven veils for electromagnetic interference shielding investigations.

The practiced operations in a conventional papermaking process are dispersion, beating/refining, metering, and blending fiber and additives. The essential elements of the papermaking machine are the headbox, wire section, press section, dryer section, and reel [69]. After making the slurry (stock suspension of fibers and water), it (the slurry) is pumped into the papermaking machine. The slurry comprises approximately 99.5% water and about 0.5% pulp fiber. When the slurry has reached the papermaking machine, it first enters the headbox (the exit point for the slurry is the “slice” or headbox opening). More significant quantities of slurry released from the head box will result in thicker papers. Mechanical compression removes water in the press section, and the sheet usually has about 65% moisture content when the paper leaves the press section.

The paper web continues to thread through the steam-heated dryers, losing moisture each step. The process evaporates tons of water, and the final paper will sometimes undergo a sizing or coating process [69].

3.1.2 Paper-making process

In the paper-making process, the consistency (also known as mass concentration) [mass of dry fibers/ mass of slurry (stock suspension of fibers and water)] (%) is necessary to produce quality/uniform non-woven mats; hence it must be defined appropriately [70]. Papermaking has a wide range of consistency (mass concentration) values. For example, laboratory handsheets can be formed at a consistency of 0.017%; and commercial paper can be created at a consistency of 0.5-1.0% [71]. The rheological properties of fiber suspensions vary significantly over the consistency ranges. The fiber-fiber contacts will transfer from occasional collisions to forced contacts or even continuous contacts as the consistency increases. The degree of fiber-fiber contacts (crowding number, N) (**eq 3.1**) is defined as the number of fibers in a volume swept by the length of one fiber [72]. It (the crowding number) can be seen as a dimensionless concentration that accounts for fiber morphology and has proven to be a helpful tool in describing fiber flocculation [73].

$$N \approx 5.0 C_m \frac{L^2}{\omega} \qquad 3.1$$

where C_m is the consistency (mass concentration) (%), L is the average fiber length (m), and ω is the fiber coarseness (mass of dry fibers/average fiber length, kg/m).

Fiber flocculation could lead to poor paper formation, which is the primary cause of papers' nonuniformity (unevenly distributed masses) [74]. Flocculation does not generally occur when N << 1, as each fiber can rotate freely and seldom hits another

fiber [75]. Such a suspension is usually called dilute, and as such, handsheets used for laboratory testing are typically made at N ≈ 1, which gives an even sheet structure thence a good formation [75]. Generally, the primary quality measure of a sheet is the mass variation in the plane, i.e., the basis-weight variation, which is referred to as the formation. Variation of the basis weight can easily be seen by holding a paper sheet in front of a light source, by which the presence of fiber flocs can then easily be detected [75].

3.1.2.1 Chemical composition of the dispersion medium (wetting/dispersion agents, binding agents/viscosity modifiers, and anti-foaming agents/defoamers)

In the usage of the paper-making process, there are two (2) significant steps: fiber dispersion and non-woven mat formation. The degree of fiber dispersion affects the quality of the manufactured non-woven mat. In turn, the degree of fiber dispersion is affected by the chemical types and their compositions. To estimate the right amount of chemical composition of the dispersion medium (wetting/dispersion agents, binding agents/viscosity modifiers, and anti-foaming agents/defoamers), reference was made to the works of Wong [76], wherein the effects of different chemicals and their constituents were examined for wetting/dispersion agents, and binding agents/viscosity modifiers. The dosages of the wetting/dispersing agent, Brij 35 non-ionic surfactant from Fisher Scientific, were examined by increasing the dosing from 0.6 g/l to 0.9 g/l and finally to 1.2 g/l. No significant improvement in the fiber dispersion was observed for the increases in the dosages. It was noted that a 4.5 g/l of hydroxyethyl cellulose binding agent/viscosity modifier from Dow Chemical Company Ltd., Middlesex, UK was enough to increase the viscosity of the fiber dispersion solution, which helped in fiber dispersion. Regarding the anti-foaming agent/defoamer, a 0.3 g/l of Bevaloid

6686W anti-foaming agent from Rhodia UK Ltd., Watford, UK, was found to be enough to suppress the formation of bubbles during the dispersion [68].

3.1.3 Titanate coupling agents

During the project, an investigation was conducted into composite laminates' flexural and shear properties using a non-woven mat made of T700 and M46J rCFs. In the interpretations of the results, poor interfacial adhesion was observed. The M46J, as an example, was examined under scanning electron microscopy (SEM): traces of resin residues were found on the fibers. These resin residues could create resin compatibility issues because one does not know what epoxy resin the residues were. To avoid any resin compatibility problems, it was necessary to size the manufactured non-woven mats using a coupling agent (sizing agent).

A sizing agent is a chemical that enhances the adhesion between two phases in a composite material [77]. Using sizing agents to improve the mechanical properties of composite materials is not a straightforward process because the right sizing agent must be chosen, and the correct amount must be applied: either too little or too much can deteriorate the mechanical properties. Organosilanes coupling agents are usually used for improving interfacial adhesion for composite materials. However, according to Monte [78], titanates are better adhesion promoters than silanes because of the intrinsic multifunctional chemistry of the tetravalent organometallic titanium compared to silicone at the nano-interface where dissimilar materials meet.

Menon et al. [79] conducted a study on the surface modification of Kevlar fibers by treating them with 2%, 5%, 8% (wt. coupling agent/wt. fiber), and a few treated with less for improved adhesion of the fiber and resin in Kevlar-phenolic composites. Flexural properties of the Kevlar-fiber reinforced composites were determined: the

composite samples with the coupling agents showed an increase in flexural strength over the untreated samples, with the maximum increase of flexural strength of about 18% over the control. Menon et al. [79], in their conclusion, suggested that about 2% of coupling agent [by weight (wt.) of fiber] was the optimum amount in terms of improvement in flexural strength. However, at that 2%, there was a slight decrease in flexural modulus compared with the control, and at lower amounts of coupling agent (about 1 %), poorer properties were observed.

Furthermore, Alkadasi et al. [80] investigated the effect of titanate coupling agent (2.0 wt.%) on the mechanical properties of flyash-filled polybutadiene rubber. They concluded that the remarkable performances (tensile strength was improved by 50%, while Young's modulus also was enhanced by 209%) were because of the improved matrix-filler adhesion. In Alkadasi et al.'s [80] works, a two percent solution of the titanate coupling agent (LICA 01) was dissolved in isopropyl alcohol (i.e., dissolving 2 g of TCA in 100 ml of isopropyl alcohol) and used to apply to a 100 g of flyash.

3.1.4 Manufacture of the recycled carbon fiber and short virgin aramid fiber non-woven mats

The virgin aramid fibers (vAFs), poly (p-phenylene terephthalamide) branded as Kevlar® 29 (K29) were furnished by DuPont in chopped strands with an average length of 3.0 mm. The fiber has a diameter of 12 μm, a specific density of 1.44, an ultimate tensile strength of 2.92 GPa to 3.62 GPa, and a tensile modulus of 70.5 GPa. The recycled carbon fibers (rCFs) used are standard modulus, intermediate modulus, and high modulus Toray T700SC, Toray T800S, and M46J, respectively, reclaimed through the fluidized bed recycling process at the University of Nottingham, UK. The rCFs' lengths used were 3 mm, 6 mm, and 12 mm. According to Pimenta et al. [81],

typical rCFs recovered from the fluidized bed process are estimated to suffer between 25% and 50% decrement in tensile strength. **Figure 3.1** (a) and **Figure 3.1** (b) show a picture of 75% of T700 and 25% of M46J rCFs, respectively. **Figure 3.2** (a) shows a picture of the vAFs.

The titanate coupling agent (TCA-L12) was purchased from Capatue Chemical Co., Ltd., Nanjing, P. R. China, and the isopropyl alcohol was purchased from Macklin. The rCFs and vAFs in the formation of 60 g/m^2 mats [examples seen in **Figure 3.1** (c) and **Figure 3.2** (b)] were used as the interleaving materials, and a commercially available unidirectional carbon (UD) fiber/epoxy prepreg, Toray T700SC carbon fiber (12K) prepregs were used as the base material to fabricate the composite laminates. The prepreg, which has an areal density of 200 g/m^2, ply thickness of 0.20 mm and resin content of 35 wt.%. The resin film has an areal density of 125 g/m^2, a thickness of 0.10 mm and 100 wt.% resin contents. The resin content from the prepreg could have been enough for the single mat configurations. However, the resin films were included because the study covered the effect of including more layers of rCF mats: the highest number was five, and the resin content from the prepregs would not suffice. The resin films were included for normalization purposes, irrespective of single or more mats. The UD carbon fiber prepreg and the resin film have the same resin system, YPH-42T, supplied by CA composites limited, Shanghai, PR China.

Shown in **Figure 3.3** is the front view of the in-house rig used to manufacture the non-woven mat utilizing a papermaking technique. The wet papermaking technique was used to manufacture both the recycled carbons and short virgin aramid fibers into rectangularly shaped non-woven mats ($340 \times 240\ mm^2$) with an areal density of 60 g/m^2 using the in-house rig. The 60 g/m^2 was chosen based on the works of Nazhad

et al. [82] and the manufacturing processing limitations. The technique comprises three stages: fiber dispersion, filtration, and non-woven mat drying.

Eqs 3.1-3.4 were used to calculate the parameters needed to manufacture the non-woven mats.

$$\text{Mass of dry fibers (in grams, g)} = \text{LBW} \tag{3.2}$$

Mass (dry fibers) = $0.34 \times 0.24 \times 60 = 4.896 \cong 4.90$

where L and B are the length (m) and breadth (m) respectively of the mesh of the sheet former, and W is the areal density (g/m^2) of the non-woven mat.

The consistency,C_m (%) = 0.05 was chosen based on the works of Kerekes [71] and Cai et al. [74].

Mass of stock suspension (slurry) (in grams, g) $= \frac{\text{mass of dry fibers (in grams,g)}}{\text{the consistency,} C_m \ (in\ \%)} = \frac{4.896}{0.05} =$ 9792

In the dispersion section, the height, h, and volume, v of the suspension (fiber slurry) were calculated using **eqs 3.3** and **3.4**, respectively.

$$\text{h, cm} = \frac{\text{mass of slurry (in grams,g)}}{\rho(g/cm^3)\times\pi r^2(cm^2)} = \frac{9792\ g}{1 \times \pi \times 15^2} \cong 13.9 \tag{3.3}$$

$$\text{v, liters (l)} = \frac{\pi r^2 h}{1000} = \frac{\pi \times 15^2 \times 13.853}{1000} \cong 9.792 \tag{3.4}$$

where ρ is the density of water (in g/cm^3), and r is the radius of the dispersion tank (in cm).

As an example, 13.9 cm of water is first measured (to use the resultant solution as many times as possible, a factor of 2.5 was introduced), the chemical compositions seen in **Table 3.1** (these values were based on the works of Wong [76] and Wong [68])

were measured in grams, g (they were calculated by multiplying them by 9.792 l) (to use the resultant solution as many times as possible, a factor of 2.5 was introduced) (there were no significant changes in the viscosity of the solution when used several times) and cautiously added to the water in the dispersion tank. The chemical solution was thoroughly mixed for 8 hours using a high-shear radial impeller at about 1200 ± 50 rpm. The final solution is pumped into the storage tank, and the required quantity is pumped from the storage tank into the dispersion tank for mixing with fibers and, subsequently, for manufacturing the mats.

Regarding the steel mesh size on which the mat will lie after manufacturing, the masses of the rCFs and the vAFs are measured in grams and added to the resultant solution in the dispersion tank separately. The measured rCFs are T700SC and M46J in the percentage ratio of 75:25-the percentage ratio was based on the processing limitations associated with the M46J rCFs (the two rCFs were added to the solution simultaneously).

The rCFs measured were in the percentage ratio of 75:25 (T700SC: M46J and T700SC: T800S) (varied rCF lengths utilized depending on the factors being investigated) (see details in chapter 5): -the percentage ratio was because of the processing limitations associated with the M46J rCFs. For the 3 mm, 6 mm, and 12 mm rCF lengths only, the 100-percentage ratio was measured. The mats with both rCFs and vAFs were in the percentage ratios of 50:25:25 (see **Figure 3.4**) and 25:25:50 for the T700SC: M46J: vAF (all 3 mm in length) and T700SC: M46J: vAF (all 3 mm in length), respectively and were added simultaneously to make the resultant mat. Subsequently, the fiber suspension is mixed for 30 ± 5 minutes with a high-shear radial impeller at about 1200 ± 50 rpm. The speed and time stated here were the best-compromised

values that resulted in the manufacturing of good mats. They (the rate and time) were based on the works of Hubbe et al. [83].

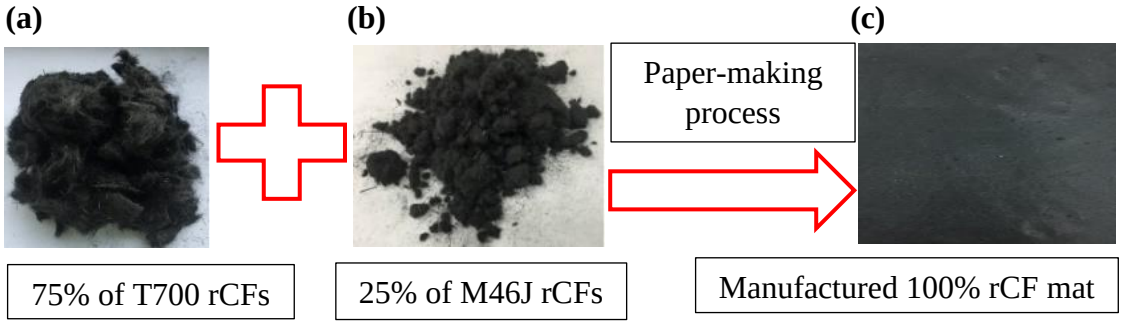

Figure 3.1. (a) 75% of T700 rCFs, (b) 25% of M46J rCFs and (c) manufactured 100% rCF non-woven mat (the mat used to interleave all laminates with 100% rCF mat; being it single, triple, or quintuple non-woven mats).

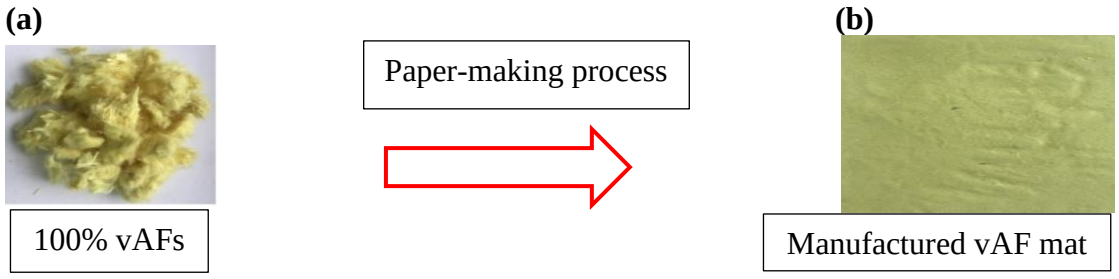

Figure 3.2. (a) vAFs and (b) manufactured vAF non-woven mat.

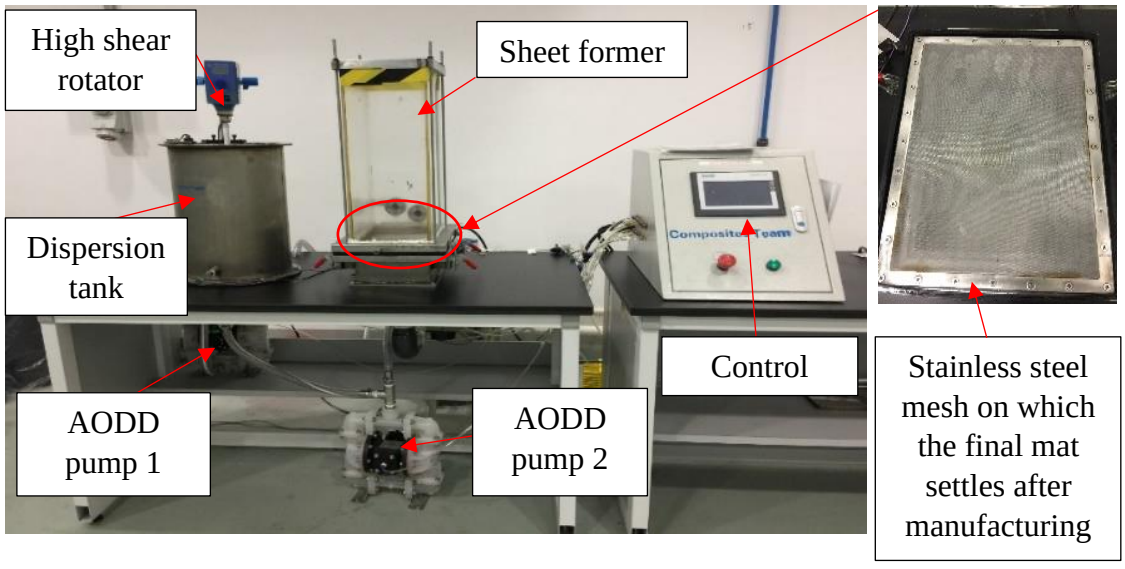

Figure 3.3. Front view of the non-woven mat rig.

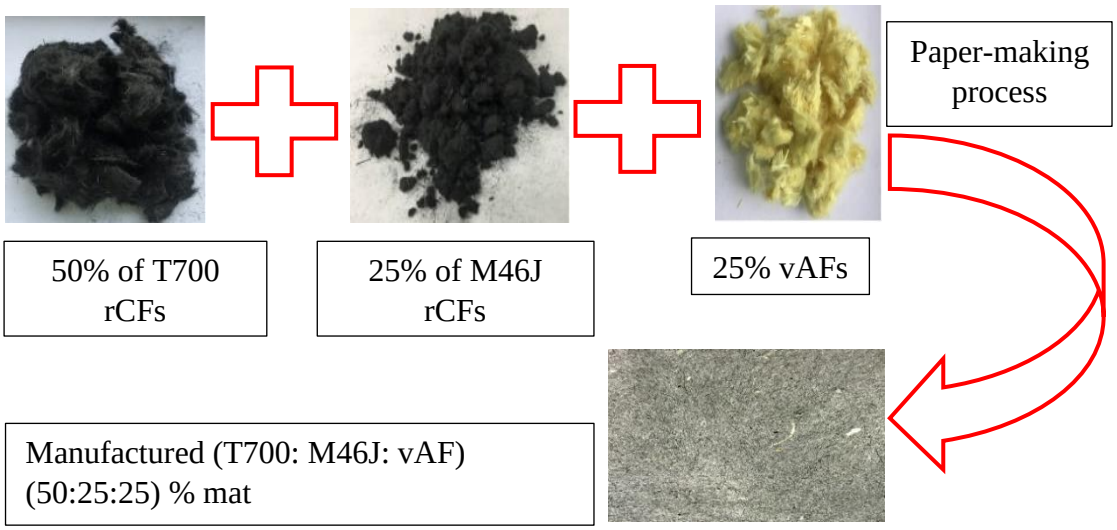

Figure 3.4. Manufacturing of the (T700: M46J: vAF) (50:25:25) % non-woven mat (**Laminate V's non-woven mat**).

Next, the fiber-slurry is pumped into the sheet former and the fiber-slurry sieve through a stainless-steel mesh with the aid of a vacuum pump. The resultant mat is wet and frail at this stage; hence, it is carefully removed from the stainless-steel mesh and dried at 100℃ in the oven for 10 minutes. The measured vAF was in the percentage ratio of 100 and manufactured the same way as the rCF mats. Some random mats were selected and weighed to understand fiber losses in manufacturing the non-woven mats. Shown in **Table 3.2** are the results. The average weight of 4.84 g (measured after the manufacturing of the non-woven mat) pegged against the 4.90 g (measured weight before the manufacturing of the non-woven mat) leaves a low percentage of 1.22, which is almost negligible (that is 0.06 g). This shows that the stringent precautions (notably, 1. the joints to the various stages were regularly cleaned; 2. it was ensured that almost all the fiber slurry was sent from the dispersion tank to the sheet former, and 3. the gasket was tightly fixed to prevent slurry from leaking out of the sheet former) taken in the manufacturing of the non-woven mats was successful.

Table 3.1. Chemical compositions

Chemicals	**Supplier**	**Functionality**	**Composition (g/l)**
Hydroxyethyl Cellulose	Macklin	Binding and Viscosity Modifier	5.5
Brij 35 non-ionic surfactant	Aladdin	Wetting and Dispersing Agent	1.0
Tributyl phosphate	Aladdin	Anti-foaming agent	0.5

Table 3.2. Measurements of some selected random non-woven mats

Sample mat no.	**Measured weight (in grams, g)**	**Sample mat no.**	**Measured weight (in grams, g)**
1	4.80	**8**	4.77
2	4.78	**9**	4.85
3	4.85	**10**	4.86
4	4.87	**11**	4.86
5	4.86	**12**	4.85
6	4.85	**13**	4.84
7	4.87	**14**	4.87
Average	**4.84**		
Standard deviation	**0.03**		
Coefficient of variation (COV) (%)	**0.7**		

3.1.5 Preparation of sizing agent and the treatment of the non-woven mats with it

In this study, an investigation was conducted into the flexural and shear properties of composite laminates manufactured using a non-woven mat made of T700 and M46J rCFs. In the interpretations of the results, poor interfacial adhesion was observed. As such, the M46J as an example was examined under scanning electron microscopy (SEM): traces of resin residues were found on the fibers (see **Figure 5.3**). These resin residues could create resin compatibility issues because one does not know what epoxy resin the residues were. To avoid resin compatibility problems, it was necessary to size the manufactured non-woven mats using a coupling agent (same as a sizing agent).

In choosing the appropriate sizing agent, references were made to the works of Monte et al. [78]. In estimating the proper dosages, references were made to the works of Menon et al. [79] and Alkadasi et al. [80]. Taking cues from the results of Monte et al. [78], Menon et al. [79], Alkadasi et al. [80], and taking into consideration the densities of the mats being manufactured, a titanate coupling agent and the following percentage ratios were chosen: 0.5%, 1%, 1.5%, and 3.0% (wt. coupling agent/wt. non-woven mat) to study the effect of sizing on the non-woven mats. As an example, to find the amount of sizing in grams (g) for a 0.5% ratio, a non-woven mat that weighs 4.86g is multiplied by 5×10^{-3} to get a 0.0243g sizing agent to be measured.

A Mettler Toledo laboratory scale (0.0001g) is then used to measure the 0.0243g sizing agent and dissolved in a 7.854g isopropyl alcohol in a beaker. All other respective ratios of the TCA-L12 were measured and dissolved in a 7.854g isopropyl alcohol in a beaker. The resulting mixture was thoroughly stirred for about 5 minutes with a stirring rod to make a solution. The solution was then sprayed uniformly as much as possible

onto the mats and dried at 100°C in an oven for about 4 hours for the alcohol's complete evaporation, leaving only the TCA-L12 on the mats.

3.2 PROCEDURE FOR THE MANUFACTURING/FABRICATION OF THE COMPOSITE LAMINATES

3.2.1 Introduction

Various production technologies are utilized to create composite laminates for high-performance aerospace goods. Some (manufacturing procedures) are only compatible with thermoset resins, whereas others can handle both thermoset and thermoplastic resins. Continuous fiber reinforcements are used in some (manufacturing procedures), while short fiber reinforcements are used in others [84]. Regardless, a manufacturing process that facilitates the production of high-performance composite laminates is preferable when selecting a manufacturing method for composite laminate fabrication. To make high-quality composite laminates, a combination of pressure, time, and temperature must be optimized. As illustrated in **Figure 3.5** [85], advanced resin matrix composites' processing and manufacturing methods are grouped into two types: 1. resin-impregnated fiber methods and 2. fiber preform/liquid processing methods.

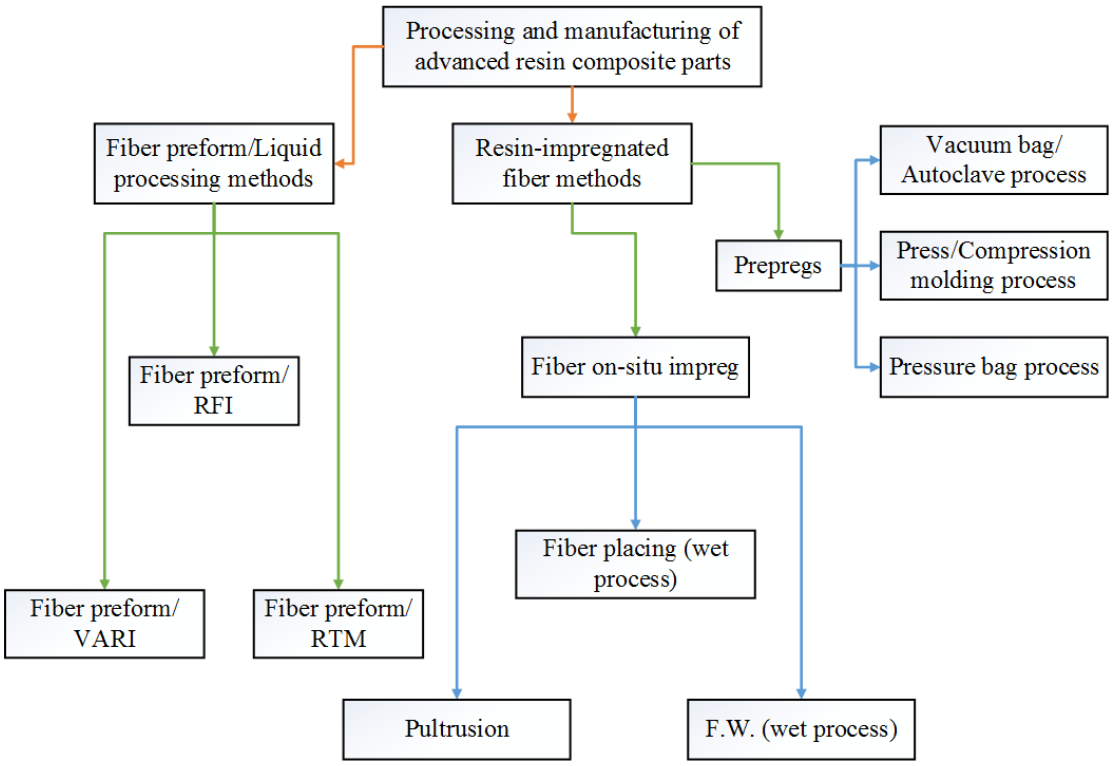

Figure 3.5. The classification of processing and manufacturing technologies (F.W.: Filament winding; RTM: Resin transfer molding; RFI: Resin film infusion; VARI: Vacuum-aided resin injection) [85].

3.2.2 Art of interleaving

As stated in **section 1.6**, the project's purpose is to introduce the appropriate amount/concentrations of recycled carbon fibers from non-woven mats into conventional/virgin fiber composites to create structural damping composite laminates. Considering the various manufacturing methods, as shown in **Figure 3.5**, to produce quality composite laminates using prepregs and nonwoven mats, reference must be made to the art of interleaving. The concept of interleaving is an old art used in the aircraft industry to enhance acoustic damping and improve damage tolerances for several years.

Shivakumar et al. [86] reviewed interleaved polymer matrix composites and noted three types of interleaving: particle, film, and nanofiber. Particle interleaving is the uniform sprinkling of fine particles to a required areal weight over prepregs or fabrics before using a suitable manufacturing method to cure the modified prepregs or assemblage into laminates. Film interleaving is the lacing of prepregs or fabrics with films (epoxy films, nonwovens, etc.) of varied thicknesses before using a convenient manufacturing technique to cure the modified prepregs or assemblage into laminates. As the name suggests, nanofiber interleaving is the lacing of prepregs or fabrics with nanofibers. Although interleaving remains an art, it can effectively control mechanical properties and vibrations in composite laminates. As such, film interleaving was used in this study.

3.2.3 Vacuum bag/autoclave process

Regarding **Figure 3.6**, Prepreg/vacuum bag–autoclave, pressure bag, and vacuum bag processes are essentially included in compression bag/half-mold (male or female only) processing techniques. The main differences among them are the different operating pressures and temperatures used in the curing processes. The prepreg press molding processing method uses a pair of matched molds (assembled molds). The closed molds containing the composite parts are heated or put into an oven for high-temperature applications. Pressure is applied either by mold body interference or by expandable rubber and airbags attached within the part. In this way, the prepregs are finally cured into composite parts [85].

The Autoclave curing process is used to fabricate high-quality aerospace composite products. The process involves using a pressurized vessel and in-process consumables such as vacuum bag, bleeder, breather, sealant putty, etc., making it

relatively expensive. An autoclave is a pressure vessel with provisions for heat input to the circulating air/gas inside the chamber. A vacuum system for applying negative pressure, a temperature and pressure monitoring system, and a control system for controlling the operating parameters are the other essential features of an autoclave [87].

The autoclave process could be mimicked using the vacuum-assisted compression molding (VACM) technique to manufacture somewhat high-quality composite laminates, which are relatively less expensive. The method employs a vacuum bagging and a hot press machine. **Figure 3.6** [88] shows a schematic representation of a vacuum bagging process.

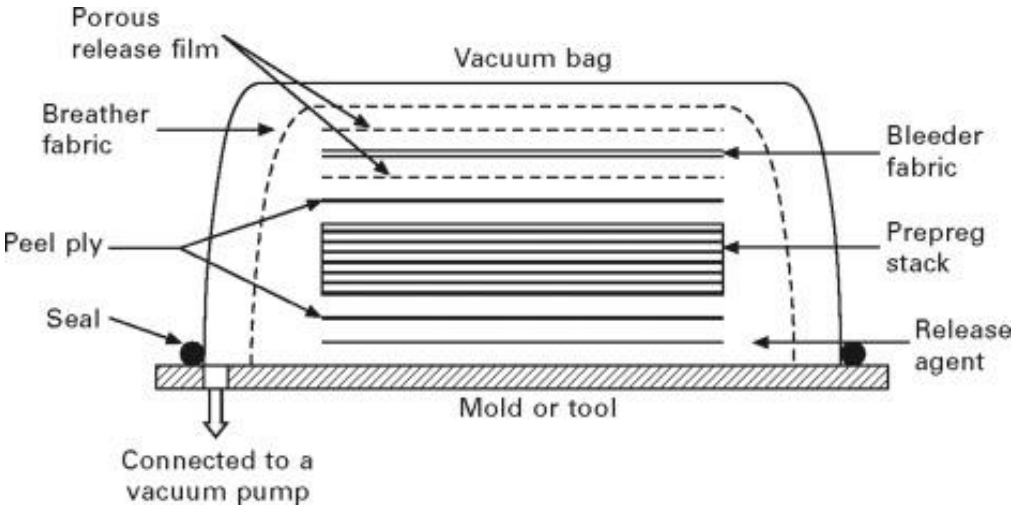

Figure 3.6. The schematic of a vacuum bagging set-up [88].

Source: Copyright 2022, Taylor and Francis Group LLC.

3.2.4 Fabrication of composite laminates

The composite laminates were manufactured using the vacuum bagging-assisted compression molding method. The Toray T700SC UD carbon fiber (12K) epoxy prepregs and mats were cut to 328×228 mm^2. The prepregs were cut using a ply cutter, and the non-woven mats were cut using a paper cutter. The configurations with mats had single, triple, and quintuple mats. Each mat was sandwiched between two resin

films (F_2) before being used to interleave the 12 prepregs (P_{12}). **Figure 3.7** shows the schematic layup sequences (the front view) for all the composite laminates manufactured. The stainless-steel mold and frame were cleaned with Acetone before being subsequently wiped with the mold releasing agent, Chemlease® PMR EZ, to help remove the cured composite laminate.

Afterward, the preforms were fitted into a $330 \times 230\ mm^2$ (inner dimensions) stainless steel frame mold with two nonporous polytetrafluoroethylenes (PTFEs) release films to cover the frame's top and bottom. After that, the assemblage was placed on a $600 \times 500 \times 4\ mm^3$ stainless steel plate that had sealant tapes, a breather is laid on top and vacuum bagged using the sealant tape. A vacuum pump is then connected, and the preforms are degassed at room temperature till the vacuum pressure reaches 0.1MPa. **Figure 3.8** shows the bagging schematic. Afterward, the assemblage was transferred to the hot press and dwelled at 80℃ for 30 min. At the 30th minute, an additional 5 MPa pressure from the hot press was applied, and the curing temperature was increased to 130℃ in about 25 minutes, and it dwelled at 130℃ for 120 minutes. The cured composite laminate was removed from the hot press at the 120th minute and allowed to cool to about room temperature with the vacuum still being applied (vacuum was applied throughout). **Figure 3.9** and **Figure 3.10** show the curing cycle and the manufacturing setup, respectively. After manufacturing the laminates, the samples for the various tests were cut using a water jet cutter. The pieces were then cleaned and dried in the oven at 100℃ for 24 hours before testing.

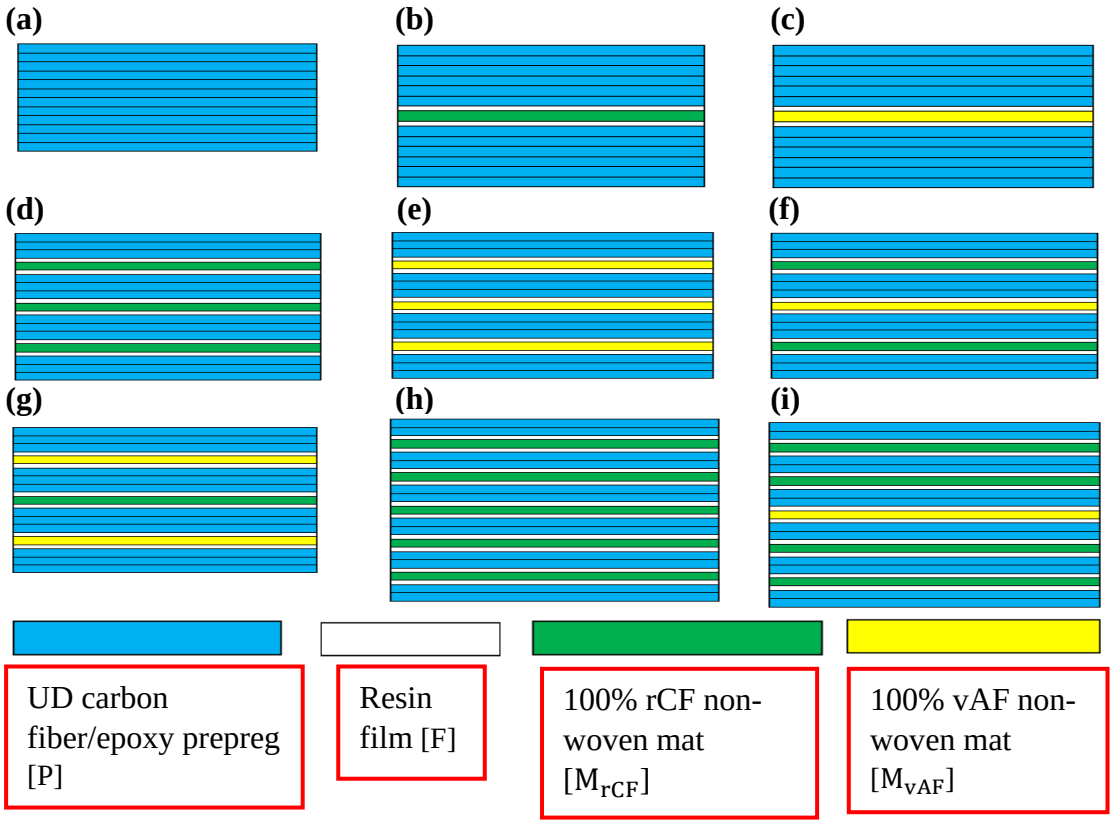

Figure 3.7. (a) Control sample ($[P_{12}]$) (**Laminate A**) (b) UD CFRP with 1 rCF mat ($[P_6F_1M_{rCF}F_1P_6]$) (**Laminate B**) (c) UD CFRP with 1 vAF mat ($[P_6F_1M_{vAF}F_1P_6]$) (**Laminate C**) (d) UD CFRP with 3 rCF mats ($[P_3F_1M_{rCF}F_1P_3F_1M_{rCF}F_1P_3F_1M_{rCF}F_1P_3]$) (**Laminate I**) (e) UD CFRP with 3 vAF mats ($[P_3F_1M_{vAF}F_1P_3F_1M_{vAF}F_1P_3F_1M_{vAF}F_1P_3]$) (**Laminate J**) (f) UD CFRP with (2 rCF + 1 vAF) mats ($[P_3F_1M_{rCF}F_1P_3F_1M_{vAF}F_1P_3F_1M_{rCF}F_1P_3]$) (**Laminate L**) (g) UD CFRP with (1 rCF + 2 vAF) mats ($[P_3F_1M_{vAF}F_1P_3F_1M_{rCF}F_1P_3F_1M_{vAF}F_1P_3]$) (**Laminate M**) (h) UD CFRP with 5 rCF mats ($[P_2F_1M_{rCF}F_1P_2F_1M_{rCF}F_1P_2F_1M_{rCF}F_1P_2F_1M_{rCF}F_1P_2F_1M_{rCF}F_1P_2]$) (**Laminate K**) (i) UD CFRP with (4 rCF + 1 vAF) mats ($[P_2F_1M_{rCF}F_1P_2F_1M_{rCF}F_1P_2F_1M_{vAF}F_1P_2F_1M_{rCF}F_1P_2F_1M_{rCF}F_1P_2]$) (**Laminate N**).

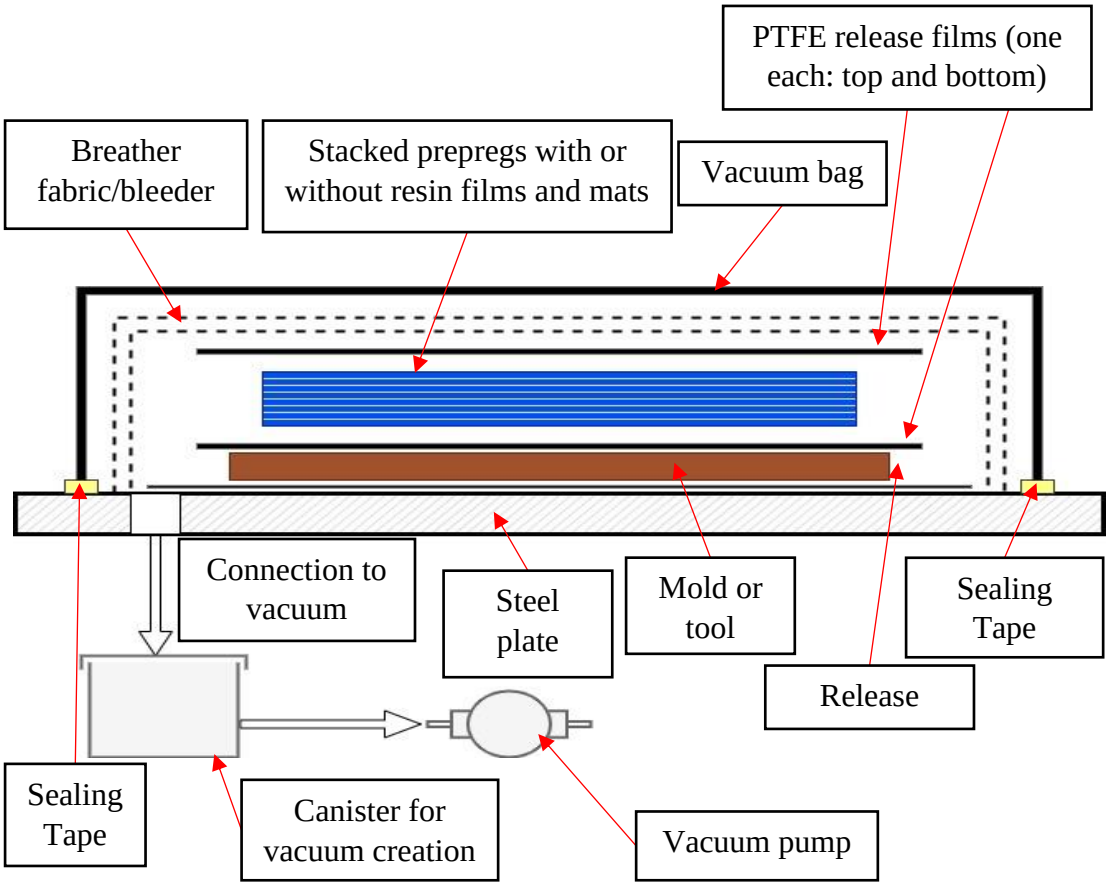

Figure 3.8. The schematic diagram for the laminate vacuum bagging process.

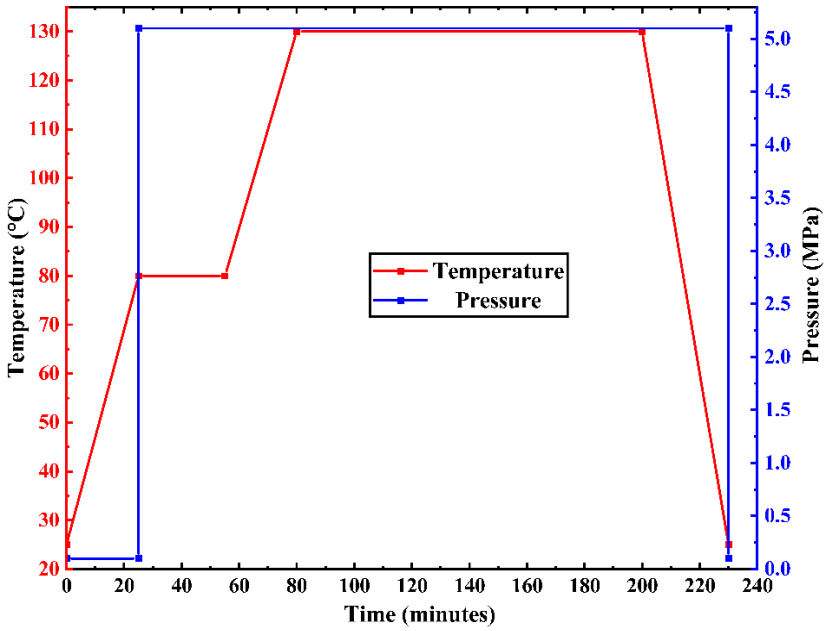

Figure 3.9. The curing cycle: temperature and pressure profile for the composite laminate.

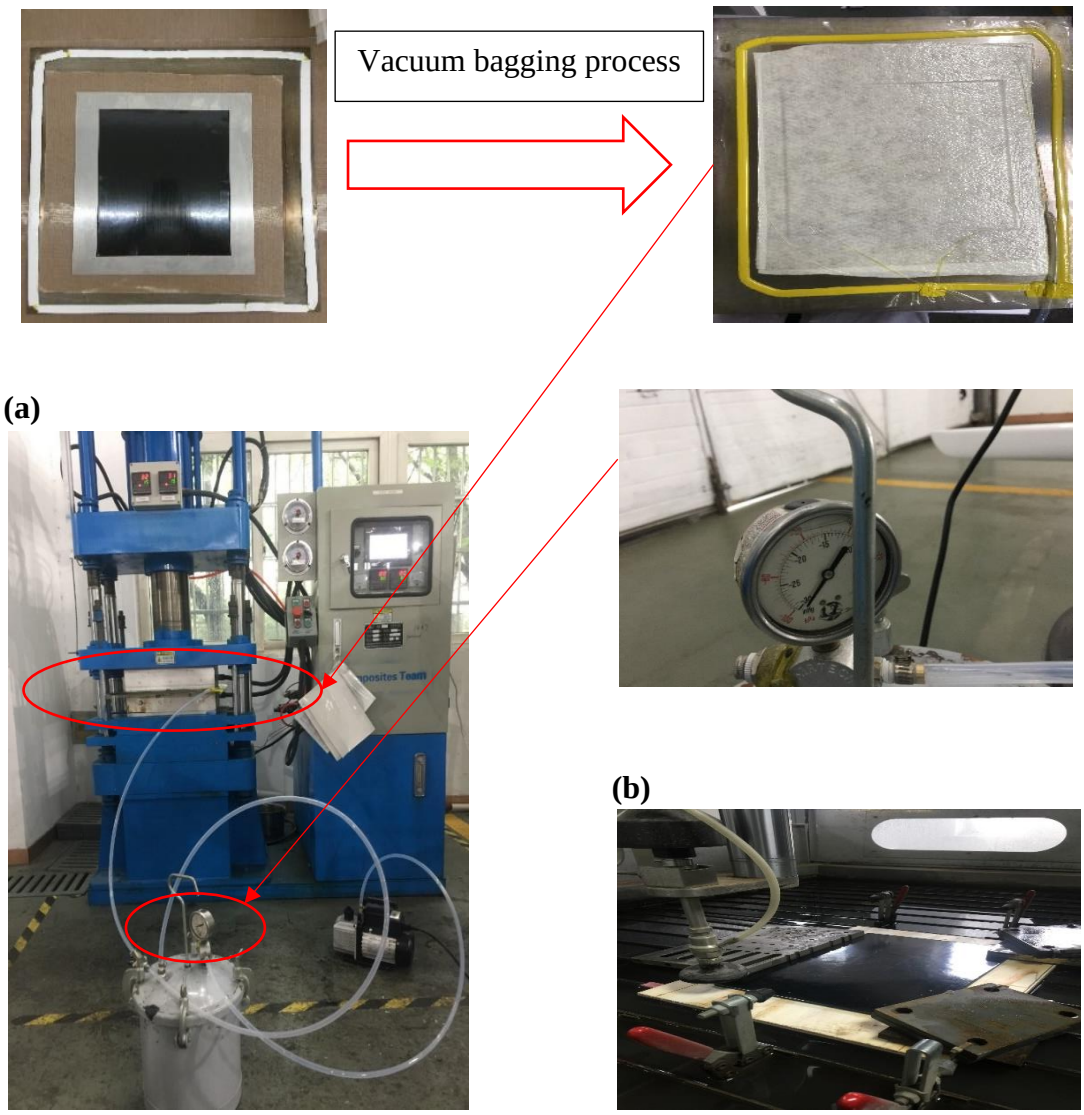

Figure 3.10. (a) The manufacturing setup for the composite laminates' manufacturing and (b) fabricated laminate about to be cut with the water jet.

4 CHARACTERIZATIONS OF COMPOSITE LAMINATES

4.1 INTRODUCTION

Undesirable vibrations can result in excessive stresses of composite structures or the complete failure of composite materials components due to resonance. These unwanted vibrations in composites can be reduced through passive or active methods. Irrespective of the kind of control, mechanical vibrations can be classified into two (2) general types: free vibration and forced vibration. Structural materials possessing high stiffness and damping are in high demand for passive vibration controls. However, the development of enhanced passive damping materials with high stiffness is hindered by the mutually exclusive nature of these mechanical properties (stiffness and mechanical damping) [89]. The DMA is utilized to study the mutually exclusive nature of these mechanical properties (stiffness and mechanical damping) (the viscoelastic behavior). Using a DMA to study the viscoelastic behavior of composite materials can be expensive; another way to reduce cost is using the free vibration-bending technique [40]. Subsequently presented is the working principle and theory behind the DMA, free vibration, and bending.

This chapter enumerates characterizing the fiber-reinforced polymer laminates used for the project. The characterizations were dynamic mechanical analysis (DMA), bending (flexural moduli and the flexural strength determinations) and shear (short beam shear strength determinations) tests, free vibration tests, surface electron microscopy (SEM), Fourier-transform infrared (FTIR) spectrometry, density, and fiber volume contents. Subsequently are the reasons and how the tests were carried out.

4.2 DYNAMIC MECHANICAL ANALYSIS (DMA) PROPERTIES

The viscoelastic behavior of fiber-reinforced polymer composites can be studied using dynamic mechanical analysis (DMA) (see **Figure 4.1** for a schematic representation). The technique allows the rapid scanning of a material's storage (elastic) and loss (viscous) moduli as a function of temperature, strain, or frequency [90]. The DMA operates by the application of oscillatory force to a sample. The sample can be subjected to either controlled stress or strain. The stress or strain application causes a sinusoidal deformation (the sample deforms to a certain amount sinusoidally). By measuring both the amplitude of the deformation at the peak of the sine wave and the lag between the stress and strain sine waves, quantities like the moduli (Elastic and Loss) and the damping (loss factor) can be computed [91]. **Figure 4.2** shows the schematic of available sample geometries used in DMA testing. Among is the three-point (or simply supported) bending mode deformation, which has the following advantages [92]: (1). the best mode for measuring medium to high modulus materials such as fiber-reinforced thermosets (composites); (2). this mode of deformation (purest deformation mode) yields the most accurate moduli values since clamping effects are avoided; and (3). this geometry also applies a small strain amplitude for a given dynamic displacement amplitude.

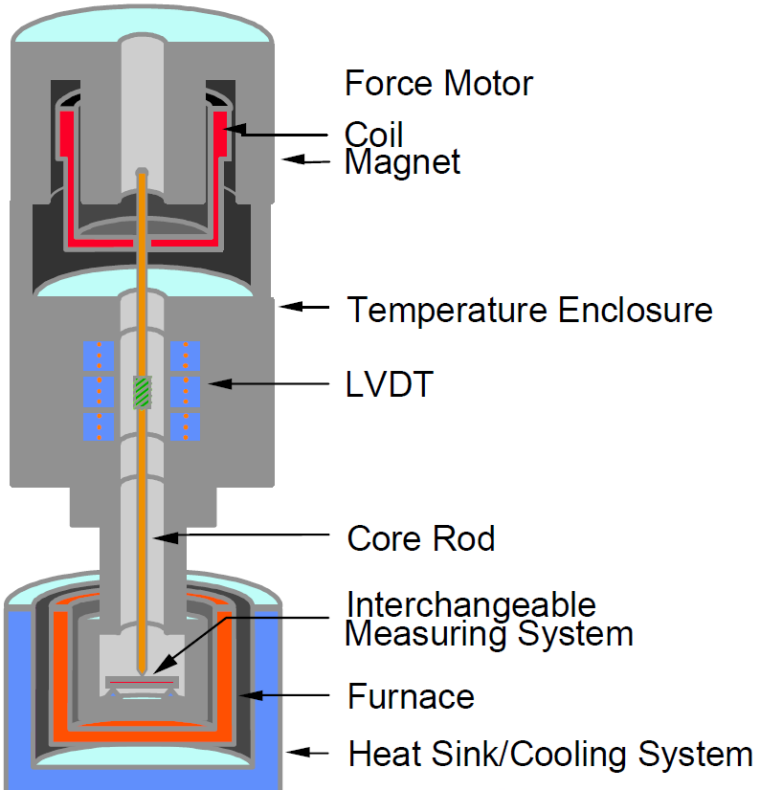

Figure 4.1. The Schematic of a Perkin-Elmer DMA 7e machine [93].

LVDT: Linear Vertical Displacement Transducer

Source: Copyright 2022, Taylor and Francis Group LLC.

A sample will deform sinusoidally if a constant dynamic force is applied to it (i.e., the load is applied sinusoidally). The oscillating load (stress) and its reaction (strain) are shown in Error! Reference source not found.: stress-strain relationship in DMA [93]. A n intricate pendulum clamps the sample between its arms. The electromechanical transducer moves the arms carrying the sample system. A linear variable differential transformer (LVDT) is utilized to monitor the frequency and amplitude of vibration, and the LVDT's feedback is used to operate the electromechanical transducer. Applying a constant dynamic force (i.e., applying the load sinusoidally) to a sample will deform it sinusoidally. **Figure 4.3** shows the oscillatory load (stress) and its response (strain): stress-strain relation in DMA [93].

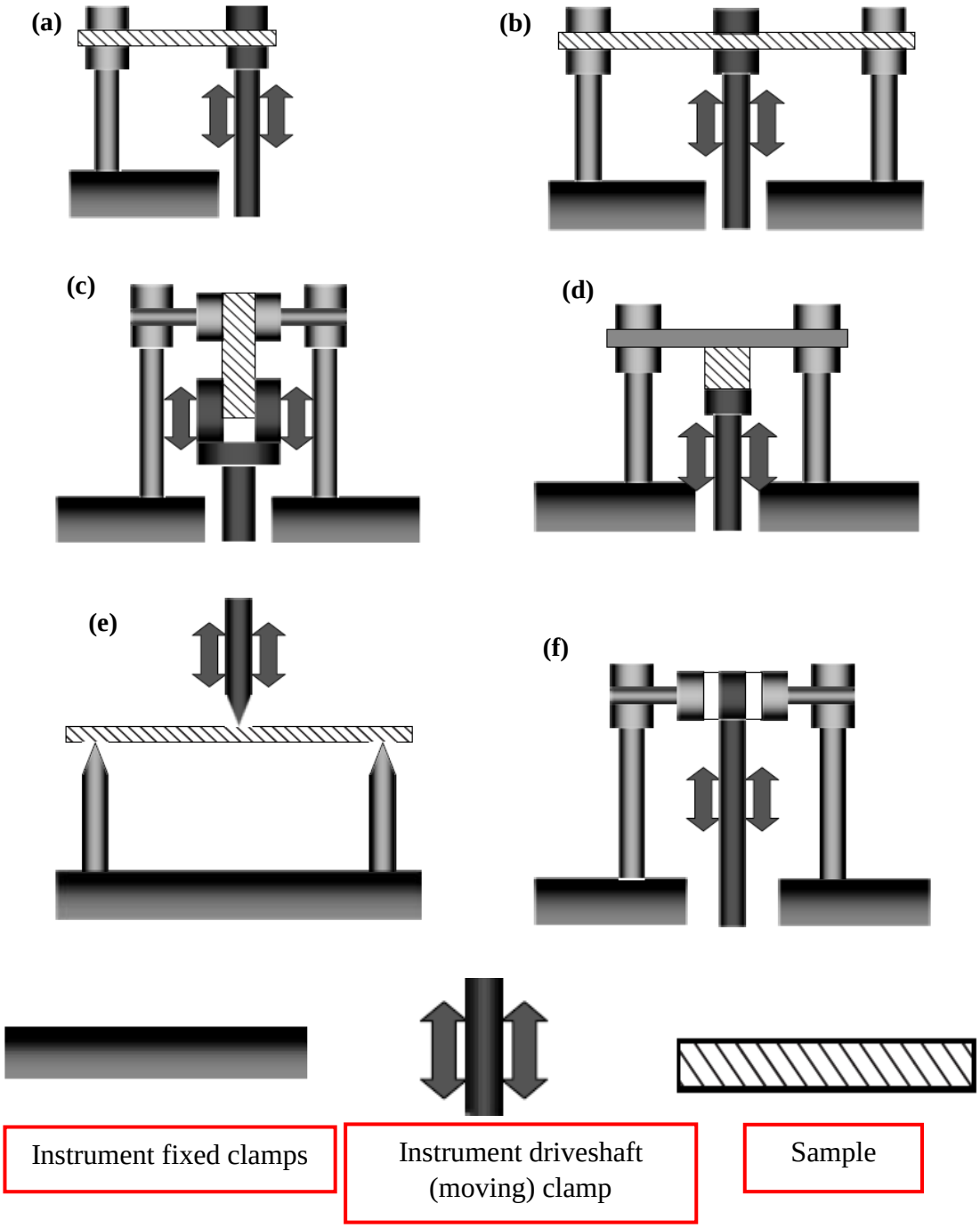

Figure 4.2. The Schematic of available sample geometries: (a) Top left – single cantilever bending; (b) top right – dual cantilever bending; (c) middle left – tension; (d) middle right – compression; (e) bottom left –three-point bending; (f) bottom right – shear. The sample length, l, is always taken as the distance between the fixed clamp and the driveshaft clamp in these definitions [92].

Source: Copyright 2022, Blackwell and John Wiley & Sons.

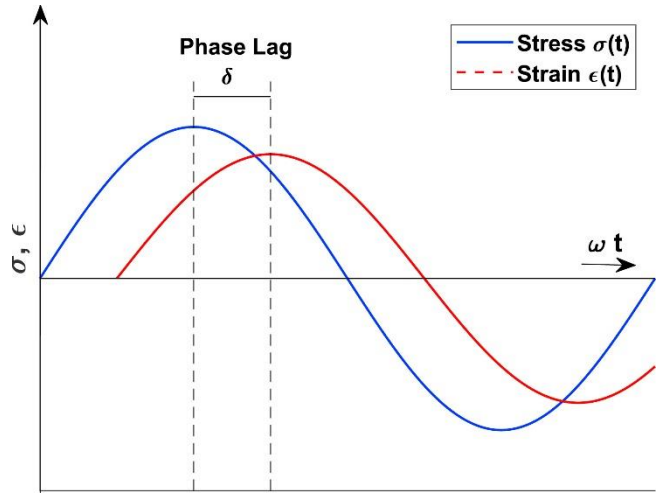

Figure 4.3. The stress-strain relation in a DMA [93].

Source: Copyright 2022, Elsevier Ltd.

Eqs 4.1-4.6 are the mathematical formulations for the DMA working principle [93]:

$$\sigma(t) = \sigma_o \sin(\omega t) \quad 4.1$$

$$\varepsilon(t) = \varepsilon_o \sin(\omega t - \delta) \quad 4.2$$

where $\sigma(t)$ is the oscillatory load (stress) as a function of time, t; σ_o is the amplitude of the oscillatory load (stress); ω is the angular frequency in radians per second; $\varepsilon(t)$ is the response (strain) as a function of time, t; ε_o is the amplitude of the response (strain); δ is the phase angle between the oscillatory load (stress) and the response (strain).

The one-dimensional stress-strain relation in the frequency domain is expressed in **eq 4.3**.

$$\sigma(\omega) = E(\omega)^* \varepsilon(\omega) = [E(\omega)' + jE(\omega)'']\varepsilon(\omega) = E(\omega)'[1 + j\eta(\omega)]\varepsilon(\omega) \quad 4.3$$

where $E(\omega)^*$ is the complex modulus; $E(\omega)'$ is the real part (also known as the storage modulus); $E(\omega)''$ is the imaginary part (also known as the loss modulus); and $\eta(\omega)$ is the ratio between the imaginary part (also known as the loss modulus) and the real part

(also known as the storage modulus), which is expressed in **eq 4.4** (also known as the loss factor or the damping) [all expressed as a function of the angular frequency].

$$\eta(\omega) = \frac{E(\omega)''}{E(\omega)'} = \tan\delta \quad 4.4$$

The real part (also known as the storage modulus) and the imaginary part (also known as the loss modulus) are respectively expressed in **eqs 4.5** and **4.6**.

$$E(\omega)' = \frac{\sigma_o}{\varepsilon_o}\cos[\delta(\omega)] \quad 4.5$$

$$E(\omega)'' = \frac{\sigma_o}{\varepsilon_o}\sin[\delta(\omega)] \quad 4.6$$

4.2.1 DMA procedure

The viscoelastic behavior of the composite laminates was investigated by a third-party entity using the dynamic mechanical analyzer, PerkinElmer, DMA 8000, according to the standard test method for plastics-dynamic mechanical properties-in flexure (three-point bending), American Society for Testing and Materials (ASTM) D5023-15 [94]. The samples' sizes are 46×10×t mm^3 (t had varied thicknesses: see **chapter 5**); span length was approximately 30 mm for all samples. The testing temperature was from 30℃ to 250℃ at a heating rate of 2℃/min, an amplitude of 20 μm, and a frequency of 1 Hz. The storage (elastic) modulus (E'), and loss factor (tan delta) (η) as a function of temperature were found. The glass transition temperature (T_g) was taken as the peak of the tan delta against the temperature graph. About 1420 data points were plotted for the various charts. The storage modulus (E') was used to multiply the loss factor (η) as seen in **eq 4.7** to find the damping capacities (quantified as a figure of merit) of the laminates under considerations [49]:

$$\text{Figure of merit} = E' \times \eta \quad 4.7$$

4.3 FLEXURAL MODULUS AND FLEXURAL STRENGTH

4.3.1 Introduction

Three-point bending tests are used to study the bending characteristics of the materials under consideration. As shown in **Figure 4.4**, this is accomplished by placing a load, P, in the center of a beam that is simply supported by two rollers.

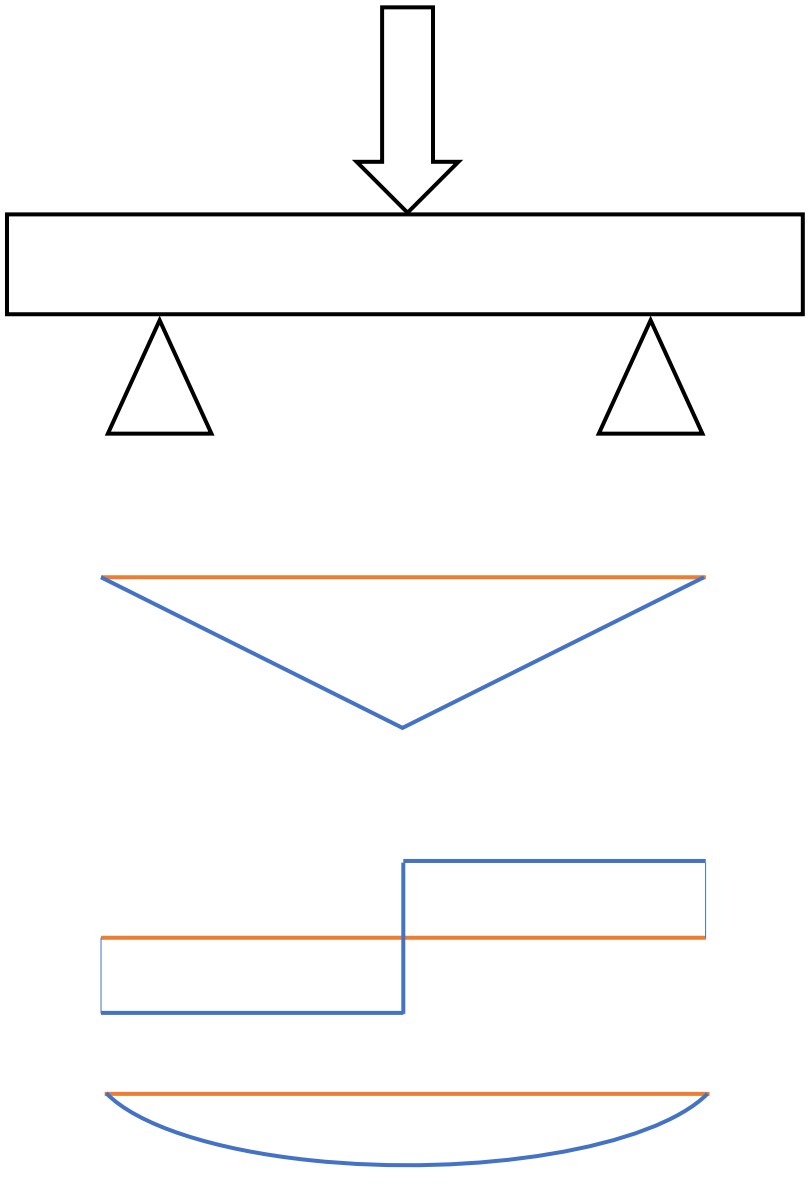

Figure 4.4. Schematic of a beam with length, L under three-point bending with a load, P (top), with bending moment (M), shear (Q), and deflection (δ) graphs.

The maximum deflection (δ_{max}) (it occurs in the center of the beam) is defined by **eq 4.8** [95].

$$\delta_{max} = \frac{PL^3}{48EI} \quad 4.8$$

where E is Young's modulus, and I is the second moment of area about the neutral axis, defined by **eq 4.9** [95].

$$I = \frac{bt^3}{12} \quad 4.9$$

where b and t are the beam's width and thickness, respectively. Young's modulus of the material can be estimated by knowing the maximum deflection, the applied load (force), and the geometry (length, width, and thickness) of the beam under consideration.

4.3.2 Flexural modulus and flexural strength determination procedure

The flexural modulus and the flexural strength of the composite laminates were investigated in a three-point bending mode according to the standard, ASTM D790-2017 [96]. The specimen had a dimension of $130\ mm \times 12.7\ mm$ with varied average thicknesses (see the results and discussion section). The rate of crosshead motion was in the order of $4.0\frac{mm}{min}$ and $4.5\ \frac{mm}{min}$ for the UD CFRP configurations with no mat (the control laminate) and single mat, respectively, while in the order of $5.1\ \frac{mm}{min}$ and $5.7\ \frac{mm}{min}$ for the UD CFRP configurations with triple mats and quintuple mats, respectively. The support span-to-thickness ratio was 32, and the rate of crosshead motion was in the order of $4.0\frac{mm}{min}$ and $4.5\ \frac{mm}{min}$ for the control and configurations with mats, respectively. The rate of crosshead motion for the configurations with mats falls within the ±10 % allowance as specified by the ASTM D790-17 standard [96]. All tests were done at room temperature using the MTS universal testing machine (UTM) Exceed 45.105, a

load cell of 50 kN. Shown in **Figure 4.5** is the test being conducted, and five specimens for each laminate were tested.

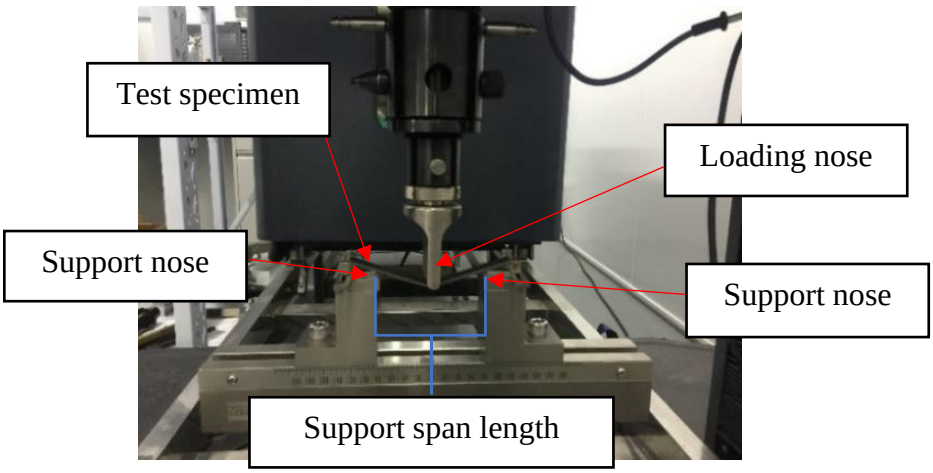

Figure 4.5. Flexural testing.

The flexural modulus and flexural strength were evaluated using **eq 4.10** and **eq 4.12**, respectively [96]:

$$E_f = \frac{L^3 m}{4bh^3} \qquad 4.10$$

where: E_f is the flexural modulus (in MPa), L is the support span (in mm), b is the width of beam tested (in mm), h is the thickness of beam tested (in mm), and m is the slope of the tangent to the initial straight-line portion of the load-deflection curve (in $\frac{N}{mm}$ of deflection); m is calculated by drawing a straight line to the steepest initial bit of the load-deflection curve.

In order to compute the flexural strength when the support span length-to-depth ratios are not greater than 16, **eq 4.11** is used. However, according to the standard, when large support span length-to-depth ratios are used (ratios greater than 16) (32 was used in this project), significant-end loads are developed at the support noses. This will affect the moment in a simply supported beam; hence **eq 4.11** includes additional terms that

are an approximate correction factor to cater to these end loads influences; thus, **eq 4.12** was used to estimate the flexural strength.

$$\sigma_f = \frac{3PL}{2bd^2} \tag{4.11}$$

where: σ_f is the flexural strength (in MPa), P is the maximum load encountered before failure (in N), L is the support span (in mm), b is the width of beam tested (in mm), and d is the thickness of beam tested (in mm).

$$\sigma_f = \frac{3PL}{2bd^2}\left[1 + 6\left(\frac{D}{L}\right)^2 - 4\left(\frac{d}{L}\right)\left(\frac{D}{L}\right)\right] \tag{4.12}$$

where: σ_f, P, L, b, and d are the same as for **eq 4.11**, and D is the deflection of the centerline of the specimen at the middle of the support span or maximum deflection encountered before failure (in mm).

4.4 SHORT BEAM SHEAR STRENGTH

According to the standard, ASTM D2344-2016 [97], a short beam shear test was conducted to evaluate the composite laminates' interfacial adhesions. The interlaminar shear strength was computed to quantify the interfacial adhesion. The specimen had the dimension 8 mm × 6 mm with thicknesses of 2.31 mm, 2.51 mm, and 2.52 mm for the UD CFRP configurations with no mat (the control), configurations with rCF mat, and vAF mats, respectively. The support span length-to-thickness ratio was approximately 4. The shear tests were carried out at room temperature with a 1.0 mm/min crosshead rate using the same universal testing machine used in the flexural tests. Shown in **Figure 4.6** is the test being conducted, and five specimens for each laminate were tested.

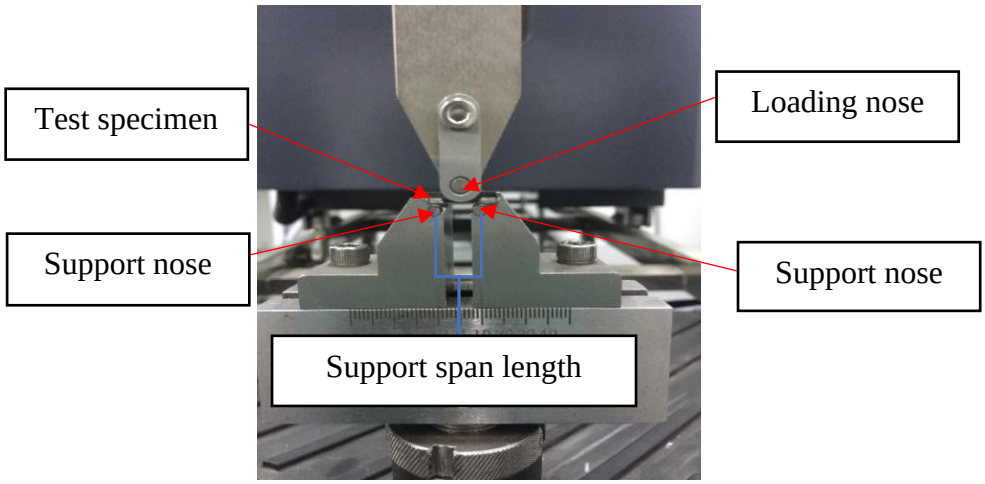

Figure 4.6. Shear testing.

The short beam shear strength was calculated using **eq 4.13** [97]:

$$F^{sbs} = 0.75 \times \frac{P_m}{b \times h} \qquad 4.13$$

where: F^{sbs} is the short-beam shear strength (in MPa); P_m is the maximum load observed during the test (in N); b is the measured specimen width (in mm), and h is the measured specimen thickness (in mm).

4.5 FREE VIBRATIONS

Free vibration refers to a motion caused by no external force. Initial circumstances, such as an initial displacement of the mass element of the system from an equilibrium position or an initial velocity, are the primary cause of motion. It is undamped if there is no energy loss throughout the system's motion. This is the case of the most straightforward vibratory system (see **Figure 4.7**), which consists of an inertia element (a mass), a damper element (a dashpot), and an elastic element (a spring) which produces a restoring force that tends to restore the inertia element to its equilibrium position. The elastic element (a spring) stores energy as potential energy, the inertia

element (a mass) stores energy as kinetic energy, and the damper element (a dashpot) dissipates energy into heat.

The mathematical models that govern the free vibration of single degree of freedom (one DOF) systems can be described in terms of homogeneous second-order ordinary differential equations that contain displacement (kx), velocity ($c\dot{x}$), and acceleration ($m\ddot{x}$) terms. The displacement coefficient (k) describes the stiffness of the elastic member. The velocity coefficient (c) defines the damping, which determines the amount of energy dissipated, and the acceleration coefficient (m) represents the inertia of the system [98].

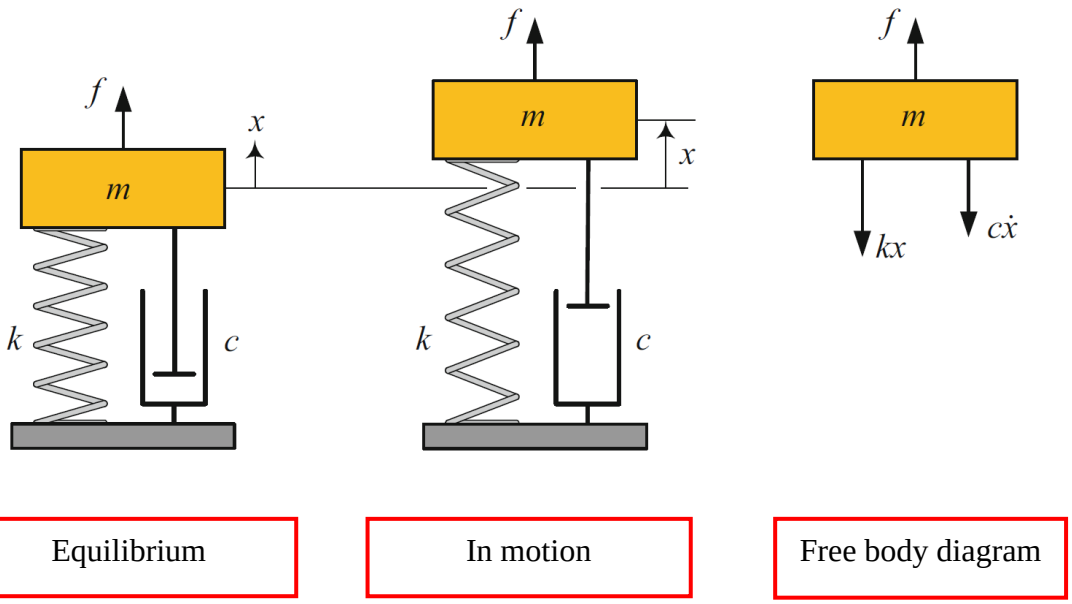

Figure 4.7. A one DOF vibrating systems [99].

Source: Copyright 2022, Springer Int.

From **Figure 4.7**, **eq 4.14** is written:

$$m\ddot{x} + c\dot{x} + kx = f \qquad 4.14$$

For free vibration, $f = 0$.

To measure a loss factor (η) which is then used in a free vibration-bending technique, the structure under consideration must be excited to measure the frequency response functions (FRFs). According to Avitabile [100], whether the measured FRF comes from a shaker test (using a shaker machine) or an impact test (using an impact hammer), the measured FRF will be the same if all precautions are followed correctly. The usage of the DMA testing for characterizations will suffice. However, the author did not have access to a readily available DMA testing rig; hence, the only option was to let a third party conduct the tests. The quoted prices by the third party were exorbitant per the number of available testing samples. In that regard, there was the need to screen out selected configurations for the DMA testing. As such, the author referred to the works of Ni et al. [40], wherein a free vibration-bending technique was used to find the figure of merit (finding the figure of merit is the only reason for the free vibration tests). Ni et al. [40] stated that the figure of merit estimated in this manner should be regarded as an indicator and not a certitude for the damping capacity of a material. In the referred literature, the authors were after damping characteristics in addition to the loss factors; hence they reported the natural frequencies and modal damping values, but in this project, the free vibration test was only done to find the loss factors which will be subsequently used to calculate the figure of merit at room temperature for screening purposes to save cost.

The free vibrations were conducted according to the ASTM E756-05(2017) [101], a standard test method for measuring vibration-damping properties of materials. The test specimens had a cantilever configuration of 230 mm by 10 mm, with the fixed length being 50 mm. The thickness for the control sample is 2.31 mm, and that of the configurations with the mats is 2.51 mm. The test was conducted by exciting the cantilever beam with an instrumented hammer (PCB piezotronics, model PCB 086C03)

with a medium tip. The responses were measured using an accelerometer (PCB piezotronics) with a sensitivity of 101.7 mV/g, placed at the tip of the beam's free end using a thin layer of wax. In connection was the multiple channels data acquisition card (DAC) (Data Physics Corporation) that connected the impact hammer and the accelerometer to it. The DAC was then attached to the computer to acquire the measured response. The data obtained by the DAC is then sent to the computer, which is interfaced with the Signalcalc ACE dynamic signal analyzer software. The testing parameters were frequency range, 1000 Hz; acquisition time, 400 ms; frequency resolution, 2.500 Hz; sampling interval/time resolution, 390.6 μ s; exponential averaging, 3; and force/exponential observation window employed. The experimental setup is shown in **Figure *4.8***. The accelerometer and the instrumented hammer have transducers that use a quartz piezoelectric crystal as sensing elements and incorporate microelectronics for signal conditioning. For an applicable and consistent range of loads to be impacted, the transducers have been designed to either overload or light load if the applied load is out of range. The connected channel shows red for the overloaded channel and yellow/black for the under-ranged (light load). The response is only accepted when the channel shows green, indicating the force is in the acceptable range. The impacts were 10 mm from the fixed end of the cantilever beam, and the coherence function was observed to ensure that the noise effect was small enough not to affect the accuracy of the measured response.

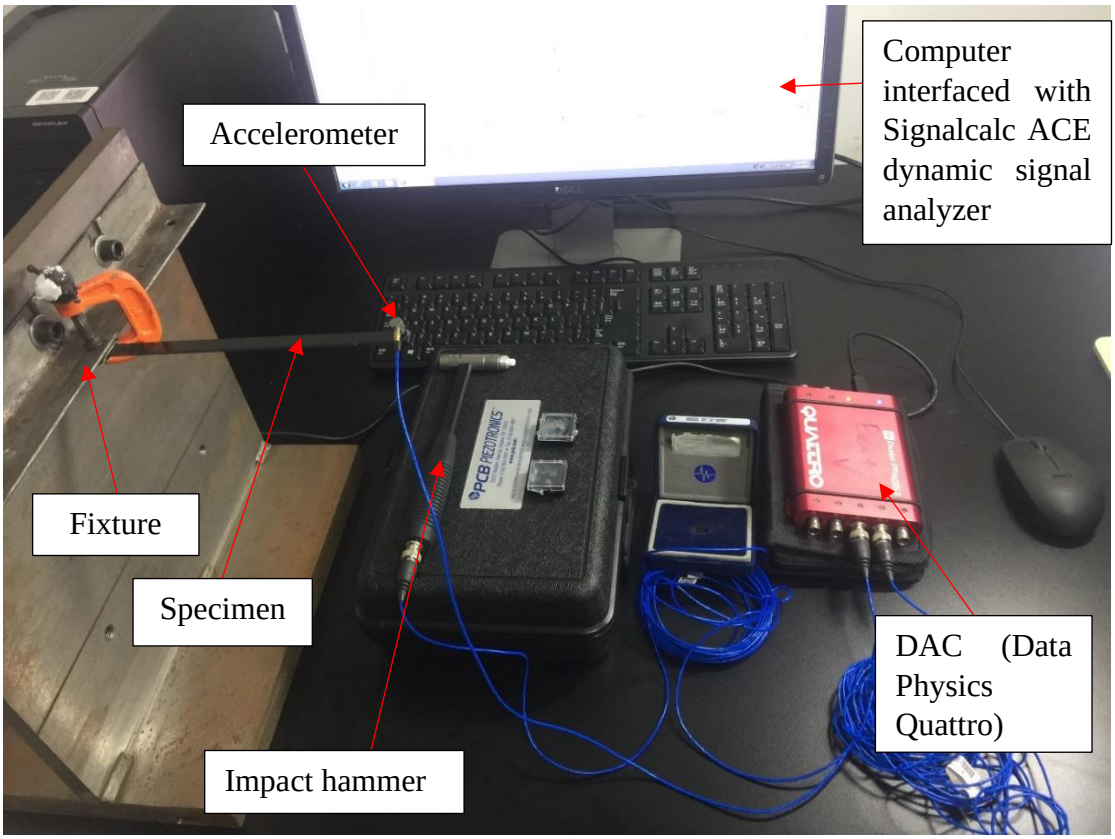

Figure 4.8. Free vibration test.

To estimate the damping capacities (quantified as the figure of merit) of the composite laminates, the loss factor for the free vibration (η) was first determined using the logarithmic decrement method. The logarithmic decrement, which measures the rate of decay of free vibrations, is a good technique used to estimate the loss factors of materials, and it is seen in **eq 4.15** and **eq 4.16** [102]:

$$\delta = \frac{1}{m} \ln \left| \frac{x_{n-1}}{x_n} \right| \qquad 4.15$$

$$\eta = \sqrt{\frac{\delta^2}{4\pi^2+\delta^2}} = \frac{\delta}{\sqrt{(2\pi)^2+\delta^2}} \qquad 4.16$$

where x_n represents a peak from the free vibration decaying graph (n > 1; i.e., $\frac{x_1}{x_2}$; $\frac{x_2}{x_3}$; etc.), δ is the logarithmic decay rate, m averages the number of cycles, and η is the loss factor. The time intervals used in calculating δ were from 0.010 s to 0.039 s (was

chosen because most responses observed for all the samples clustered around there) (all peaks less than 1.00 that fell within this time zone were neglected and if the last peak in this time zone does not approximately fall on 0.039 s, the next peak was chosen). **Eq 4.15** averages the logarithmic decay rate, and the average value is then used in estimating the loss factor using **eq 4.16**.

Bending, characterized as the flexural modulus (E_f) is very important in many applications; hence it is considered a measure of stiffness [103]. Therefore, the flexural modulus was used to multiply the calculated loss factor as seen in **eq 4.17** to estimate the damping capacities of the laminates under considerations [40]:

$$\text{Figure of merit} = E_f \times \eta \qquad 4.17$$

4.6 SURFACE ELECTRON MICROSCOPY (SEM)

The surface morphology of the recycled carbon fibers, M46J, was characterized using a Zeiss Sigma VP scanning electron microscope with an accelerating voltage (EHT) of 10.0 kV. The working distance (WD) was 11.6 mm. Secondary electron detectors (SE2) and in-lens detectors were employed in the SEM imaging. Before the SEM imaging, the fibers were coated with a thin layer of gold using Leica SCD 500 gold sputter.

4.7 FOURIER TRANSFORM INFRA-RED (FTIR) SPECTROMETRY

A Bruker Vertex 70 FTIR (Fourier-transform infrared) spectrometer used the OPUS software to confirm the sizing agent on the non-woven mat. The platinum ATR mode was used with a resolution of 5 cm^{-1} in the wavelength ranges of 400 cm^{-1} to 4000 cm^{-1}. A sample of the non-woven mat was placed on top of the platinum ATR, and the spectra of the non-woven mat were taken. The spectrometer works by shining light

through the sample chamber and then measuring the amount of radiation absorbed by the sample compared to that absorbed by the reference. A detector plots the absorbance as a function of the wavenumber. The plot gives a spectrum for the sample under investigation. The experimental setup is shown in **Figure 4.9**.

Figure 4.9. FTIR experimental setup.

4.8 DENSITY DETERMINATIONS

The density was determined according to the ASTM D3171-15 (Test method II) standard [104] by using a set of vernier calipers and a Mettler Toledo laboratory scale (0.0001 g). All thickness variations of the tested samples were measured, and the average value was determined. A 20 mm $\times$ 30 mm sample size was suitable per the standard recommendations and available materials. The density in $\frac{g}{cm^3}$ was calculated using **eq 4.18** [104]:

$$\rho_c = \frac{M_i}{A \times t \times 100} \qquad 4.18$$

where: M_i is the mass of the tested sample (in grams, g); A is the area of the tested sample (in m^2) and t is the thickness (in mm).

5 RESULTS AND DISCUSSIONS

5.1 EFFECTS OF THE SIZING AGENT (TITANATE COUPLING AGENT-L12)

By applying infrared radiation (IR) to material samples, FTIR analysis assesses the absorbance of infrared light at different wavelengths to determine the molecular composition and structure of the substance [105]. The Fourier transform spectrometer translates the unprocessed data from the broad-band light source into each wavelength's absorbance level. Infrared libraries have been developed with thousands of IR spectra of diverse compounds. When evaluating an unidentified material, its IR spectrum is compared with those stored in a library. A matching coefficient is generated, which reflects the similarity between the library spectrum and the unknown spectrum. This method enables users to identify unidentified compounds based on their infrared (IR) fingerprint [105]. **Figure 5.1** depicts the chemical structure **(a)** of a TCA-L12, which has a molecular formula **(b)** of $C_{60}H_{123}O_{15}P_3Ti$. The plot in **Figure 5.2** confirms the presence of a sizing agent on the non-woven mat.

(a) **(b)**

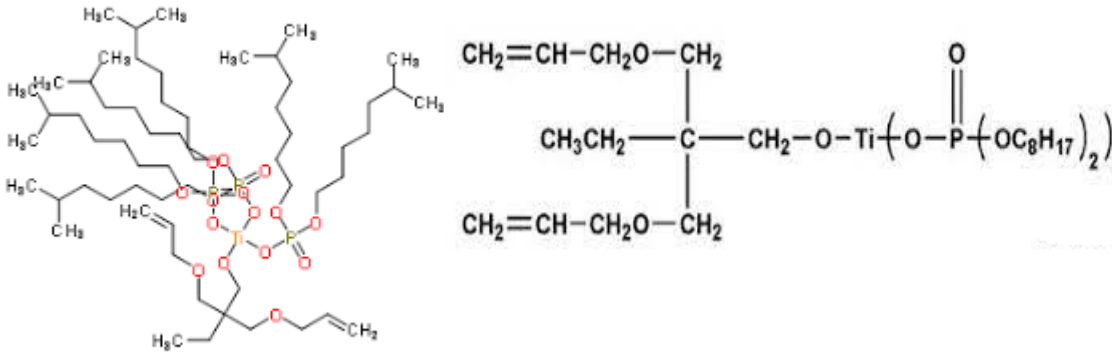

Figure 5.1. Chemical structure **(a)** and the molecular formula **(b)** of TCA-L12.

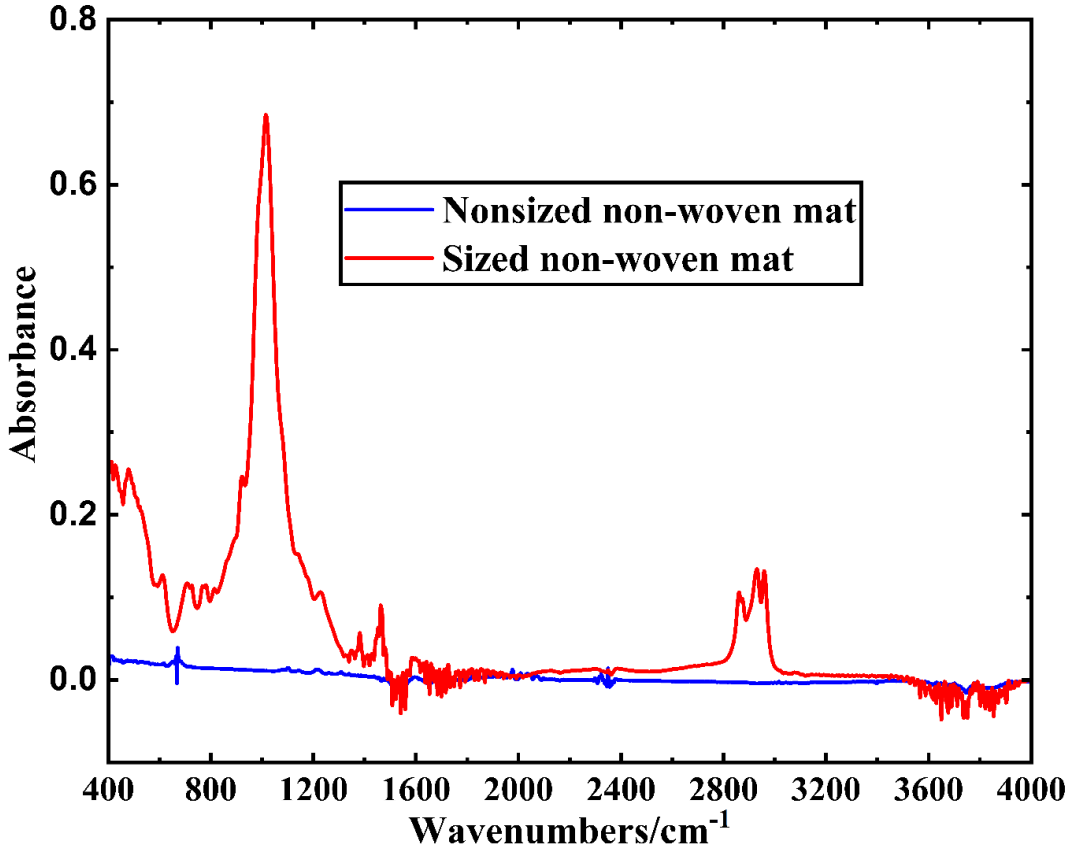

Figure 5.2. FTIR profile.

From **Figure 5.2** (it shows the FTIR spectrum of the nanosized non-woven mat and sized non-woven mat), the IR absorption at 500 and 600 cm^{-1} are attributed to the vibrations of Ti-O and P-O-Ti, respectively. The sharp and robust band at around 1000 cm^{-1} relates to the titanate coupling agent's Ti–O–C linkage. The 1350 cm^{-1} absorption band is attributed to the P=O stretching vibration. The detection of an absorption band at around 1550 cm^{-1} indicates the presence of OH groups. Stretching is attributed to the absorption bands between approximately 2800 cm^{-1} and 3100 cm^{-1}, which correspond to the CH_2 and CH_3 groups, respectively.

As shown in **Table 5.1**, the effects of the sizing agent on the flexural moduli, flexural strengths, and shear strengths have been listed. For the UD CFRP configurations with rCF mat, the 0.5 wt.% (non-woven mat used in **Laminate D**) improved the flexural

modulus, flexural strength, and shear strength by 4.8%, 9.0%, and 6.5%, respectively, compared with the 0.0 wt.% sized rCF mat (non-woven mat used in **Laminate B**). However, compared with the control sample, the improvement for the shear strength was not adequate: the shear strength was in the deficit of 0.3%. Increasing the dosage of the sizing agent from 0.5 wt.% (non-woven mat used in **Laminate B**) to 1.0 wt.% (non-woven mat used in **Laminate E**) resulted in a slight decrement of the previous improvements in the flexural properties; however, it resulted in further enhancements of the shear strength by 5.5%. Compared with the 0.0 wt.% sized rCF mat (non-woven mat used in **Laminate B**), the flexural modulus, the flexural strength, and shear strength increased by 6.8%, 15.8%, and 8.1%, respectively, when 1.5 wt.% (non-woven mat used in **Laminate F**) sizing agent was applied. At this 1.5 wt.% (non-woven mat used in **Laminate F**), the flexural modulus, flexural strength, and shear strength improved by 15.5%, 6.6%, and 1.1%, respectively, compared to the control sample (no non-woven mat was used in **Laminate A**). Doubling the dosage from 1.5 wt.% (non-woven mat used in **Laminate F**) to 3.0 wt.% (non-woven mat used in **Laminate H**) further improved flexural strength and shear strength by 0.7% and 3.0%, respectively, but resulted in a decrement of the flexural modulus of 3.2%. The only ratio that improved one of the most important properties (flexural modulus) compared to the control sample (no non-woven mat was used in **Laminate A**) was the 1.5 wt.% (non-woven mat used in **Laminate F**).

Among the factors that affect the flexural moduli are the constituents' properties and the lamina hybridization (inter-ply/inter-layer/layer-by-layer hybridization) [106]. Notwithstanding the slight decrement in the mechanical properties of the rCFs, the flexural moduli performances of the UD CFRP with vAF mat (**Laminate G**) compared with the UD CFRP with rCF mats (**Laminates B, C, D, E, and H**) can be attributed to

the positive lamina hybridization of the vAF mat with the UD CFRPs. A positive lamina hybrid occurs when layers of different reinforcements provide the combined benefits of both involving layers (in this context, positive synergistic effects between the UD CFRP layers and the layer of the vAF mat) [106]. There is also a positive synergistic effect between the UD CFRP layers and the layer of the rCF mat, but it is not as pronounced as in the case of the vAF mat layer. In addition, Singh et al. [107] noted in a study about the characterization of Kevlar fiber and its composites that Kevlar fibers can be viewed as nylons with extra benzene rings in their polymer chains: this unique nature of the Kevlar fibers results in better flexural modulus and strength. The aramid ring gives them (the aramid fibers) thermal stability, while the para structure gives high strength and modulus [108].

Moreover, the configurations with single mats can be considered a "classic" sandwich structure with six skins (upper and bottom each) separated by a core material (the non-woven mats). The core material behaves like the web in an I-beam, which increases the moment of inertia without much increment in weight, thereby producing an efficient structure for sustaining bending (characterized as flexural modulus) and buckling loads [109]. The slightly thicker vAF mat makes the moment of inertia a little more significant than the rCF mat, thereby increasing the flexural modulus for the UD CFRP with the vAF mat compared with the UD CFRP with the rCF mat.

The good interfacial adhesion between the fibers and their polymer matrix often leads to better mechanical properties (often because other factors such as environmental factors could cause degradation in mechanical properties irrespective of a generally good interfacial bonding). Aramid fibers have high crystallinity, smooth, and chemically inert surfaces that result in poor interfacial adhesions of their composites if their surfaces are not modified to improve their chemical bonding and mechanical

interlocking between their fiber and their polymer matrix [110]. For the short-beam strength performances of the UD configurations with 0.0 wt.% sizing mats, the vAF mat (non-woven mat used in **Laminate C**) performed slightly better than that of the rCF mat (non-woven mat used in **Laminate B**) regardless of the smooth and chemically inert surfaces of the aramid fibers. Generally, the rCF mat (non-woven mat used in **Laminate B**) should have had better short-beam strength values than the vAF mat (non-woven mat used in **Laminate C**). However, during a related investigation, it was observed that the M46J rCF fibers, for example, had some resin residues on their fibers (see **Figure 5.3**). Although the M46J rCFs were recovered from polymer composites, one does not know what kind of polymer epoxy the M46J rCFs were exposed to in their previous applications; hence the issue of resin compatibility arises as a result. Resin incompatibilities occur when fiber reinforcements get exposed to two different polymer epoxies.

On the performance of the flexural strengths, it should be noted that flexural strength is a fiber-dominated property. Hence, incorporating the mats generally should lead to better flexural strength values, but that was not the scenario for some laminates (see **Table 5.1**). From **Table 5.1**, for the UD CFRPs interleaved with 0.0 wt. % sizing mats (**Laminates B** and **C**), the slightly thicker vAF mat (non-woven mat used in **Laminate C**) performed somewhat better in short-beam strength compared with that of the rCF mat (non-woven mat used in **Laminate B**), which had a slightly poor short-beam strength. Additionally, regardless of the extra fibers in the form of the rCF mat, the UD CFRP with no mats (**Laminate A**) had a better flexural strength value than the UD CFRP with the rCF mat (**Laminate B**). The performance of the UD CFRP with no extra fibers (**Laminate A**) could be attributed to the better interfacial adhesions (short-beam strengths) [6.9% and 6.3%, respectively, better than the UD CFRP configurations with

0.0 wt.% sizing rCF mat and 0.0 wt.% sizing vAF mat (**Laminates B** and **C** respectively)]. When it comes to the performances of the UD CFRP with sized mats (**Laminates D**, **E**, **F**, **G**, and **H**) for their properties (flexural modulus, flexural strength, and short-beam strength), the argument becomes different because of the nature of the sizing agent (it is the same as coupling agents). Titanate coupling agents (TCAs) are organometallic catalysts often utilized in the polymer industry to invigorate polymeric composites by enhancing the affinity of the particles to the matrix. Their molecular formula (TCAs) is $XO-Ti-(OY)_3$. The $XO-$ is the alkoxy group interacting with an inorganic substrate, and the $-OY$ is the organofunctional fragment. The Y part has different groups reacting with thermosets [111]. The interaction increases the van der Waals' forces that enhance the fiber-matrix bonding, leading to improved interfacial adhesion and, subsequently, better mechanical properties. In a nutshell, the TCAs act like a molecular bridge that links the filler (non-woven mats) to the matrix (epoxy resin) [112] that ends up influencing the mechanical properties positively or negatively. The molecular bridge weakens or strengthens if the TCAs are too little or too much: an optimum quantity 'balances' the system, leading to better mechanical properties (as such has been the observations found in **Table 5.1**). Compared with the 0.0 wt. % sized rCF mats (non-woven mat used in **Laminate B**), increasing the sizing dosage from 0.5 wt. % to 3.0 wt. % for rCF mats (non-woven mat used in **Laminates D** and **H,** respectively) improved the flexural and short-beam strengths (see **Table 5.1**). All in all, since the flexural modulus is one of the most critical indicators in this project, the 1.5 wt. % (non-woven mat used in **Laminate F**) was selected and used to treat all the mats subsequently utilized in the project. For comparison purposes, a vAF mat was treated with the 1.5 wt. % (non-woven mat used in **Laminate G**) of the sizing agent. Compared with the 1.5 wt.% sized rCF mat (non-woven mat used in **Laminate F**), the vAF mat (non-woven

mat used in **Laminate G**) decreased by 0.3%, 5.8%, respectively, in flexural modulus and flexural strength; but increased by 0.5% in short-beam strength. The performance of the 1.5 wt.% sized single vAF mat (non-woven mat used in **Laminate G**) pegged against the 1.5 wt.% sized single rCF mat (non-woven mat used in **Laminate F**) is not surprising because regardless of the actual loss in mechanical properties (being it stiffness or strength) (Pimenta et al. [81] estimated that for typical rCFs recovered from the fluidized bed process, they would suffer between 25% and 50% decrement in tensile strength), per the stiffness of virgin T700SC and M46J which is 230 GPa and 436GPa respectively, the overall resultant stiffness for the rCF mat will be higher than that of the vAF mat (has a stiffness of 70.5GPa) with all things being equal.

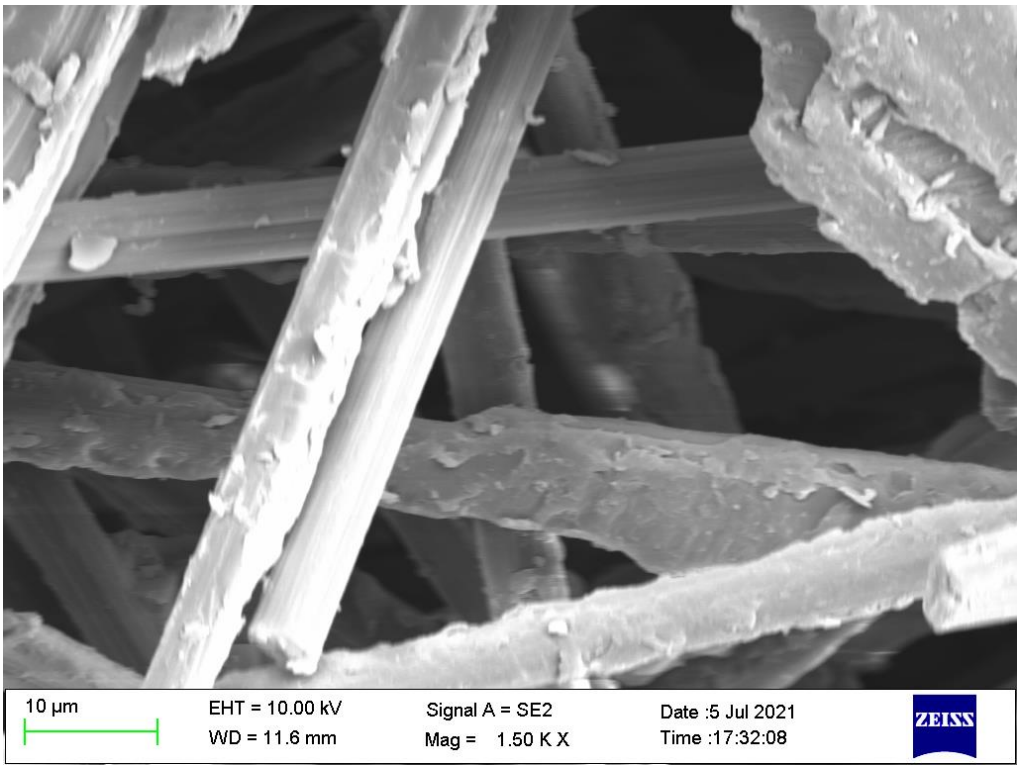

Figure 5.3. SEM images of the M46J rCFs.

In a nutshell, because carbon fibers have higher stiffness compared with that of vAFs, the CFRP configurations involving vAF mats that performed better than the configurations with rCFs (see **Table 5.1**) can be attributed to 1. the better positive

synergistic effect of the involving layers, 2. the resin residues found on some rCFs thereby reducing the performances of the rCFs because of the issue of resin compatibility (sizing was done as a result), 3. the moment of inertia generated with the slightly thicker single vAF mat configurations, and 4. the para structure of the vAFs. Using the flexural modulus values only, the control sample (**Laminate A**), UD CFRP with 1.5 wt.% sized rCF (same as UD CFRP with 1 rCF mat) (**Laminate F**), and UD CFRP with 1.5 wt.% sized vAF (same as UD CFRP with 1 vAF mat) (**Laminate G**) were selected for the quantifications of their damping capacities which is expressed as the figure of merit using DMA (see **Table 5.2**).

Table 5.1. Flexural properties and shear strength of the UD CFRP interleaved with non-woven mats composite laminates

Samples	**Flexural modulus, E_f /GPa**	**Flexural strength /MPa**	**Shear strength /MPa**	**Average thickness/mm**
Control (Laminate A)	125.1 ±3.1	1567.6 ±74.3	87.1 ±5.3	2.31
UD CFRP with 0.0 wt.% sized rCF mat (Laminate B)	135.3 ±5.1	1444.1 ±187.6	81.5 ±3.4	2.51
UD CFRP with 0.0 wt.% sized vAF mat (Laminate C)	140.1 ±3.3	1585.3 ±89.3	81.9 ±2.1	2.52

UD CFRP with 0.5 wt.% sized rCF mat (Laminate D)	141.8 ±6.5	1574.0 ±161.3	86.8 ±3.3	2.51
UD CFRP with 1.0 wt.% sized rCF mat (Laminate E)	135.8 ±5.3	1508.4 ±155.9	91.6 ±1.2	2.51
UD CFRP with 1.5 wt.% sized rCF (same as UD CFRP with 1 rCF mat) (Laminate F)	144.5 ±2.2	1671.7 ±157.9	88.1 ±3.3	2.51
UD CFRP with 1.5 wt.% sized vAF (same as UD CFRP with 1 vAF mat) (Laminate G)	144.1 ±2.4	1579.7 ±122.5	88.5 ±2.6	2.52
UD CFRP with 3.0 wt.% sized rCF mat (Laminate H)	140.0 ±1.8	1683.8 ±85.4	90.7 ±1.8	2.51

The damping capacities quantified as the figure of merit are dependent on the storage moduli and the loss factors, as seen in **Table 5.2**. The storage moduli and the loss factors are mutually exclusive parameters. **Figure 5.4** (a) and (b) are plots of the loss factor-temperature and storage modulus-temperature, respectively.

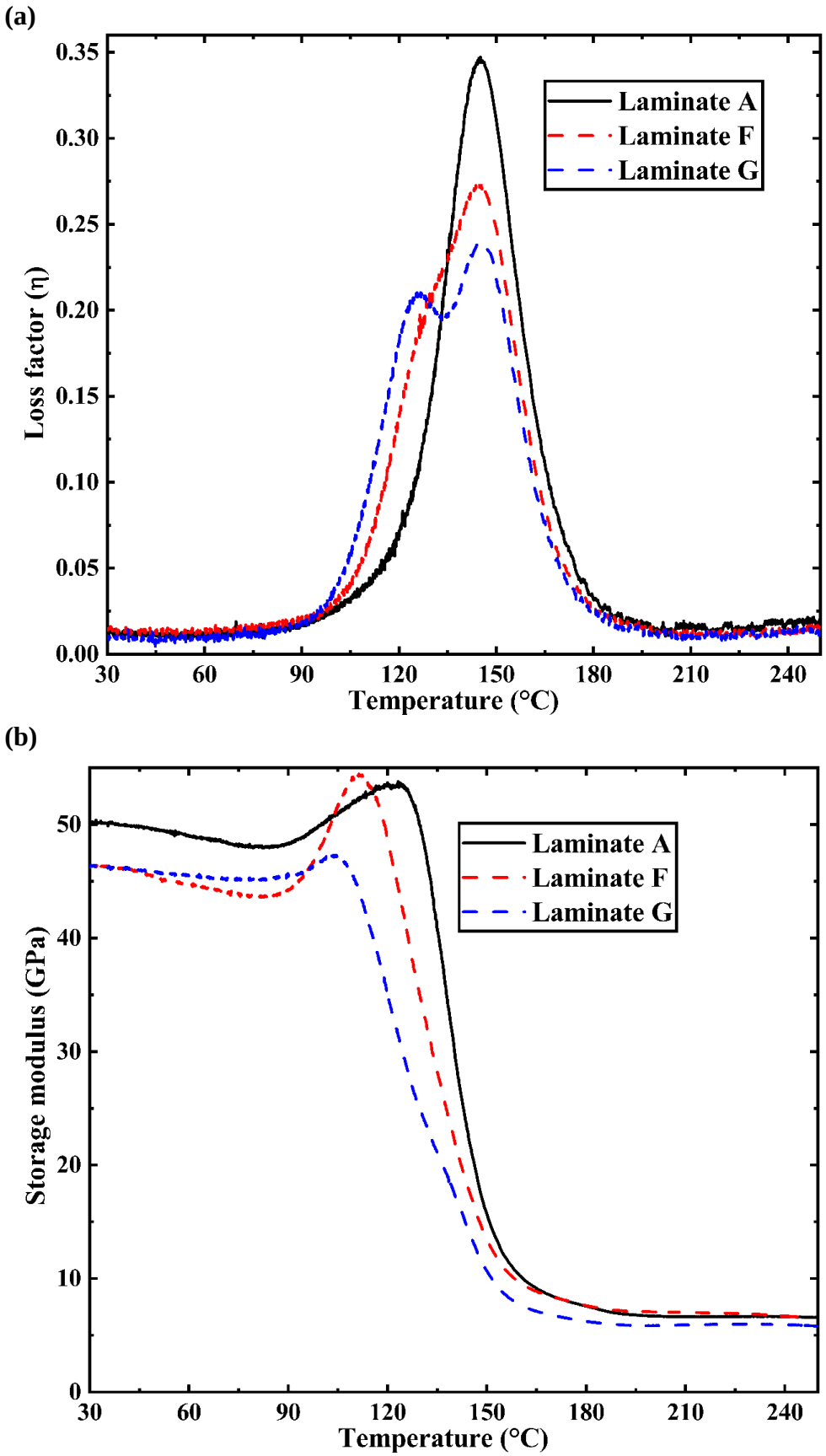

Figure 5.4. (a) Loss factor-temperature (b) storage modulus-temperature of the UD CFRP interleaved with non-woven mats composite laminates showing sizing effect.

Ordinarily, the following phases predominately exist for the DMA of polymer composites: glassy region, glass transition region, and rubbery plateau region [113]. Per the respective definitions using temperatures, regarding all the laminates under consideration (for all loss factor-temperature and storage modulus-temperature plots), the glassy, glass transition, and the rubbery plateau regions occur grossly between 30℃ to 124℃; 125℃ to 159℃; and 160℃ to 250℃ respectively. From **Figure 5.4** (a), primarily, the UD CFRP interleaved with 1.5 wt.% sized non-woven mats (both the rCF and the vAF) (**Laminates F** and **G** respectively) composite laminates had better damping abilities or had higher loss factor values compared with the control sample (**Laminate A**) at lower temperatures. Taking an approximate temperature of 65.1℃ for an example, the measured loss factor for the control sample, the UD CFRP with 1.5 wt.% sized rCF mat and vAF mat (**Laminates F** and **G** respectively) respectively, were 0.0094, 0.0143, and 0.0107. However, as the temperature increases towards the glass transition temperature (the peak of the tan delta-temperature curve) for the respective configurations, the control sample (**Laminate A**) performed better, as seen in **Table 5.2**.

Molecular relaxations in polymer composites have to do with the mobility of their molecules. For polymeric composites, beta transition/relaxation occurs in the glassy state, and in the glass transition region, the alpha transition/relaxation exists. Generally, for a plot of loss factor against temperature, the beta relaxation is not a clearly defined peak. The alpha relaxation, synonymous with the glass transition temperature, is primarily a well-defined peak [114]. In **Figure 5.4** (a), the UD CFRP with 1.5 wt.% sized vAF mat (**Laminate G**) had two peaks at the temperatures of 127.0℃ (loss factor at this temperature was 0.2105) (this possibly corresponds to the beta relaxations) and 144.5℃ (this corresponds to the glass transition temperatures). In a

nutshell, the beta-relaxation has to do with the localized atomic or molecular motion when the temperature increases (this corresponds to a secondary peak) before further increment in temperature causes a phase-shift that results in a primary peak called the glass transition temperature [115].

Additionally, composite materials are defined as a combination of two or more materials: they are not the same in their properties, but upon mixing, they usually bind with each other physically, chemically, physics-chemically, and mechanically [116]. "Binding" here does not mean "solving," but rather, it signifies overlapping between the two phases [116]. The phase could cause the system (the polymer composite laminate) to be unbalanced, resulting in phase separation. This phenomenon could also account for showing two peaks in **Figure 5.4** (a). Only the UD CFRP with the 1.5 wt.% sized vAF mat (Laminate G) had two peaks in the loss factor-temperature plot. The other configurations (**Laminates A and F**) had only single peaks corresponding to their glass transition temperatures, meaning they had balanced systems.

Table 5.2. DMA properties of the composite laminates under consideration

Samples	**Storage modulus, E′ @30℃/GPa**	**Loss factor, tan δ (η) @30℃**	**Loss factor, tan δ (η) @T_g**	**Glass transition temperature, T_g/℃**	**Figure of merit (ηE′)/ GPa**
Control (Laminate A)	50.23	0.0118	0.3472	145.1	0.59
UD CFRP with 1.5 wt.% sized	46.40	0.0146	0.2733	144.8	0.68

rCF (same as UD CFRP with 1 rCF mat) (Laminate F)					
UD CFRP with 1.5 wt.% sized vAF (same as UD CFRP with 1 vAF mat) (Laminate G)	46.42	0.0090	0.2403	144.5	0.42

Damping (loss factor) in composites is generally induced by different factors such as the viscoelastic nature of the matrix and the fiber materials, the fiber-matrix interface, etc. [117]. In this section, the damping performance of the UD CFRP with no mats (control sample, **Laminate A**) @30℃ and the glass transition temperature can be attributed to either or all the factors above by Berthelot et al. [117]. For example, incorporating a non-woven mat into the UD CFRP will probably increase the interphase friction that can limit the movement of the molecular chain structure of the epoxy resin. This can subsequently restrict the ability of the laminate with the mats to dissipate energy (damping) efficiently at higher temperatures, as observed in **Table 5.2** (see **loss factor (η) @T_g**). Aramid fibers are considered polymeric fibers that exhibit viscoelastic behaviors [118]. At the fiber-matrix interface of the UD CFRP with the vAF mat, both (the vAF and the matrix) behave as viscoelastic material [119]. Viscoelastic materials (they can store and dissipate mechanical energy simultaneously) have been used for increased damping performance in structures for a very long time. These materials have long molecular chains that offer a combination of elasticity and viscosity [120]. Under

loading, there is deformation; the damping occurs from the recovery of these chains after deformation [120]. This unique characteristic of the aramid fibers (viscoelastic nature) gives them inherent damping abilities. However, regardless of their intrinsic damping abilities, the UD CFRP with vAF mats (**Laminate G**) could not outperform those with the rCF mats (**Laminate F**) because, from Crema et al. [119], damping is related to Young's modulus. The rCFs irrespective of their slight decrement in mechanical properties, are expected to have a higher Young's modulus than those of the vAFs. Storage modulus measures the amount of energy stored or absorbed. It (storage modulus) is a function of the fiber contents (see **eq 5.1**); hence, incorporating the non-woven mats was expected to result in comparatively higher storage modulus values, but that was not the observation at lower temperatures. From **Table 5.2**, for example, @30℃, the control sample (**Laminate A**) had the best storage modulus value of 50.23 GPa, whiles the UD CFRP with the 1.5 wt.% sized rCF mat (**Laminate F**) and 1.5 wt.% sized vAF mat (**Laminate G**) had an almost storage modulus value in GPa of 46.40 and 46.42 respectively. All things being equal, it appears that the possible explanation for the storage modulus @30℃ for the laminates under consideration in this section (**Laminates A**, **F**, and **G**) could be the differences in their void contents. Furthermore, from **Figure 5.4** (b), the UD CFRP with the 1.5 wt.% sized rCF mat (**Laminate F**) had its largest storage modulus of 54.44 GPa at 111.3℃ whiles the control sample (**Laminate A**) had its biggest storage modulus of 53.78 GPa at 123.2℃. The UD CFRP with the 1.5 wt.% sized vAF mat (**Laminate G**) had its biggest storage modulus of 47.35 GPa at 103.1℃.

Generally, the storage modulus gradually decreases from the glassy region as the temperature increases for the storage modulus-temperature plot. With a further increment in temperature, there is a phase shift from the glassy area to the glass

transition region: a sudden loss of stiffness causes a significant drop in the storage modulus. Further increment in the temperature results in a rubbery plateau region where the storage modulus is somewhat constant (although it gradually decreases with increasing temperature). In the glassy part, there is little mobility in the molecular chains of the polymer composites [121], thereby creating avenues for the participating fiber reinforcements to reinforce themselves for a while until the temperatures get high enough for a phase-shift to occur; then, there will be a considerable drop in the value of the storage modulus as seen in **Figure 5.4** (b). A similar storage modulus pattern (although not as prominent as in this project) was observed for the prototype 1 sample in Fig.3 of Bosze et al.'s [122] investigation into the high-temperature strength and storage modulus in unidirectional hybrid composites. Bosze et al. [122] stated that for engineering purposes, the useful operating range of a thermoset epoxy is the range over which the storage modulus is nearly constant; hence considering the behavior of their prototype 1, the valuable range was where the storage modulus begins to decrease very steeply. Consequently, the useful storage modulus range for the UD CFRP with no mats (**Laminate A**), 1.5 wt.% sized rCF mat (**Laminate F**), and 1.5 wt.% sized vAF mat (**Laminate G**) are temperatures up to 123.2℃, 111.3℃ and 103.1℃ respectively.

5.2 EFFECTS OF THE INTERLEAVED RCFS MAT'S NUMBERS AND LOCATION/POSITION

After finding the appropriate sizing wt.% to be 1.5 wt.%, all mats used to study the effect of the interleaved rCFs mat's numbers and location/position were sized with the 1.5 wt.%. Found in **Table 5.3** are the flexural moduli of the composite laminates under consideration here. For the effect of the number of rCF mats, from **Table 5.3**, the flexural modulus decreased from 144.5 GPa for UD CFRP with one rCF mat to 128.9

GPa for the configuration with 3 rCF mats. A further decrement from 128.9 GPa to 105.8 GPa was seen when rCF mats were increased to 5. The UD CFRPs with single mats can be considered as “classic” sandwich materials, and under dynamic loading, they depend on their skins, core structure, and skin-core interfaces [123]. As explained in the preceding section, the core structure has the essential function of generating a moment of inertia that results in higher mechanical properties. The experimental results from Foo et al. [124] showed that the face-sheet (skin) thickness played a significant role in the mechanical properties of the sandwich panels under investigation. As the number of rCF mats increases, the skin thickness reduces [see **Figure 3.7** (b), (d), and (h)] (regarding the classical definition of a sandwich structure, as the number of mats increases, the configurations act like a combination of several sandwich structures with decreasing skin thicknesses), resulting in lower flexural moduli.

Now that it has been established that using one rCF mat will suffice, from the perspectives of hybridizations, it will be interesting to see the effect of the rCF mats when interleaved with the short virgin aramid fibers' mat (vAF mat). Furthermore, from **Table 5.3**, sandwiching one vAF mat between two rCF mats produced a flexural modulus of 133.4 GPa, but with the reverse, the flexural modulus decreased to 121.7 GPa. Doubling the rCF mats from two to four and inserting a single vAF mat in-between did not improve the flexural modulus; instead, it further decreased to 113.9 GPa. This observation concerns the positive hybridization of the involving fibers: the positive hybridization weakened with more vAF mats. To quantify the damping capacities of the laminates under consideration here, the figure of merit must be employed, as in the case of the preceding section. As done in **section 5.1**, DMA tests for selected samples were conducted, and tabulated in **Table 5.4** are the DMA properties of the composite laminates showing the effects of the factors under consideration here. **Figure 5.5** (a)

and (b) are the loss factor-temperature plots showing the results of the interleaved rCF mat numbers and their location/position effect, respectively.

Table 5.3. Flexural moduli of the composite laminates under consideration here

Samples	**Flexural modulus, E_f /GPa**	**Average thickness/mm**
Control [Laminate A]	125.1 ±3.1	2.31
UD CFRP interleaved with 1.5 wt.% sized rCF (same as UD CFRP with 1 rCF mat) [Laminate F]	144.5 ±2.2	2.51
UD CFRP interleaved with 1.5 wt.% sized vAF (same as UD CFRP with 1 vAF mat) [Laminate G]	144.1 ±2.4	2.52
UD CFRP interleaved with 3 rCF mats [Laminate I]	128.9 ±1.5	2.91
UD CFRP interleaved with 3 vAF mats [Laminate J]	125.4 ±2.0	2.94
UD CFRP interleaved with 5 rCF mats [Laminate K]	105.8 ±2.7	3.31

UD CFRP interleaved with (2 rCF + 1 vAF) mats [Laminate L]	133.4 ±3.0	2.92	
UD CFRP interleaved with (1 rCF + 2 vAF) mats [Laminate M]	121.7 ±0.6	2.93	
UD CFRP interleaved with (4 rCF + 1 vAF) mats [Laminate N]	113.9 ±1.1	3.32	

Table 5.4. DMA properties of the composite laminates showing the effects of the factors under consideration

Samples	**Storage modulus, E′ @30℃/GPa**	**Loss factor, tan δ (η) @30℃**	**Loss factor, tan δ (η) @T_g**	**Glass transition temperature, T_g/℃**	**Figure of merit (ηE′)/ GPa**
Control (Laminate A)	50.23	0.0118	0.3472	145.1	0.59
UD CFRP interleaved with 1.5 wt.% sized rCF (same as UD CFRP interleaved with	46.40	0.0146	0.2733	144.8	0.68

1 rCF mat) (Laminate F)					
UD CFRP interleaved with 1.5 wt.% sized vAF (same as UD CFRP interleaved with 1 vAF mat) (Laminate G)	46.42	0.0090	0.2403	144.5	0.42
UD CFRP interleaved with 3 rCF mats (Laminate I)	33.71	0.0149	0.3267	140.5	0.50
UD CFRP interleaved with 3 vAF mats (Laminate J)	36.48	0.0149	0.3465	139.3	0.54
UD CFRP interleaved with 5 rCF mats (Laminate K)	29.39	0.0177	0.3572	141.4	0.52

UD CFRP interleaved with (2 rCF + 1 vAF) mats (Laminate L)	38.44	0.0190	0.2962	139.0	0.73

As shown in **Table 5.4**, the figure of merit is a function of the loss factors and the storage moduli. Each interleaved mat was sandwiched between two resin films before being used; hence 3 and 5 interleaved mats, respectively, mean 6 and 10 resin films being introduced into the composite laminate. This ensures that all things are equal; there will be no resin starvations in the manufactured laminate. From Ni et al. [40], the addition of the resin films will result in resin-rich zones that could consume some vibration energy through friction between the molecular chains of the epoxy and the interfaces.

From **Table 5.4** and seen in **Figure 5.5** (a) @30℃, the incorporation of more rCF mats increased the loss factors: UD CFRP interleaved with 1.5 wt.% sized rCF (same as UD CFRP interleaved with 1 rCF mat) (**Laminate F**), UD CFRP interleaved with 3 rCF mats (**Laminate I**), and UD CFRP interleaved with 5 rCF mats (**Laminate K**) had loss factors of 0.0146, 0.0149, and 0.0177 respectively. The resin-rich zones gradually increased with an increasing number of the rCF mats, resulting in the gradual increase of loss factors of the composite laminates. Hence, the UD CFRP interleaved with 5 rCF mats (**Laminate K**) having the highest loss factor. Additionally, these increments can further be explained with **eq 5.1** [125]:

$$\tan\delta = \eta = \frac{E''}{E'} = \frac{\text{loss modulus (generally a function of resin contents)}}{\text{storage/elastic(generally a function of fiber contents)}} \quad 5.1$$

where tanδ and η are the same, which is the loss factor. As seen in **eq 5.1**, E″ is directly proportional to the loss factor (tanδ); hence generally, a higher loss factor and E″ means appreciable values of resin contents. The lowest (0.0090) and highest (0.0190) loss factors measured were for the UD CFRP interleaved with 1.5 wt.% sized vAF (same as UD CFRP interleaved with 1 vAF mat) (**Laminate G**) and UD CFRP interleaved with (2 rCF + 1 vAF) mats (**Laminate L**), respectively. As already shown above, the UD CFRP interleaved with 1.5 wt.% sized vAF (same as UD CFRP interleaved with 1 vAF mat) (**Laminate G**) was not as competitive as the UD CFRP interleaved with 1.5 wt.% sized rCF (same as UD CFRP interleaved with 1 rCF mat) (**Laminate F**), but since vAFs have inherently good damping properties, combining the vAF and rCF mats should yield a competitive configuration which was precisely the observation as shown in **Table 5.4** (see the loss factor at @30℃ for **Laminate L**).

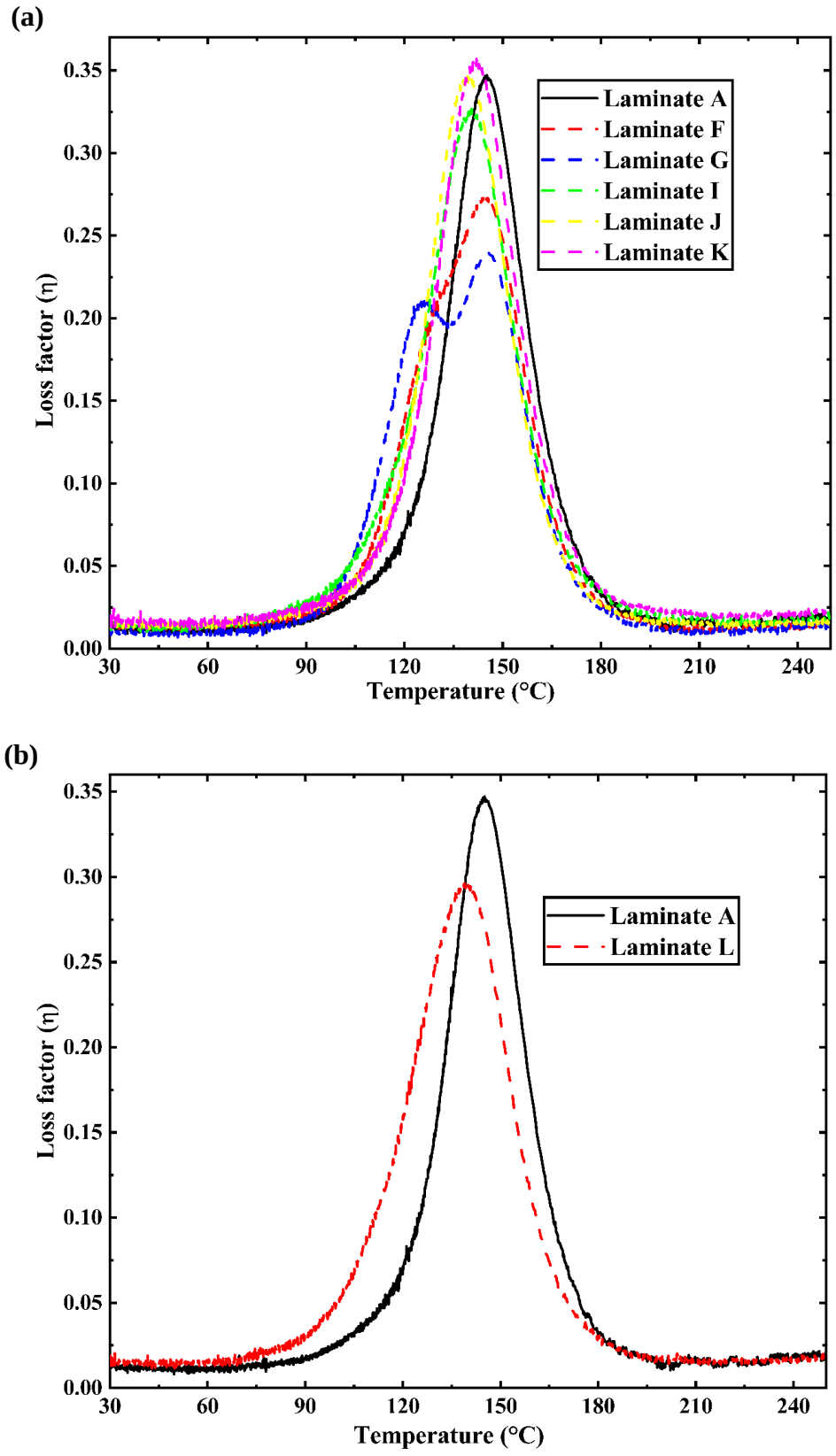

Figure 5.5. (a) Loss factor-temperature plot showing the effects of the interleaved rCF mat's numbers (b) loss factor-temperature plot for the interleaved rCF mat's location/position.

About **Figure 5.5** (a), at higher temperatures, in terms of loss factors, the UD CFRP interleaved with 5 rCF mats (**Laminate K**) performed very well compared with all configurations inclusive of the control sample (**Laminate A**) (in the study of the other factors in the preceding sections such was not the case for the competing configurations: the control sample had high loss factor at high temperature). The most significant recorded loss factor at the glass transition temperature (0.3572) was the UD CFRP interleaved with 5 rCF mats (**Laminate K**). Also, regarding **Figure 5.5** (b), the loss factor performance of the UD CFRP interleaved with (2 rCF + 1 vAF) mats (**Laminate L**) compared to the control sample (**Laminate A**) was remarkable at lower temperatures. From **Table 5.4**, an increment in the number of rCF mats for the storage modulus resulted in a decrement in the storage modulus @30℃. The storage modulus @30℃ for the UD CFRP interleaved with 1.5 wt.% sized rCF (same as UD CFRP interleaved with 1 rCF mat) (**Laminate F**), UD CFRP interleaved with 3 rCF mats (**Laminate I**), and UD CFRP interleaved with 5 rCF mats (**Laminate K**) respectively are 46.40 GPa, 33.71 GPa, and 29.39 GPa. The reasoning for this trend has the explanations as the trend observed for the flexural moduli in **Table 5.4** in the preceding sections. A decrement was also observed when the UD CFRP interleaved with 1.5 wt.% sized vAF (same as UD CFRP interleaved with 1 vAF mat) (**Laminate G**) was increased to UD CFRP interleaved with 3 vAF mats (**Laminate J**): from 46.42 GPa for the UD CFRP interleaved with 1.5 wt.% sized vAF (same as UD CFRP interleaved with 1 vAF mat) (**Laminate G**) to 36.48 GPa for the UD CFRP interleaved with 3 vAF mats (**Laminate J**). Regarding the UD CFRP interleaved with (2 rCF + 1 vAF) mats (**Laminate L**), its measured storage modulus was very competitive (although not the highest among the lot) because its recorded loss factor @30℃ was the highest among the lot. These performances resulted in a very competitive figure of merit. **Figure 5.6**

further depicts the trend established in **Table 5.4** to effectively show the interleaved rCFs mat's numbers and location/position effects.

(a)

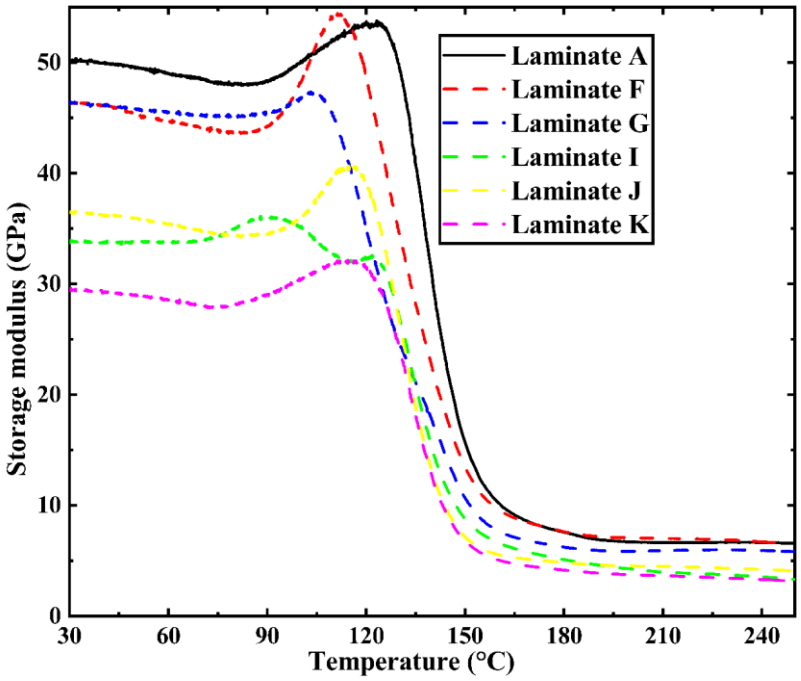

(b)

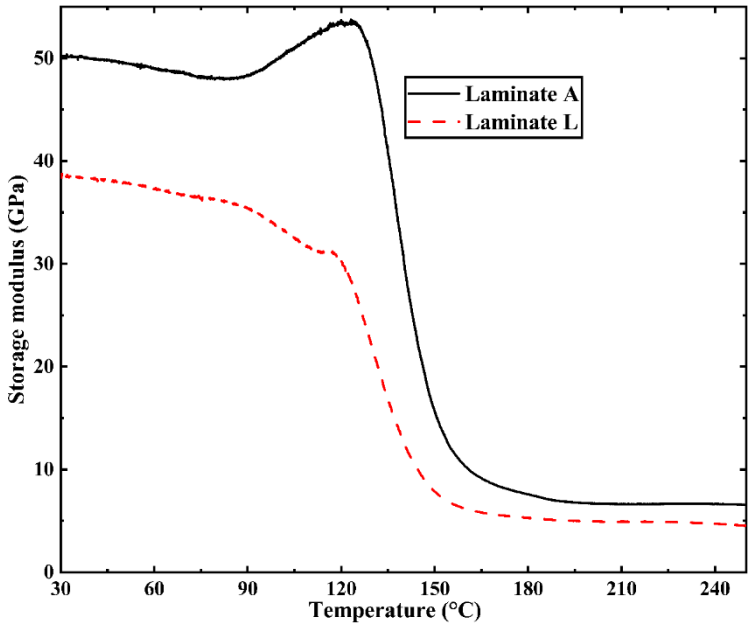

Figure 5.6. (a) Storage modulus-temperature plot showing the effects of the interleaved rCF mat's numbers (b) storage modulus-temperature plot for the interleaved rCF mat's location/position.

5.3 Effects of Recycled Carbon Fibers' Lengths and Their Combinations

Table 5.5 shows the influence of the recycled carbon fibers' lengths and their combinations; recycled carbon fibers' types; and micro-hybridization with short virgin aramid fibers. The effect of the rCFs' fiber lengths was studied using the UD CFRP interleaved with T700 (3mm) mat [**Laminate O**]; UD CFRP interleaved with T700 (6mm) mat [**Laminate Q**], and UD CFRP interleaved with T700 (12mm) mat [**Laminate R**]. From **Table 5.5**, it was observed that an increment in the fiber length from 3 mm to 6 mm (UD CFRP interleaved with T700 (3mm) mat [**Laminate O**], and UD CFRP interleaved with T700 (6mm) mat [**Laminate Q**] respectively) resulted in an increment in the flexural modulus (from 131.0 GPa to 140.2 GPa).

Table 5.5. Flexural moduli and loss factors of all the composite laminates under consideration

Samples	**Flexural modulus, E_f /GPa**	**Loss factor, tan δ (η) @25℃**	**Figure of merit (ηE_f)/ GPa**
Control [Laminate A]	125.1 ±3.1	0.0063	0.788 ±0.02
UD CFRP interleaved with 1.5 wt.% sized rCF (same as UD CFRP interleaved with 1 rCF mat) [same as UD CFRP interleaved with (T700 +	144.5 ±2.2	0.0062	0.896 ±0.01

M46J) (3mm + 3mm) mat] [same as UD CFRP interleaved with (T700 + M46J + vAF) (75% + 25% + 0%) mat] [Laminate F]			
UD CFRP interleaved with T700 (3mm) mat [Laminate O]	131.0 ±2.8	0.0059	0.773 ±0.02
UD CFRP interleaved with (T700 + T800) (3mm + 3mm) mat [Laminate P]	137.3 ±2.8	0.0062	0.851 ±0.02
UD CFRP interleaved with T700 (6mm) mat [Laminate Q]	140.2 ±4.4	0.0078	1.094 ±0.03
UD CFRP interleaved with T700 (12mm) mat [Laminate R]	142.8 ±9.3	0.0045	0.643 ±0.04
UD CFRP interleaved with (T700 + M46J) (6mm + 6mm) mat [Laminate S]	135.6 ±3.3	0.0091	1.234 ±0.03

UD CFRP interleaved with (T700 + M46J) (3mm + 6mm) mat [Laminate T]	135.4 ±0.8	0.0092	1.246 ±0.01
UD CFRP interleaved with (T700 + M46J) (6mm + 3mm) [Laminate U]	132.6 ±1.8	0.0084	1.114 ±0.02
UD CFRP interleaved with (T700 + M46J + vAF) (50% + 25% + 25%) mat [Laminate V]	135.4 ±1.8	0.0065	0.880 ±0.01
UD CFRP interleaved with (T700 + M46J + vAF) (25% + 25% + 50%) mat [Laminate W]	138.3 ±2.4	0.0043	0.595 ±0.01

A further increment in the fiber length from 6 mm to 12 mm (UD CFRP interleaved with T700 (6mm) mat [**Laminate Q**] and UD CFRP interleaved with T700 (12mm) mat [**Laminate R**] respectively) further resulted in the increment of the flexural modulus: increment from 140.2 GPa to 142.8 GPa. These observations can be attributed to the interactions between fiber-fiber and fiber-matrix (epoxy resin). In the works of Li et al. [126], wherein the effects of fiber volume fraction, fiber length, and fiber orientation on the mechanical performances of short fiber-reinforced composite materials were investigated, it was concluded that the fiber length played a prominent role in achieving higher mechanical performances compared with the other investigated factors: when

the fiber length was increased from 2.5 mm to 10 mm, the elastic modulus increased by 123.9 %. Furthermore, the reason ascribed to such an observation was that as the fiber length increases, the number of fiber bundles in the matrix would decrease; the longer fiber lengths could bear higher loads than the shorter fiber lengths.

The increment in fiber length that resulted in an increment in the elastic modulus was well in line with existing literature [127]. To investigate the effect of the fiber lengths on the damping capacities, a look at the figure of merit must be taken. From **Table 5.5**, the figure of merit was increased when the fiber length was increased from 3 mm to 6 mm (from 0.773 GPa to 1.094 GPa) (UD CFRP interleaved with T700 (3mm) mat [**Laminate O**], and UD CFRP interleaved with T700 (6mm) mat [**Laminate Q**] respectively). A further increment in fiber length from 6 mm to 12 mm resulted in a decrement in the figure of merit (from 1.094 GPa to 0.643 GPa) (UD CFRP interleaved with T700 (6mm) mat [**Laminate Q**] and UD CFRP interleaved with T700 (12mm) mat [**Laminate R**] respectively). These observed variations are synonymous with the interpretations by the loss factors: it increased from 0.0059 to 0.0078 when the fiber length increased from 3 mm to 6 mm (UD CFRP interleaved with T700 (3mm) mat [**Laminate O**] and UD CFRP interleaved with T700 (6mm) mat [**Laminate Q**] respectively) and decreased from 0.0078 to 0.0045 when the fiber length was increased from 6 mm to 12 mm (UD CFRP interleaved with T700 (6mm) mat [**Laminate Q**] and UD CFRP interleaved with T700 (12mm) mat [**Laminate R**] respectively). This behavior can be explained by the fact that the fibers are randomly distributed in the matrix in short fiber-reinforced composites. Therefore, there is an interaction between the fibers and the matrix (resin); the shorter the fiber lengths, the more influential the interactions. Moreover, since the loss factor is generally a matrix function, the more meaningful the interactions (meaningful interactions here mean that the fibers are well

randomly distributed without many spaces being spared by either the fibers or the matrix), the better the loss factor values.

A few lengths were combined to further study the fiber lengths' effect. The samples used were UD CFRP interleaved with 1.5 wt.% sized rCF (same as UD CFRP interleaved with 1 rCF mat) [same as UD CFRP interleaved with (T700 + M46J) (3mm + 3mm) mat] [same as UD CFRP interleaved with (T700 + M46J + vAF) (75% + 25% + 0%) mat] [**Laminate F**]; UD CFRP interleaved with (T700 + M46J) (6mm + 6mm) mat [**Laminate S**]; UD CFRP interleaved with (T700 + M46J) (3mm + 6mm) mat [**Laminate T**]; and UD CFRP interleaved with (T700 + M46J) (6mm + 3mm) [**Laminate U**]. From **Table 5.5**, the UD CFRP configuration with D, E, F, and G mats had a flexural modulus of 144.5 GPa, 135.6 GPa, 135.4 GPa, and 132.6 GPa: that is a decreasing trend. But the loss factors were 0.0062, 0.0091, 0.0092, 0.0084 respectively for the UD CFRP interleaved with 1.5 wt.% sized rCF (same as UD CFRP interleaved with 1 rCF mat) [same as UD CFRP interleaved with (T700 + M46J) (3mm + 3mm) mat] [same as UD CFRP interleaved with (T700 + M46J + vAF) (75% + 25% + 0%) mat] [**Laminate F**]; UD CFRP interleaved with (T700 + M46J) (6mm + 6mm) mat [**Laminate S**]; UD CFRP interleaved with (T700 + M46J) (3mm + 6mm) mat [**Laminate T**]; and UD CFRP interleaved with (T700 + M46J) (6mm + 3mm) [**Laminate U**] (that is, it increased up to the UD CFRP interleaved with (T700 + M46J) (3mm + 6mm) mat [**Laminate T**] and decreased for the UD CFRP interleaved with (T700 + M46J) (6mm + 3mm) [**Laminate U**]). The variations observed for the various configurations in terms of their flexural moduli and loss factors can be explained by the fact that there is an optimum operating fiber length for short fiber reinforcements (critical fiber length).

Regarding the figure of merit, the same trend as the trend established by the loss factors was observed for the various configurations. The figure of merit increased from 0.896 GPa to 1.234 GPa for the UD CFRP interleaved with 1.5 wt.% sized rCF (same as UD CFRP interleaved with 1 rCF mat) [same as UD CFRP interleaved with (T700 + M46J) (3mm + 3mm) mat] [same as UD CFRP interleaved with (T700 + M46J + vAF) (75% + 25% + 0%) mat] [**Laminate F**]; and UD CFRP interleaved with (T700 + M46J) (6mm + 6mm) mat [**Laminate S**] respectively. With the combination of the 3 mm length of T700 and the 6 mm length of M46J, the figure of merit increased further to 1.246 GPa (UD CFRP interleaved with (T700 + M46J) (3mm + 6mm) mat [**Laminate T**]). However, there was a decrement in the figure of merit (1.114 GPa) when the 6 mm fiber length of T700 was combined with the 3 mm fiber length of M46J (UD CFRP interleaved with (T700 + M46J) (6mm + 3mm) [**Laminate U**]). All the variations in the figure of merit can be seen in **Figure 5.7** (a) and **Figure 5.7** (b) [**Figure 5.7** (a) Figure of merit showing the effect of the recycled carbon fibers' lengths and **Figure 5.7** (b) figure of merit showing the effect of the combinations of the recycled carbon fibers' lengths]. These observed variations are in line with existing literature, where it was observed that the mechanical and vibration (DMA) properties depended on their fiber lengths. Specifically, from the works of Capela et al. [60], wherein there was an investigation into the effects of fiber length on tensile and DMA properties of low content of short fiber-reinforced composites and noted in the conclusions that the stiffness and the tensile strength increased in the order of 25% when the fiber length increased from 2 mm to 4 mm, but afterward tends to decrease for the 6 mm fiber length composites. Also, the DMA elastic modulus increased when fiber length increased from 2 mm to 4 mm, and still increased slightly when fiber length increased from 4 mm to 6 mm.

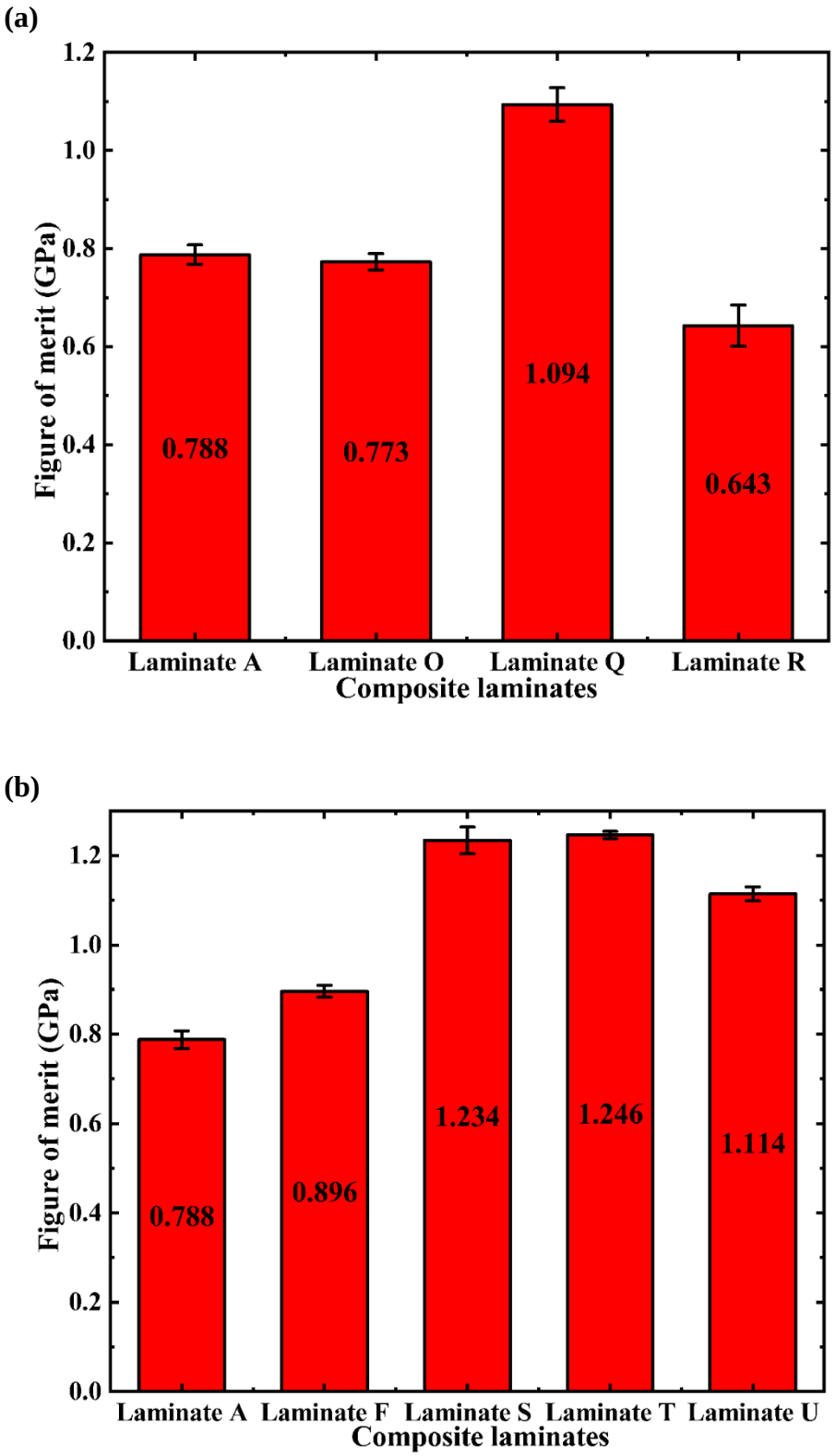

Figure 5.7. (a) Figure of merit showing the effect of the recycled carbon fibers' lengths and (b) figure of merit showing the effect of the combinations of the recycled carbon fibers' lengths respectively plots. The error bars show the standard deviation values.

Some composite laminates were chosen for DMA testing. In addition to the control sample (**Laminate A**), the UD CFRP interleaved with T700 (3mm) mat [**Laminate O**]; and UD CFRP interleaved with T700 (6mm) mat [**Laminate Q**] were chosen to study the effect of recycled carbon fibers' lengths. And the UD CFRP interleaved with 1.5 wt.% sized rCF (same as UD CFRP interleaved with 1 rCF mat) [same as UD CFRP interleaved with (T700 + M46J) (3mm + 3mm) mat] [same as UD CFRP interleaved with (T700 + M46J + vAF) (75% + 25% + 0%) mat] [**Laminate F**]; and UD CFRP interleaved with (T700 + M46J) (3mm + 6mm) mat [**Laminate T**] were chosen to study the effect of the fiber length combinations. **Figure 5.8** shows the loss factor-temperature plots. The loss factors are low at low temperatures, then rise to a maximum in the transition zone (around 145℃) before reducing somewhat at high temperatures.

The rise occurs because of sliding between molecules, which generates a frictional loss, which increases with increasing temperature. At the highest temperatures, the friction forces reduce, reducing the loss factor despite a high amount of sliding. The peak of **Figure 5.8** is the glass transition temperature; hence it can be said to demonstrate the matrix's transition zone (about 135℃ to 175℃), which exhibits a considerable rise in loss factor. **Figure 5.9** shows the storage modulus-temperature plots. Superimposing **Figure 5.8** and **Figure 5.9**, it can be said that the change in the behavior of the graphs with increasing temperatures is because of the dynamics of the molecular rearrangements that govern the relaxation behavior (due to the relaxation phenomena during the glass transition). A progressive drop follows the glass transition phase in the storage modulus.

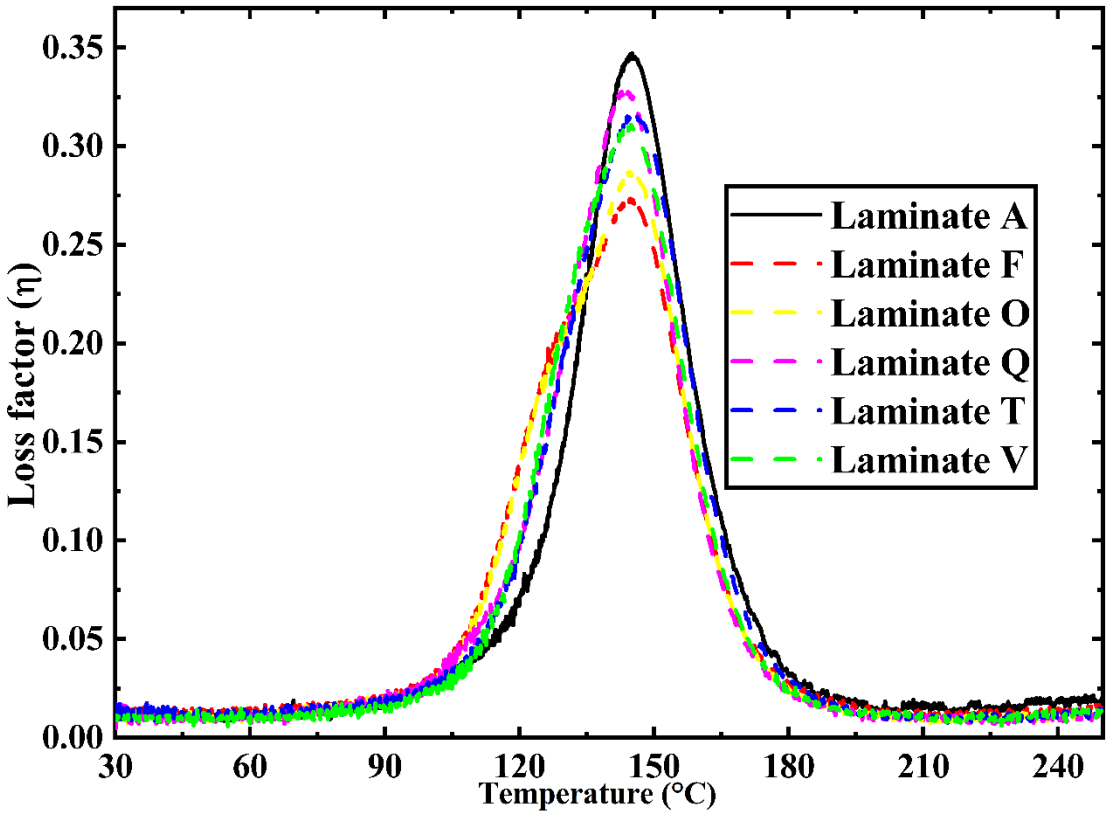

Figure 5.8. Loss factor-temperature plot showing the effect of the fiber lengths, the effect of the combination of fiber lengths, the effects of the recycled carbon fibers' types, and the effects of the recycled carbon fibers' micro-hybridization with short virgin aramid fibers.

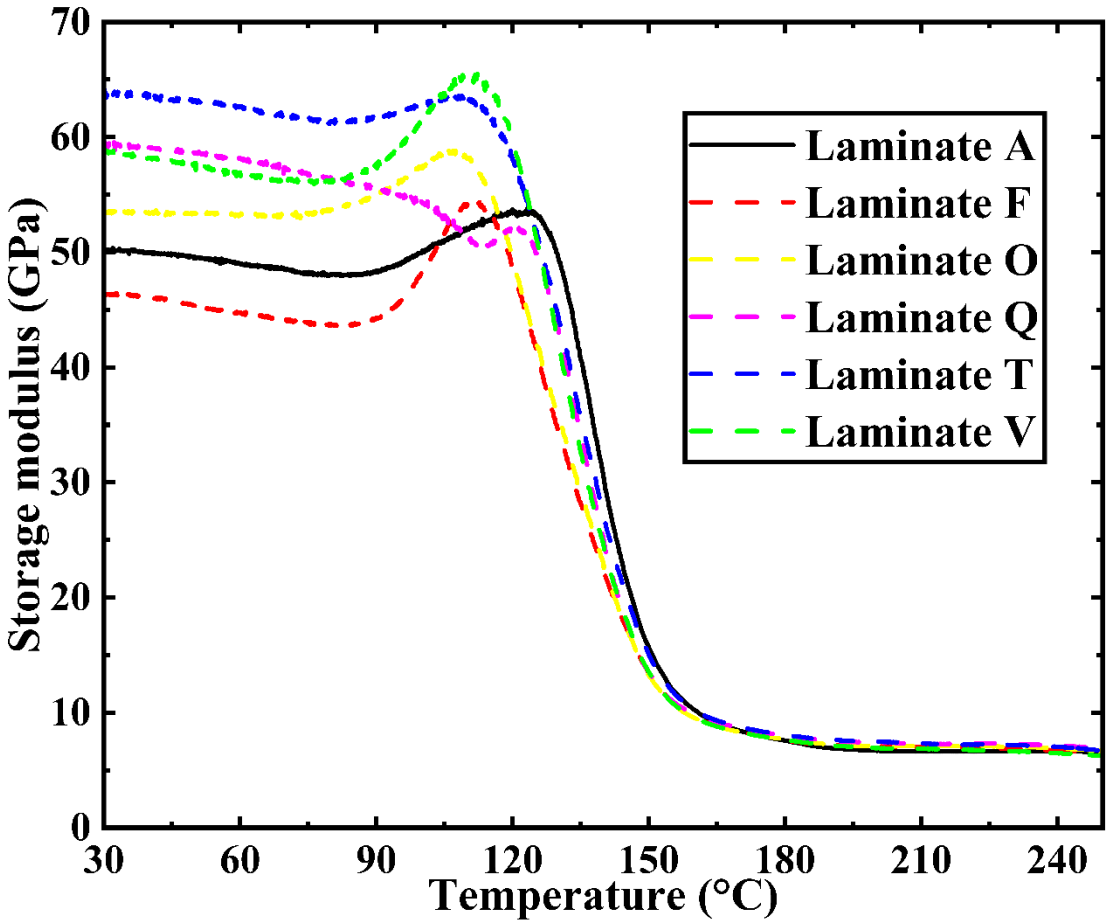

Figure 5.9. (a) Storage modulus-temperature plot showing the effect of the fiber lengths, the effect of the combination of fiber lengths, the effects of the recycled carbon fibers' types, and the effects of the recycled carbon fibers' micro-hybridization with short virgin aramid fibers.

Also, **Figure 5.6** shows the DMA properties. From **Table 5.6**, at 30℃, concerning the effect of the rCFs' lengths, compared with the control sample (**Laminate A**), the UD CFRP interleaved with T700 (6mm) mat [**Laminate Q**] increased the loss factor from 0.0118 to 0.0132; there was a corresponding increment in the storage modulus as well (from 50.23 GPa to 59.43 GPa). At 30℃, compared with the control sample (**Laminate A**), the UD CFRP interleaved with T700 (3mm)

mat [**Laminate O**] decreased in loss factor (to 0.0105 from 0.0118), but for the storage modulus, there was an increment from 50.23 GPa to 53.45 GPa.

Table 5.6. DMA properties of the composite laminates showing the effects of the factors under considerations

Samples	**Storage modulus, E′ @30℃/GPa**	**Loss factor, tan δ (η) @30℃**	**Loss factor, tan δ (η) @T_g**	**Glass transition temperature, T_g/℃**	**Figure of merit (ηE′)/ GPa**
Control (Laminate A)	50.23	0.0118	0.3472	145.1	0.59
UD CFRP interleaved with 1.5 wt.% sized rCF (same as UD CFRP interleaved with 1 rCF mat) [same as UD CFRP interleaved with (T700 + M46J) (3mm + 3mm) mat] [same as UD CFRP interleaved with (T700 + M46J +	46.40	0.0146	0.2733	144.8	0.68

vAF) (75% + 25% + 0%) mat] [Laminate F]					
UD CFRP interleaved with T700 (3mm) mat [Laminate O]	53.45	0.0105	0.2871	145.4	0.56
UD CFRP interleaved with T700 (6mm) mat [Laminate Q]	59.43	0.0132	0.3292	143.1	0.78
UD CFRP interleaved with (T700 + M46J) (3mm + 6mm) mat [Laminate T]	63.72	0.0143	0.3170	146.2	0.91
UD CFRP interleaved with (T700 + M46J + vAF) (50% + 25% + 25%) mat [Laminate V]	58.75	0.0110	0.3110	144.9	0.65

Regarding the effect of fiber length combinations, from **Table 5.6**, the combination of 3 mm of T700 and 3 mm of M46J (UD CFRP interleaved with 1.5 wt.% sized rCF (same as UD CFRP interleaved with 1 rCF mat) [same as UD CFRP interleaved with (T700 +

M46J) (3mm + 3mm) mat] [same as UD CFRP interleaved with (T700 + M46J + vAF) (75% + 25% + 0%) mat] [**Laminate F**]) resulted in the improvement of the loss factor: compared with the control sample (**Laminate A**), 23.7% improvement; and compared with the UD CFRP interleaved with T700 (3mm) mat [**Laminate O**], 39.0% improvement. Regarding the storage modulus, a decrement was observed when the 3 mm of T700 and 3 mm of M46J were combined (UD CFRP interleaved with 1.5 wt.% sized rCF (same as UD CFRP interleaved with 1 rCF mat) [same as UD CFRP interleaved with (T700 + M46J) (3mm + 3mm) mat] [same as UD CFRP interleaved with (T700 + M46J + vAF) (75% + 25% + 0%) mat] [**Laminate F**]): compared with the control sample (**Laminate A**), 8.3 % decrement; and compared with the UD CFRP interleaved with T700 (3mm) mat [**Laminate O**], 15.2 % decrement. Maintaining the 3 mm of T700 and increasing the length of the M46J to 6 mm (that is, UD CFRP interleaved with (T700 + M46J) (3mm + 6mm) mat [**Laminate T**]) results in improvements in both the storage modulus and loss factor when compared with the control sample (**Laminate A**). For example, there was a 26.9% and 21.2% improvement in the storage modulus, and the loss factor of UD CFRP interleaved with (T700 + M46J) (3mm + 6mm) mat [**Laminate T**] compared with the control sample (**Laminate A**), respectively. From **Figure 5.8** and **Figure 5.9**, the UD CFRP interleaved with T700 (3mm) mat [**Laminate O**] and the UD CFRP interleaved with T700 (6mm) mat [**Laminate Q**] were competitive from 30℃ to about 120℃.

The storage modulus and loss factor performances exhibited by the configurations under consideration were reflective in their figure of merit performances, as shown in **Table 5.6**. At approximately 80 degrees Celsius, the material begins to flow, accompanied by a rapid fall in storage modulus and an increase in tan delta. As stated previously, the glass transition results from relaxation. Each figure contains three zones,

one of which is a glassy state zone consisting of the horizontal portion of the initial test region in which the material is in a solid state. The relatively flat areas of each polymer at lower temperatures are referred to as their glassy state. In this region, segmental movement within the material's structure is restricted, and the material's modulus is high. The composite glass transition (T_g) begins at the beginning of the curves' initial downward bend. All curves indicate a significant decrease above this level due to a substantial softening and rubbery flow. Due to the importance of glass transition temperature in assessing the viscoelastic properties of polymer matrix composites, this region is the most relevant and crucial. The final zone is a glassy zone in which the material's state is stabilized, and the storage modulus does not vary considerably. The loss modulus is a sensitive indicator of molecular changes and an extremely helpful parameter for failure investigation. This metric, known as the specimen's damping characteristics, helps predict the viscous response of a material. As stated previously, the observed variations in the effect of the fiber lengths and their combinations in DMA properties are collaborated by the works of Capela et al. [63]. In a nutshell, there is an optimum length for the fibers to perform (critical fiber length); they reach a plateau upon the increment of the lengths and decrease in performance: the same trend was observed for the combination of two lengths.

5.4 Effects of The Recycled Carbon Fibers' Types and Their Micro-Hybridization with Short Virgin Aramid Fibers

The achievement of good mechanical properties is critically dependent on the stress transfer efficiency from the matrix to the fibers when discontinuous fibers are utilized as reinforcements in composites. Additionally, the critical fiber length for the efficient stress transfer to the fiber is a unique function of the ratio between Young's elastic moduli of the fiber and matrix (E_f/E_m) [128-130]. Generally, all things being

equal, the higher the E_f/E_m ratio, the better the flexural moduli of the composite. To evaluate the effect of the fiber type, 3 mm length of T700, and its combination with 3 mm each of M46J and T800 to form three separate composite laminates. That is, the UD CFRP interleaved with T700 (3mm) mat [**Laminate O**]; UD CFRP interleaved with 1.5 wt.% sized rCF (same as UD CFRP interleaved with 1 rCF mat) [same as UD CFRP interleaved with (T700 + M46J) (3mm + 3mm) mat] [same as UD CFRP interleaved with (T700 + M46J + vAF) (75% + 25% + 0%) mat] [**Laminate F**]; and UD CFRP interleaved with (T700 + T800) (3mm + 3mm) mat [**Laminate P**]. For the effect of the recycled carbon fibers' micro-hybridization with short virgin aramid fibers, UD CFRP interleaved with 1.5 wt.% sized rCF (same as UD CFRP interleaved with 1 rCF mat) [same as UD CFRP interleaved with (T700 + M46J) (3mm + 3mm) mat] [same as UD CFRP interleaved with (T700 + M46J + vAF) (75% + 25% + 0%) mat] [**Laminate F**]; UD CFRP interleaved with (T700 + M46J + vAF) (50% + 25% + 25%) mat [**Laminate V**]; and UD CFRP interleaved with (T700 + M46J + vAF) (25% + 25% + 50%) mat [**Laminate W**].

To explore the effects of the fiber type, a reference was made to the flexural moduli values in **Table 5.5**. Accordingly, the UD CFRP with no mat (**Laminate A**) had 125.1 GPa, the UD CFRP interleaved with T700 (3mm) mat [**Laminate O**]; UD CFRP interleaved with (T700 + T800) (3mm + 3mm) mat [**Laminate P**]; and UD CFRP interleaved with 1.5 wt.% sized rCF (same as UD CFRP interleaved with 1 rCF mat) [same as UD CFRP interleaved with (T700 + M46J) (3mm + 3mm) mat] [same as UD CFRP interleaved with (T700 + M46J + vAF) (75% + 25% + 0%) mat] [**Laminate F**] respectively had 131.0 GPa, 137.3 GPa, and 144.5 GPa: that is an increasing trend. These variations follow the fact that T700S, T800S, and M46J are standard modulus, intermediate modulus, and high modulus carbon fibers, respectively: from the E_f/E_m

ratio, the elastic moduli of the fibers are directly proportional to the effective stress transfer that inadvertently affect the flexural moduli of the composite laminates. For the figure of merit (see **Table 5.5**), there was a little switch in the above-established trend, which is explained by **eq 4.8**, wherein the figure of merit depended on both the flexural moduli and the loss factors. From **Table 5.5**, the control sample (**Laminate A**) performed slightly better than the UD CFRP interleaved with T700 (3mm) mat [**Laminate O**] in terms of the figure of merit evaluations [the control sample (**Laminate A**) had 0.788 GPa, and the UD CFRP interleaved with T700 (3mm) mat [**Laminate O**] had 0.773 GPa]. However, the UD CFRP interleaved with T700 (3mm) mat [**Laminate O**] had a better flexural modulus value compared to the control sample (**Laminate A**). Such a discrepancy is because of the loss factor: the control sample (**Laminate A**) recorded a loss factor of 0.0063, while the UD CFRP interleaved with T700 (3mm) mat [**Laminate O**] recorded 0.0059.

Concerning the effect of the recycled carbon fibers' micro-hybridization with short virgin aramid fibers, a reference must be made to the hybridization concept. Hybridization is the combination of more than one type of fibers, and in hybridizations, there is either a positive or negative synergistic effect. The positive synergistic effect happens when the resultant composite laminates take up their fibers' merits. The negative synergistic effect is where the final composite laminates take up the demerits of their participating fibers [131-133]. In reference to the three configurations under considerations here, that is, the UD CFRP interleaved with 1.5 wt.% sized rCF (same as UD CFRP interleaved with 1 rCF mat) [same as UD CFRP interleaved with (T700 + M46J) (3mm + 3mm) mat] [same as UD CFRP interleaved with (T700 + M46J + vAF) (75% + 25% + 0%) mat] [**Laminate F**]; UD CFRP interleaved with (T700 + M46J + vAF) (50% + 25% + 25%) mat [**Laminate V**]; and UD CFRP interleaved with (T700 +

M46J + vAF) (25% + 25% + 50%) mat [**Laminate W**], from **Table 5.5**, the introduction of the vAFs weakened the positive hybridization achieved by the introduction of M46J rCFs into the T700 rCFs (see values for **Laminates F**, **O**, **P**, and **V**) as discussed under the effect of fiber type (the weakness affected all properties as listed in **Table 5.5** for the laminates under consideration here). The weakness in the positive hybridization became more prominent with the introduction of more vAFs, that is, when the vAF percentage was increased from 25 to 50 (see values for **Laminates V** and **W**). **Figure 5.10** (a) and **Figure 5.10** (b) depict the effect of the recycled carbon fibers' types and their micro-hybridization with short virgin aramid fibers, respectively, in terms of the figure of merits much clearly.

Under the effects of the recycled carbon fibers' lengths and their combinations, some selected samples (see **Figure 5.8** and **Figure 5.9**) were used to undertake DMA tests for further investigations. **Table 5.6** shows the DMA properties of the selected composite laminates showing the effects of the factors under consideration.

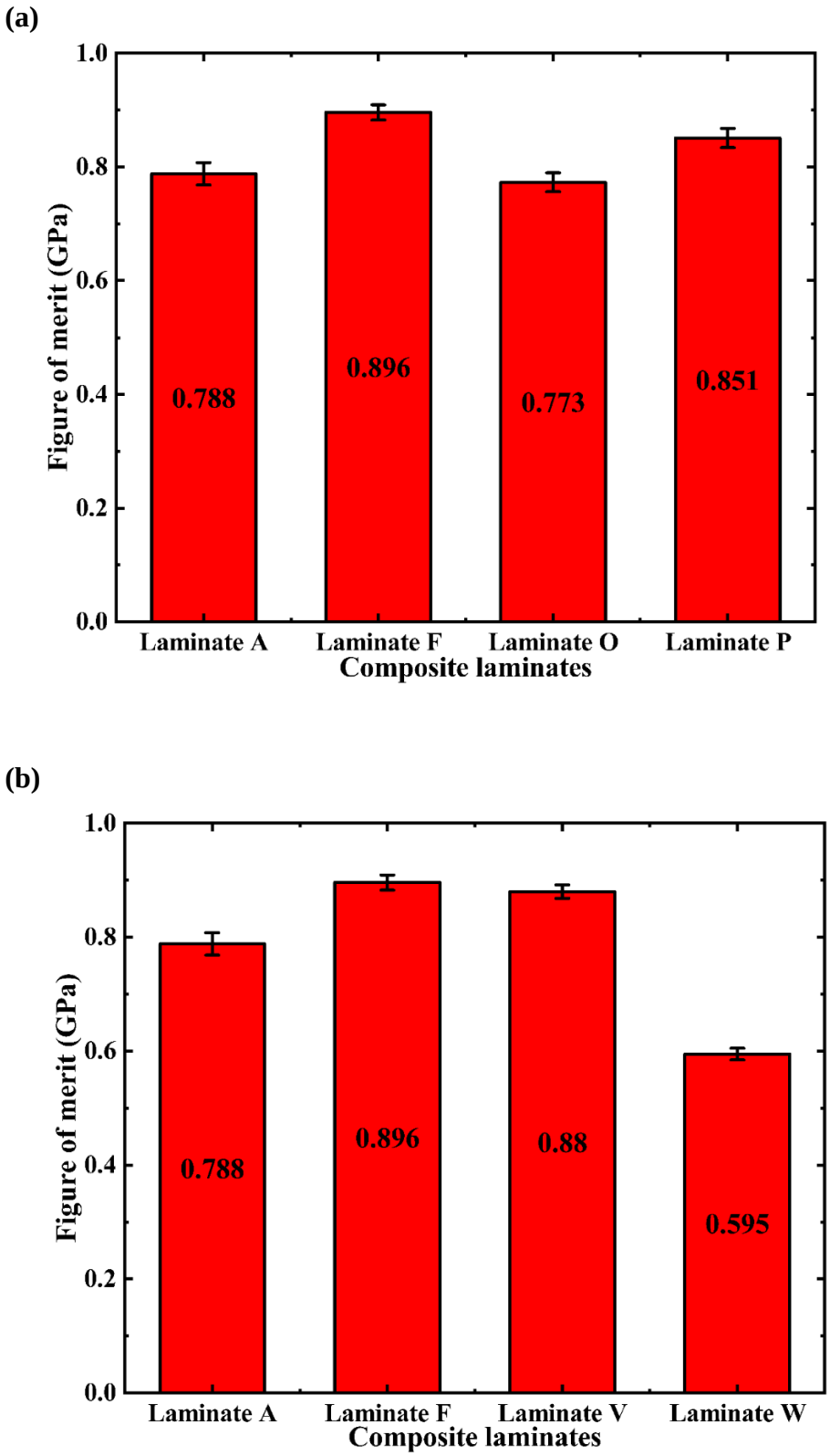

Figure 5.10. (a) The effects of the recycled carbon fibers' types (b) the effect of the recycled carbon fibers' micro-hybridization with short virgin aramid fibers: figure of merit. The error bars show the standard deviation values.

The short (recycled) carbon fibers, irrespective of their slight decrement in mechanical properties, have higher stiffness and strength than the virgin aramid fibers. This inherent stiffness results in the overall stiffness of the composite laminates with recycled carbon fiber non-woven mats. Stiffness is synonymous with the flexural moduli in bending and storage moduli in DMA. These performances are well depicted in **Figure 5.9**. Generally, the storage modulus decreases as temperature increases. This is normal for polymer composites as heating increases the mobility of molecules, thereby making the material easier to deform.

At 30℃, compared with the control sample, regarding the effect of the fiber type, from **Table 5.6**, the loss factor increased only for the UD CFRP interleaved with 1.5 wt.% sized rCF (same as UD CFRP interleaved with 1 rCF mat) [same as UD CFRP interleaved with (T700 + M46J) (3mm + 3mm) mat] [same as UD CFRP interleaved with (T700 + M46J + vAF) (75% + 25% + 0%) mat] [**Laminate F**] by 23.7 % and decreased by 12.4 % for the UD CFRP interleaved with T700 (3mm) mat [**Laminate O**]. Regarding the storage modulus, compared with the control sample (**Laminate A**), the reversed trend was observed; the UD CFRP interleaved with 1.5 wt.% sized rCF (same as UD CFRP interleaved with 1 rCF mat) [same as UD CFRP interleaved with (T700 + M46J) (3mm + 3mm) mat] [same as UD CFRP interleaved with (T700 + M46J + vAF) (75% + 25% + 0%) mat] [**Laminate F**] decreased by 8.3 %, and increased by 6.4 % for the UD CFRP interleaved with T700 (3mm) mat [**Laminate O**]. At lower temperatures up to about 110℃, compared with the control sample, as shown in **Figure 5.9**, the UD CFRP interleaved with 1.5 wt.% sized rCF (same as UD CFRP interleaved with 1 rCF mat) [same as UD CFRP interleaved with (T700 + M46J) (3mm + 3mm) mat] [same as UD CFRP interleaved with (T700 + M46J + vAF) (75% + 25% + 0%) mat] [**Laminate F**]; and UD CFRP interleaved with T700 (3mm) mat [**Laminate O**]

had better performances in their loss factors, but at higher temperatures, the control sample (**Laminate A**) did better. Regarding the effect of the recycled carbon fibers' micro-hybridization with short virgin aramid fibers, compared with the control sample, the storage modulus for the UD CFRP interleaved with (T700 + M46J + vAF) (50% + 25% + 25%) mat [**Laminate V**] was 17.0 %. From **Table 5.6**, at 30℃, the reduction of the 75 % of the UD CFRP interleaved with 1.5 wt.% sized rCF (same as UD CFRP interleaved with 1 rCF mat) [same as UD CFRP interleaved with (T700 + M46J) (3mm + 3mm) mat] [same as UD CFRP interleaved with (T700 + M46J + vAF) (75% + 25% + 0%) mat] [**Laminate F**] and introducing 25 % of vAF to form a UD CFRP interleaved with (T700 + M46J + vAF) (50% + 25% + 25%) mat [**Laminate V**] resulted in 26.6 % in storage modulus. From **Figure 5.8**, compared with the control sample (**Laminate A**), both the UD CFRP interleaved with 1.5 wt.% sized rCF (same as UD CFRP interleaved with 1 rCF mat) [same as UD CFRP interleaved with (T700 + M46J) (3mm + 3mm) mat] [same as UD CFRP interleaved with (T700 + M46J + vAF) (75% + 25% + 0%) mat] [**Laminate F**]; and UD CFRP interleaved with (T700 + M46J + vAF) (50% + 25% + 25%) mat [**Laminate V**] had better loss factor performances at lower temperatures up to about 110℃. There was an increase in loss factor performance for the UD CFRP interleaved with (T700 + M46J + vAF) (50% + 25% + 25%) mat [**Laminate V**] with further increment in temperature to about 145 ℃ compared with the UD CFRP interleaved with 1.5 wt.% sized rCF (same as UD CFRP interleaved with 1 rCF mat) [same as UD CFRP interleaved with (T700 + M46J) (3mm + 3mm) mat] [same as UD CFRP interleaved with (T700 + M46J + vAF) (75% + 25% + 0%) mat] [**Laminate F**]. These performances with the inclusion of the aramid fibers are explained in the preceding sections.

Furthermore, from **Figure 5.8** and **Figure 5.9**, the storage modulus falls as temperature increases, while the loss modulus and tan delta reach a maximum. The glass transition effect is one of relaxation. The storage moduli exhibit a step during the glass transition, but the loss moduli and tan delta exhibit a peak. The tan delta peaks always appear at a temperature slightly higher than their corresponding loss modulus peaks. Typically, the glass transition is observed as a step-like decrease in the storage modulus, accompanied by peaks in the loss modulus and tan delta. After this, the modulus falls gradually. A little increase follows this decrease in loss modulus. **Figure 5.11** shows the mutually exclusive nature of the storage moduli and the loss factors (as established by **eq 5.1**) of the best configuration in this project.

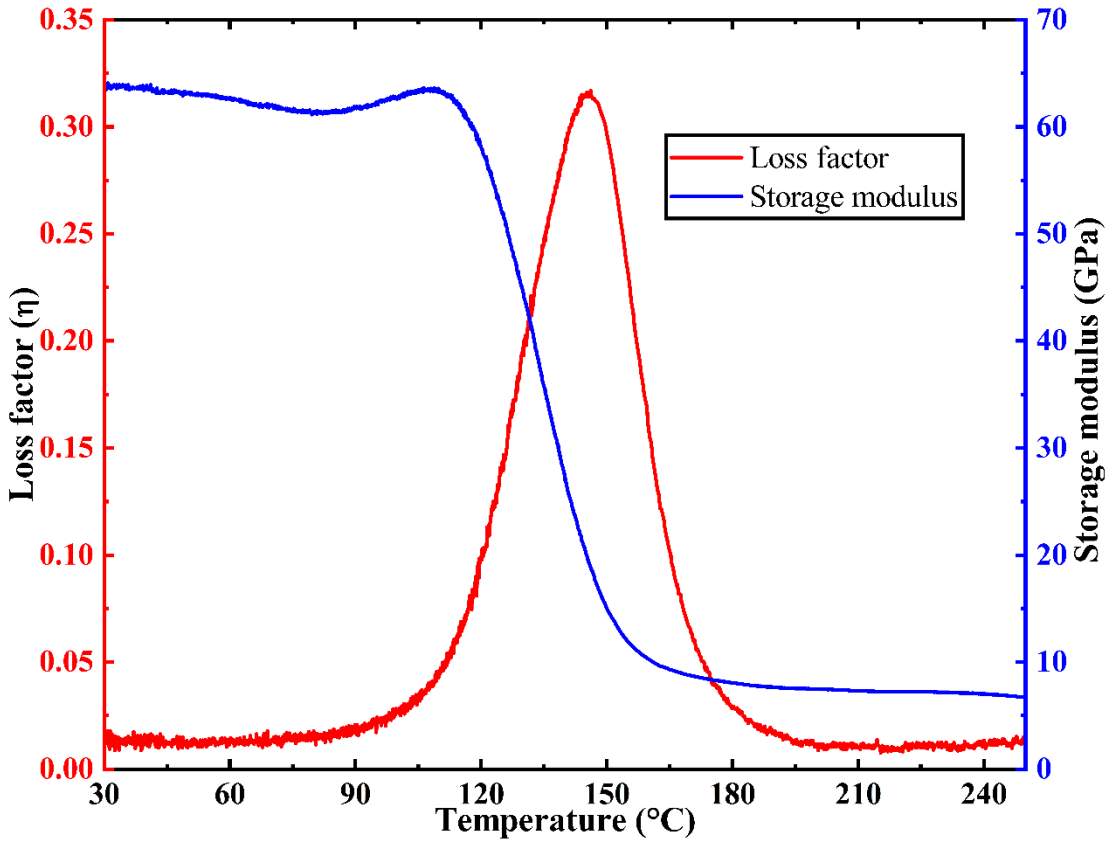

Figure 5.11. Mutually exclusive nature of the storage moduli and the loss factors of the best configuration in this project.

With an appropriate design, it is possible to simultaneously increase the storage moduli and loss factors despite their mutual exclusivity. This study demonstrated that the addition of extra fibers (in the form of non-woven mats) and additional resins (in the form of resin films) (to prevent resin starvation) led to a simultaneous increase in the storage modulus and the loss factors (damping): the storage modulus is typically a fiber-dominated property, whereas the loss factor is a resin-dominated property (it should be acknowledged that, the statement should be put in context because there are some fibers such as natural fibers that have inherent damping properties). A more detailed plot showing the trend of change of damping capacities (figure of merit) @30℃ is shown in **Figure 5.12**.

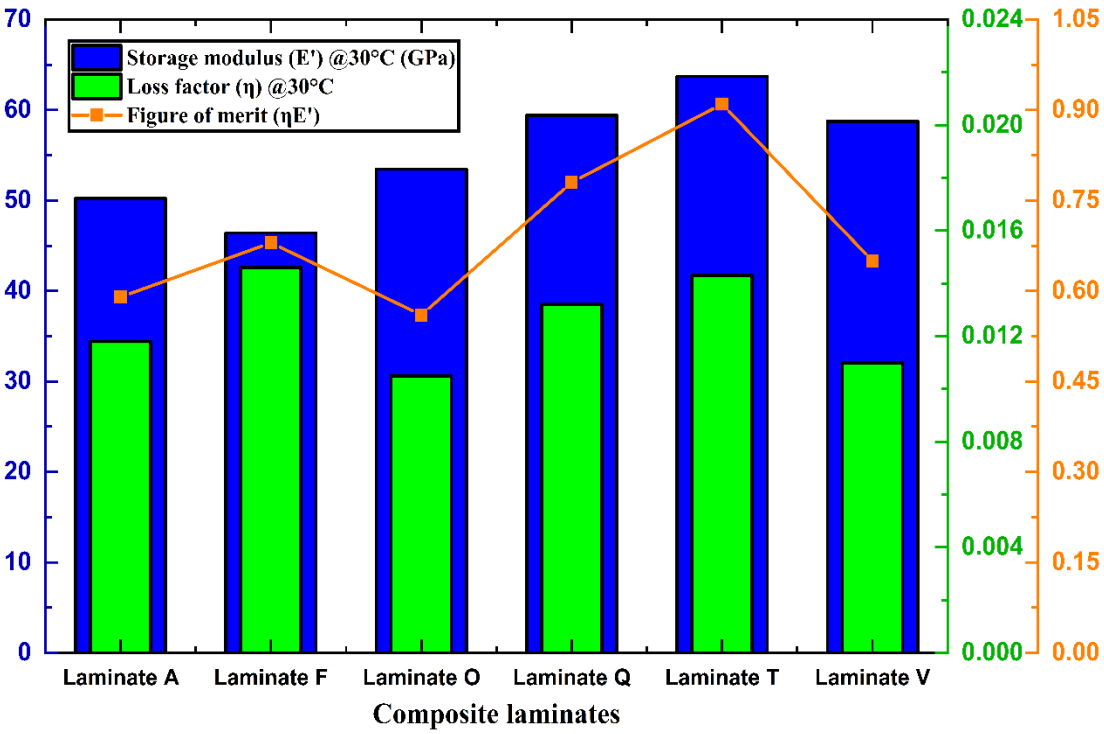

Figure 5.12. Damping capacity plot showing the effect of the fiber lengths, the effect of the combination of fiber lengths, the effects of the recycled carbon fibers' types, and the effects of the recycled carbon fibers' micro-hybridization with short virgin aramid fibers.

Table 5.7 and **Table 5.8** summarize the comparison between the best composite laminate developed in this paper and the best materials developed by other authors. **Table 5.7** compares the DMA method, and **Table 5.8** compares the free vibration-bending method. Shown in **Figure 5.13** is the Ashby plot [47], offering the best composite laminate developed. In comparison, the control sample has been very competitive; hence, their counterparts' somewhat inferior performances should not be taken out of context but rather be appreciated.

Table 5.7. Comparison using the DMA method

Method	**Samples**	**Storage modulus, E′ @30℃/GPa**	**Loss factor, tan δ (η) @30℃**	**Figure of merit (ηE′)/ GPa**	**% Improvements from Unwin et al. [48]**
DMA	Constrained high internal friction interfacial layer (best result) [48]	6.04	0.117	0.71	-
	UD CFRP interleaved with (T700 + M46J) (3mm + 6mm) mat [**Laminate T**]	63.72	0.0143	0.91	28.2

Table 5.8. Comparison using the free vibration-bending method

Method	**Samples**	**Flexural modulus, E_f /GPa**	**Loss factor, tan δ (η) @25℃**	**Figure of merit (ηE_f)/ GPa**	**% Improvements from Ni et al. [40]**
Bending and free vibration tests	High damping and high stiffness CFRP composites with aramid non-woven fabric interlayers (best result) [40]	140.1	0.0075	1.051	-
	UD CFRP interleaved with (T700 + M46J) (3mm + 6mm) mat [**Laminate T**]	135.4	0.0092	1.246	18.6

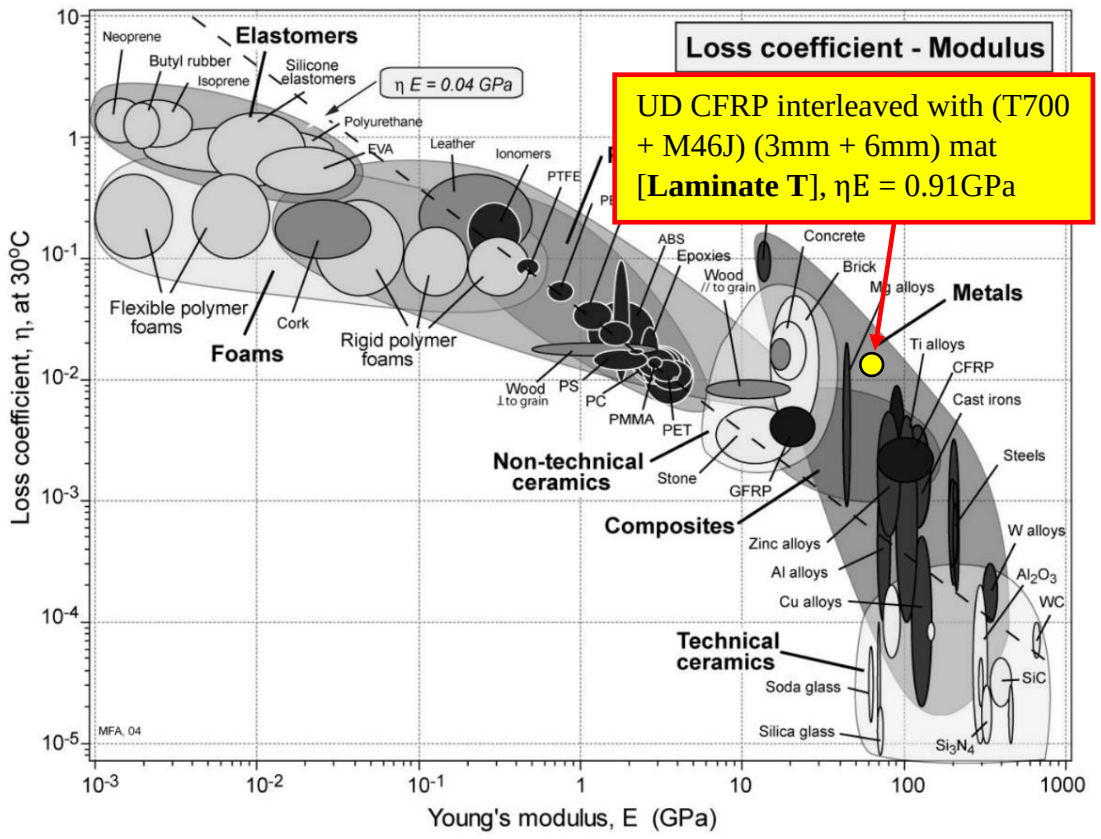

Figure 5.13. The Ashby log-log plot (the original plot was changed to grayscale, and the best result from this paper was superimposed on it) [47].

Source: Copyright 2022, Elsevier Ltd.

As seen in **Figure 5.13**, the objective of the investigations carried out in this paper has been well achieved. Compared with the control sample, the best laminate was 54.2% better in the figure of merit in the ideal direction of the Ashby log-log plot.

5.5 REPRODUCIBILITY

The part of the analyses (see **sections 5.3** and **5.4**) that utilized both the DMA and the bending-free vibration methods established the same trends regarding the figure of merits for both ways (the bending-free vibration was carried out first and selected samples were investigated further using the DMA). A reproducibility test was carried out since manufacturing processes could affect the results. To test the reproducibility of data of the developed composite laminates, the following was done:

1. Three composite laminates were manufactured by repeating the same processes used in manufacturing the original composites (the best configuration for the project, **Laminate T,** was manufactured) (herein referred to as **L−1**).
2. The bending test was conducted in the same manner as carried out in the investigation of **L−1**.
3. The mean values for the flexural moduli were calculated for the three laminates.
4. The standard deviation was also calculated for the three composite laminates (**L−2** to **L−4**).
5. The mean values and the standard deviations (the values show the reproducibility uncertainty) for the three composite laminates alongside the **L−1** were plotted on a scatter chart.

All values are shown in **Table 5.9**.

Table 5.9. Flexural moduli of the composite laminates under consideration

Samples	**Test No.**	**Flexural modulus, E_f /GPa**	**Flexural strength /MPa**	**Specific flexural modulus $\left(\frac{\mathbf{GPa}}{\mathbf{gcm^{-3}}}\right)$**	**Specific flexural strength $\left(\frac{\mathbf{MPa}}{\mathbf{gcm^{-3}}}\right)$**	**Average thickness/mm**
L−1	1	134.338	1367.782	87.550	891.408	**2.51**
	2	135.736	1896.905	88.462	1236.246	
	3	136.007	1349.595	88.638	879.555	
	4	134.668	1644.943	87.766	1072.038	
	5	136.238	1772.921	88.789	1155.444	
Average		**135.397**	**1606.429**	**88.241**	**1046.938**	
Standard deviation		**0.844**	**243.154**	**0.550**	**158.468**	
Coefficient of variation (COV) (%)		**0.6**	**15.1**	**0.6**	**15.1**	
L−2	1	134.484	1439.809	87.979	941.917	
	2	135.857	1603.480	88.877	1048.990	
	3	136.136	1521.408	89.060	995.299	
	4	134.341	1509.081	87.885	987.235	
	5	134.936	1782.479	88.275	1166.090	
Average		**135.151**	**1571.251**	**88.415**	**1027.906**	

Standard deviation		**0.809**	**131.608**	**0.529**	**86.097**
Coefficient of variation (COV) (%)		**0.6**	**8.4**	**0.6**	**8.4**
L−3	1	136.449	1496.418	89.332	979.693
	2	136.849	1561.734	89.594	1022.455
	3	135.884	1480.511	88.962	969.279
	4	135.662	1761.528	88.817	1153.259
	5	135.3	1386.878	88.580	907.978
Average		**136.029**	**1537.414**	**89.057**	**1006.533**
Standard deviation		**0.620**	**139.998**	**0.406**	**91.656**
Coefficient of variation (COV) (%)		**0.5**	**9.1**	**0.5**	**9.1**
L−4	1	135.84	1656.449	88.486	1079.008
	2	136.575	1483.242	88.965	966.182
	3	135.372	1587.519	88.181	1034.108
	4	135.84	1699.015	88.486	1106.736
	5	136.932	1560.497	89.197	1016.505
Average		**136.112**	**1597.344**	**88.663**	**1040.508**

Standard deviation	**0.629**	**84.119**	**0.410**	**54.795**
Coefficient of variation (COV) (%)	**0.5**	**5.3**	**0.5**	**5.3**

Table 5.9 shows no significant differences in the mean values of the flexural modulus measured for the composite laminates. Regarding the standard deviation values, minimal differences were observed for the various laminates. This observation is not surprising considering the difficulties of achieving consistent uniform non-woven mats. Since the test samples were cut from different parts of the laminates, the results are not dramatic. **Figure 5.14** shows the reproducibility graph.

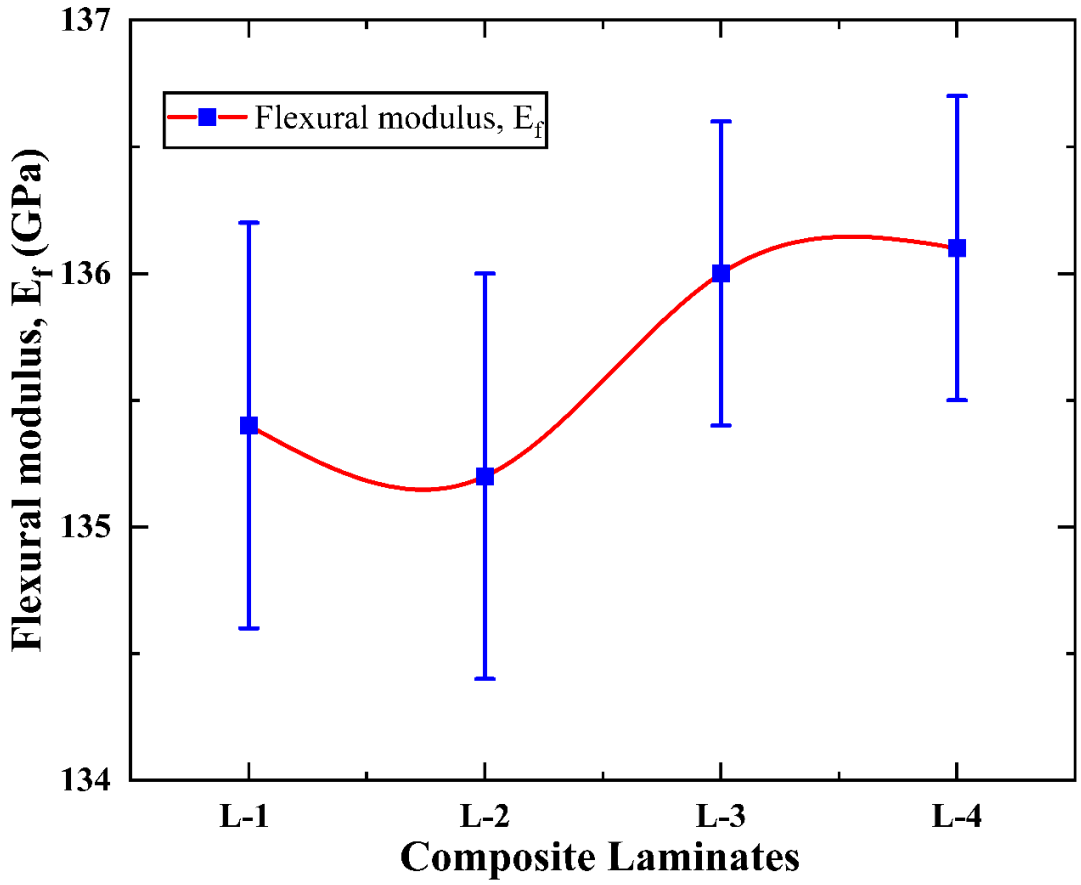

Figure 5.14. The reproducibility plots. The error bars show the standard deviation values.

Table 5.10 summarizes some parameters of the control sample and the best laminate (flexural modulus, flexural strength, specific flexural modulus, and specific flexural strength).

Table 5.10. Summary of some properties for the control sample and the best laminate

Samples	**Flexural modulus, E_f /GPa**	**Flexural strength /MPa**	**Specific flexural modulus** $\left(\frac{\mathbf{GPa}}{\mathbf{gcm^{-3}}}\right)$	**Specific flexural strength** $\left(\frac{\mathbf{MPa}}{\mathbf{gcm^{-3}}}\right)$

Control	125.1 ±3.1	1567.6 ±74.3	79.2 ±2.0	992.5 ±47.0
Laminate T	135.4 ±0.8	1606.4 ±243.2	88.2 ±0.6	1046.9 ±158.5
Differences pegging Laminate T against the control (%)	8.2	2.5	11.4	5.5

The competitiveness of the best-developed composite laminate is quite encouraging, as shown in **Table 5.10**.

6 FREE VIBRATIONS (MODAL ANALYSIS) AND FORCED VIBRATIONS (HARMONIC ANALYSIS)

6.1 INTRODUCTION

To directly quantify the inherent vibration/dynamic characteristics (natural frequencies and mode shapes) of the non-woven mats and to gain an in-depth understanding of the vibration behavior of the non-woven mats, the free (modal analysis) and forced (harmonic analysis) vibrations were simulated using the ANSYS workbench software (ANSYS STUDENT 2022 R2). A structure's natural frequencies and mode shapes can be determined using modal analysis. The modal analysis offers the natural frequencies, mode shapes, and mode participation factors (the mode participation factors tell us which modes would be excited the most) [134]. The highest vibration levels occur at the natural frequencies we seek to diminish. Therefore, the modal analysis reveals the vibrational frequencies at which the system is susceptible to harm. If the modal study finds that a structure's natural frequencies are within the range of excitation frequencies, we typically (but not always) strive to modify the structure's design so that the natural frequencies fall outside the excitation frequency range. The mode shapes illustrate how a structure tends to deform at different natural frequencies and the shape at which free vibration occurs. The mode shapes reveal the places that would be subjected to substantial stresses if the deformed shape resembled the mode shape. This shape is quite advantageous since, for instance, we do not want the weld regions of a welded structure to be high-stress zones, as this can decrease the fatigue life of the structure. The natural frequencies and mode shapes are crucial in designing a structure for dynamic loading conditions.

Additionally, modal analysis results are used in further investigations such as harmonic analysis. A time-history analysis might be computationally expensive to examine a structure under vibrating loads. Harmonic analysis is an alternate method for simulating the reaction of a structure to forced vibrations. Unlike transient dynamic analysis, harmonic analysis solves the structure's dynamics in the frequency domain instead of the time domain. Harmonic analysis can be valuable for comprehending a vital behavior such as resonance, where excessive motion, stress, noise, and vibrations occur at a specific frequency. A harmonic analysis determines the steady-state response of a structure to known-frequency sinusoidal (harmonic) loads. Pressures, forces, and displacements with known amplitude and frequency can serve as inputs (in-phase or out-of-phase with each other). Harmonic displacements and related stresses and strains are the model's outputs. Typically, harmonic analysis is conducted to (1) ensure that a design can tolerate sinusoidal loads at various frequencies and (2) assess the response of the design to the provided harmonic excitation [134]. It is a linear assessment (non-linearities are ignored).

Ansys supports two techniques for solving harmonic analysis: a computationally demanding complete technique and an efficient mode-superposition technique. Mode Superposition is the only available solution choice for ANSYS Student. Harmonic analysis is a forced vibration study, and damping must be introduced to the system to duplicate actual values. The harmonic analysis provides information on how a design may react to different types of dynamic loads and can be used as an illustration for avoiding resonance vibrations that can be destructive to structures. Resonance results in excessive motions, stress, noise, and vibrations, as well as fatigue damage and eventual failure. At a high natural frequency, resonance might be deferred.

6.2 MATERIALS AND METHODS

6.2.1 Micromechanics

Micromechanical models were applied for the prediction of material properties. Not only are many existing micromechanical models, such as self-consistent models, variational models, exact methods, etc., challenging to implement, but they are also constrained to a tiny percentage of the entire range of fiber orientation and packing geometry of interest. Halpin and Tsai approximated these sophisticated micromechanical models to produce simple empirical formulae for moduli for randomly oriented composites. The Halpin-Tsai equations, which account for the fiber aspect ratio l/d, have been demonstrated to be reasonably accurate for low fiber volume fractions ($V_f < 0.50$) [135]. Tsai-Pagano modified the Halpin-Tsai model to estimate Young's modulus [136], Shear modulus [137], and Poisson's ratio [138] of a randomly oriented fiber (ROF) system. Due to fiber entanglements, the highest fiber volume fraction that may be reached in a randomly oriented fiber (ROF) system is roughly 37 percent [138].

6.2.1.1 Derivation of non-woven mat composites' properties

The properties of non-woven mat composites were treated as isotropic materials; therefore, the parameters, elastic modulus, E; shear modulus, G; Poisson's ratio, ν; and density, ρ suffice to characterize their behaviors. The rule of mixtures; rule of hybrid mixtures; Halpin-Tsai model's equations; and Tsai-Pagano model's equations were combined and used to find the elastic modulus, E_{mat}, shear modulus or modulus of rigidity, G_{mat} and Poisson's ratio, υ_{mat} of the non-woven mat composites.

$$E_{mat} = E_m \left[\frac{3}{8}\left(\frac{1+ \zeta\eta_L V_f}{1- \eta_L V_f}\right) + \frac{5}{8}\left(\frac{1+ 2\eta_T V_f}{1- \eta_T V_f}\right)\right] \quad 6.1$$

where $\eta_L = \frac{(\frac{E_f}{E_m})-1}{(\frac{E_f}{E_m})+\zeta}$; $\eta_T = \frac{(\frac{E_f}{E_m})-1}{(\frac{E_f}{E_m})+2}$; and $\zeta = 2\left(\frac{l}{d}\right)$

$$G_{mat} = E_m\left[\frac{1}{8}\left(\frac{1+\zeta\eta_L V_f}{1-\eta_L V_f}\right) + \frac{1}{4}\left(\frac{1+2\eta_T V_f}{1-\eta_T V_f}\right)\right] \quad 6.2$$

$$\nu_{mat} = \frac{E_{mat}}{2G_{mat}} - 1 \quad 6.3$$

The rule of hybrid mixtures only was used for the calculation of the density of non-woven mats composites, ρ_{mat} :

$$\rho_{mat} = \rho_f V_f + \rho_m[1 - V_f] \quad 6.4$$

where E_m is the elastic modulus of the matrix; E_f and V_f is the elastic modulus and volume fraction of the random discontinuous fibers, respectively; ρ_f is the density; ρ_m is the density of the matrix; l is the fiber length; d is the fiber diameter; ζ is a shape parameter dependent upon reinforcement geometry and orientation; and the constant η considers the matrix's and fiber's modulus [139].

For the recycled carbon fibers (rCF) T700, l = 3 mm, d = 7 μm, ρ_{rCF} = 1800 Kgm^{-3} , E_{rCF} = 230 GPa.

For the recycled carbon fibers (rCF) M46J, l = 3 mm, d = 5 μm, ρ_{rCF} = 1840 Kgm^{-3} and E_{rCF} = 436 GPa.

For the chopped virgin aramids (vAF) (DuPont™ Kevlar® 29), l = 3 mm, d = 12 μm, ρ_{vAF} = 1440 Kgm^{-3} and E_{vAF} = 70.5 GPa.

For the epoxy matrix, ρ_m = 1200 Kgm^{-3} and E_m= 3.5 GPa. It was estimated that each mat had a constant thickness of 0.20 mm.

Using a modified variant of **eqs 6.1**, **6.2**, **6.3**, and **6.4**, the elastic modulus, shear modulus or modulus of stiffness, Poisson's ratio, and density of composites containing 100 percent rCF nonwoven mats are computed as an example:

$$E_{rCFmatComposite} = E_m \left[\left\{ \frac{3}{8}\left(\frac{1+\zeta\eta_L V_f}{1-\eta_L V_f}\right) + \frac{5}{8}\left(\frac{1+2\eta_T V_f}{1-\eta_T V_f}\right) \right\}_{T700rCF} + \left\{ \frac{3}{8}\left(\frac{1+\zeta\eta_L V_f}{1-\eta_L V_f}\right) + \frac{5}{8}\left(\frac{1+2\eta_T V_f}{1-\eta_T V_f}\right) \right\}_{M46JrCF} \right]$$

$$G_{rCFmat} = E_m \left[\left\{ \frac{1}{8}\left(\frac{1+\zeta\eta_L V_f}{1-\eta_L V_f}\right) + \frac{1}{4}\left(\frac{1+2\eta_T V_f}{1-\eta_T V_f}\right) \right\}_{T700rCF} + \left\{ \frac{1}{8}\left(\frac{1+\zeta\eta_L V_f}{1-\eta_L V_f}\right) + \frac{1}{4}\left(\frac{1+2\eta_T V_f}{1-\eta_T V_f}\right) \right\}_{M46JrCF} \right]$$

$$\upsilon_{rCFmat} = \frac{E_{rCFmat}}{2G_{rCFmat}} - 1$$

$$\rho_{rCFmat} = \rho_{T700rCF} V_{TT700rCF} + \rho_{M46JrCF} V_{M46JrCF} + \rho_m \left[1 - \left(V_{T700rCF} + V_{M46JrCF}\right)\right]$$

Where all terms and constants adhere to the definitions mentioned above. As an example, to estimate $E_{mat}, \upsilon_{mat}, \rho_{mat}$, and G_{mat} for the 100% rCF non-woven mats composites with the fiber volume fraction of 37%, the T700rCF: M46JrCF ratio (75:25)% was calculated as $V_{T700rCF}$: $\left(\frac{75}{100}\right)$ = 0.75 of 0.37 = 0.375, and $V_{M46JrCF}$ was calculated as 0.37-0.2775 = 0.0925.

6.2.2 FEA Methodology

6.2.2.1 Introduction

The free vibration behavior in terms of natural frequencies and mode shapes, as well as the forced vibration characteristics, are determined using a finite element analysis (FEA). The correlation between the FEA and theoretical conclusions was

excellent in terms of their natural frequencies. The results provide a greater understanding of the damping characteristics of the non-woven mat composites.

6.2.2.2 Mechanical ANSYS Workbench Modal and Harmonic Analysis Governing Equations

Given the general equation of motion [140],

$$[M]\{\ddot{x}\} + [C]\{\dot{x}\} + [K]\{x\} = \{f(t)\} \quad 6.5$$

where $[M], \{\ddot{x}\}, [C], \{\dot{x}\}, [K], \{x\}, \text{and } \{f(t)\}$ are respectively, the mass matrix, acceleration, damping matrix, velocity, stiffness matrix, displacement, and external load. The terms $[C]\{\dot{x}\}$ and $\{f(t)\}$ are equal to zero for modal analysis. **Eqs 6.6** and **6.7** define the displacement and acceleration, respectively [139]:

$$\{x\} = \{\phi\}_i \sin(\omega_i t + \theta_i) \quad 6.6$$

$$\{\ddot{x}\} = -\omega_i{}^2\{\phi\}_i \sin(\omega_i t + \theta_i) \quad 6.7$$

Substituting **eqs 6.6** and **6.7** into **eq 6.5** yields the eigenvalue equation (**eq 6.8**) for a modal analysis:

$$([K] - \omega_i{}^2[M])\{\phi\}_i = \{0\} \quad 6.8$$

Where $-\omega_i{}^2$ is the eigenvalue and $\{\phi\}_i$ is the eigenvector.

$([K] - \omega_i{}^2[M])$ computes the natural frequencies (the natural frequencies are reported in Hz using $\omega_i = 2\pi f_i$; where ω_i is in radians/sec and f_i is in Hz) and $\{\phi\}_i$ computes the corresponding mode shapes.

For harmonic analysis, **eqs 6.9** and **6.10** specify the displacement and applied load, respectively:

$$\{x\} = \{x_{max}\cos\phi + ix_{max}\sin\phi\}e^{i\omega t} = (\{x_1\} + i\{x_2\})e^{i\omega t} \quad 6.9$$

$$\{f(t)\} = \{f_{max}\cos\phi + if_{max}\sin\phi\}e^{i\omega t} = (\{f_1\} + i\{f_2\})e^{i\omega t} \quad 6.10$$

Eq 6.11 (the equation for harmonic analysis) is obtained by substituting **eqs 6.9** and **6.10** into **eq 6.5**:

$$(-\omega^2[M] + i\omega[C] + [K])(\{x_1\} + i\{x_2\}) = (\{f_1\} + i\{f_2\}) \quad 6.11$$

where $\{x_1\}$ and $\{x_2\}$ are the real and imaginary displacement vectors, respectively; and $\{f_1\}$ and $\{f_2\}$ are the real and imaginary force vectors, respectively.

Using the mode superposition method (it solves the harmonic equation in modal coordinates) [7], **eq 6.11** gives **eq 6.12**:

$$\ddot{y}_j + 2\omega_j\xi_j\dot{y}_j + \omega_j{}^2 y_j = f_j \quad 6.12$$

where y_j, ω_j, ξ_j , f_j are the modal coordinate, natural frequency of mode j, fraction of critical damping for mode j, and force in modal coordinates, respectively.

6.2.2.3 Modeling of the composites in ANSYS Workbench (WB) Mechanical

ANSYS WB 2022 R2 Student Version was utilized for the simulations. First, the 180 mm by 10 mm geometry was created using Ansys SpaceClaim, a direct modeling technology that eliminates geometry issues associated with various 3D CAD operations [141]. The geometry was developed per the ASTM E756-05(2017) Standard Test Method for Measuring Vibration-Damping Properties of Materials. The ANSYS Composite PrepPost (ACP) component was added to the Project Schematic by dragging it from the Component Systems menu. Using "ANSYS Composite PrepPost (ACP)," one can extract either the shell or solid geometry of the composite laminate model under consideration and quickly define the stacking sequence, stacking orientations, and number of plies (material and fabrics/stackup definitions).

The "Engineering Data" is used to define the material properties, while the "Geometry" (model) section is used to import the drawn geometry as a shell element. Using a mesh of 0.5 mm, the mesh model is constructed. The ACP (Pre) setup data is transferred into the modal project as composite shell data. Various parameters (material characteristics, rosettes, oriented element sets, and composite thicknesses) were allocated to their corresponding geometries. Then, an assignment modeling group is formed (laying order and laying thickness are defined in **Figure 6.1**, **Figure 6.2**, **Figure 6.3**, and **Figure 6.4** exhibits, in ascending order, the Ansys workbench interface, mesh details, the meshed model, and modal analysis configuration details. In this work, the structural damping coefficient is 0.01, a 1 N force was applied across the edge of the cantilevered beam, and the harmonic response across the edge was also extracted. **Figure 6.5** depicts the assignment of boundary conditions and force definition. Using a frequency range between 0 Hz and 200 Hz, two modes of the cantilevered configuration are analyzed, and solutions/results are obtained. **Figure 6.6**, **Figure 6.7**, and **Figure 6.8** depict the specifics of the harmonic analysis settings, the frequency response, and the project's general structure, respectively.

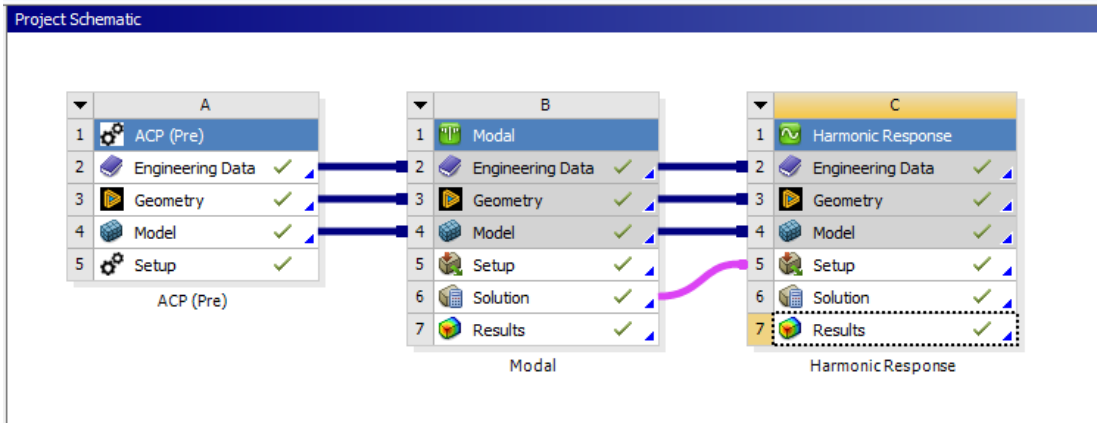

Figure 6.1. The interface of Ansys workbench.

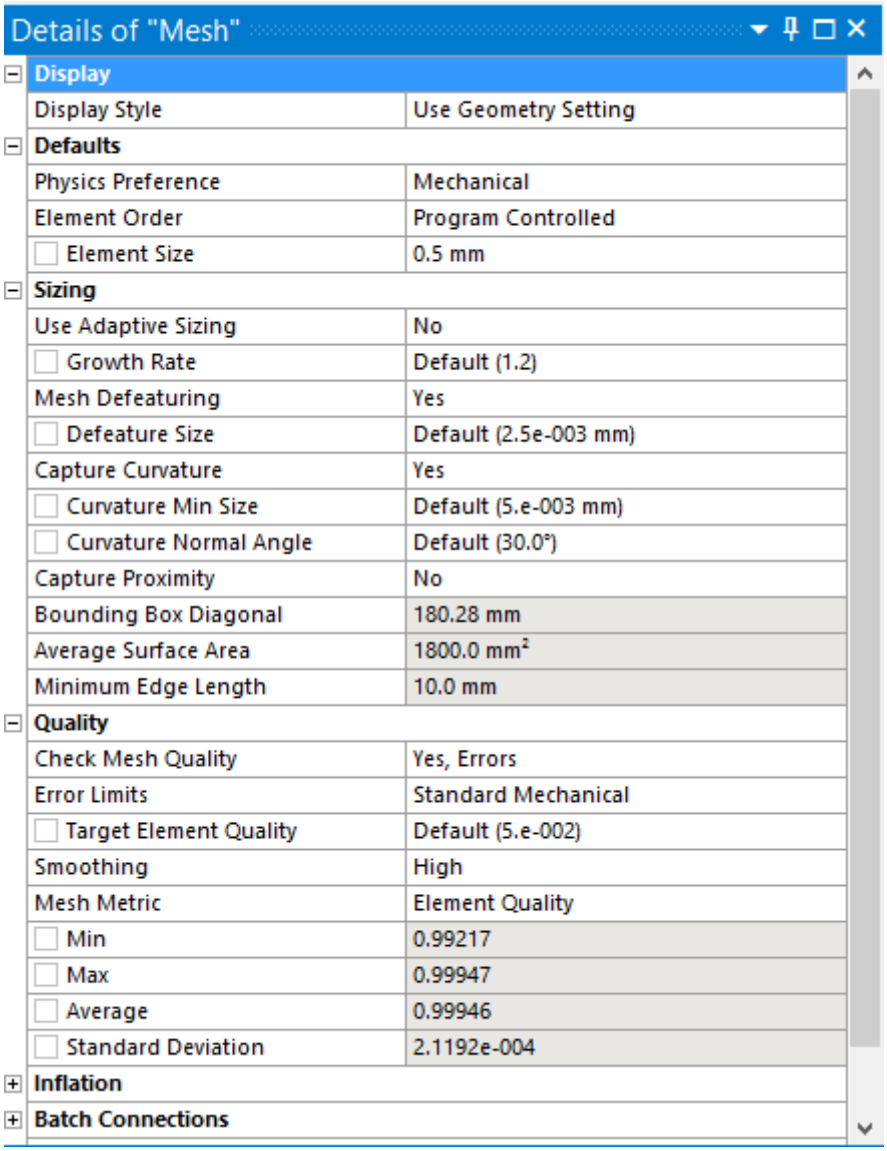

Details of "Mesh"

Display	
Display Style	Use Geometry Setting
Defaults	
Physics Preference	Mechanical
Element Order	Program Controlled
Element Size	0.5 mm
Sizing	
Use Adaptive Sizing	No
Growth Rate	Default (1.2)
Mesh Defeaturing	Yes
Defeature Size	Default (2.5e-003 mm)
Capture Curvature	Yes
Curvature Min Size	Default (5.e-003 mm)
Curvature Normal Angle	Default (30.0°)
Capture Proximity	No
Bounding Box Diagonal	180.28 mm
Average Surface Area	1800.0 mm²
Minimum Edge Length	10.0 mm
Quality	
Check Mesh Quality	Yes, Errors
Error Limits	Standard Mechanical
Target Element Quality	Default (5.e-002)
Smoothing	High
Mesh Metric	Element Quality
Min	0.99217
Max	0.99947
Average	0.99946
Standard Deviation	2.1192e-004
Inflation	
Batch Connections	

Figure 6.2. Mesh details of the model.

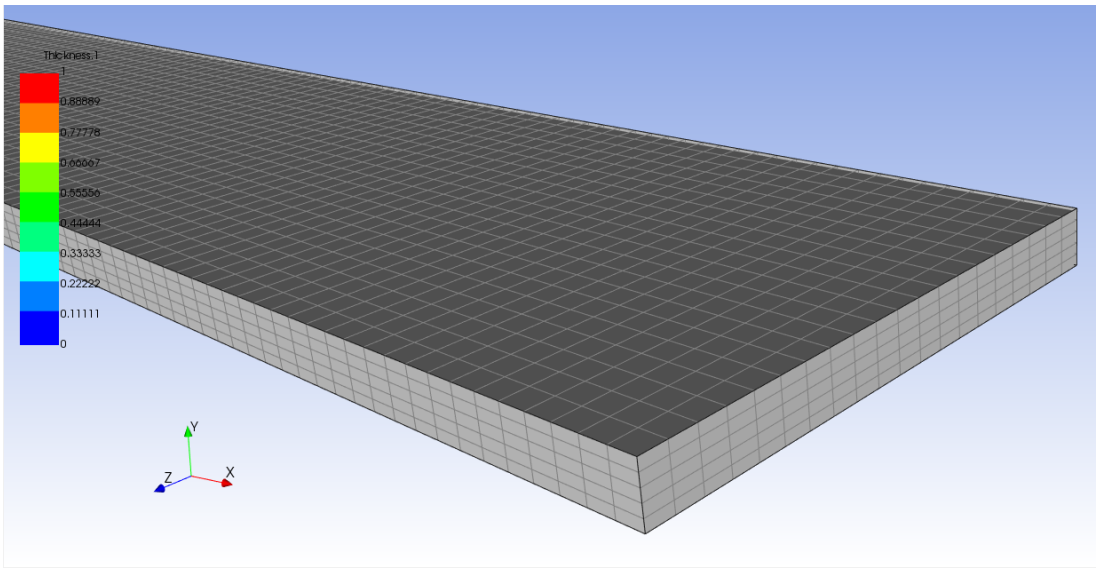

Figure 6.3. Meshed model showing the five layers for the various composites.

Details of "Analysis Settings"

Options	
Max Modes to Find	2
Limit Search to Range	Yes
Range Minimum	0. Hz
Range Maximum	200. Hz
On Demand Expansion	No
Solver Controls	
Damped	No
Solver Type	Program Controlled
Rotordynamics Controls	
Advanced	
Output Controls	
Stress	Yes
Surface Stress	No
Back Stress	No
Strain	Yes
Contact Data	No
Nodal Forces	Constrained Nodes
Volume and Energy	No
Euler Angles	No
Calculate Reactions	Yes
Store Modal Results	No
General Miscellaneous	No
Result File Compression	Program Controlled
Analysis Data Management	

Figure 6.4. Details of the analysis settings for the modal analysis.

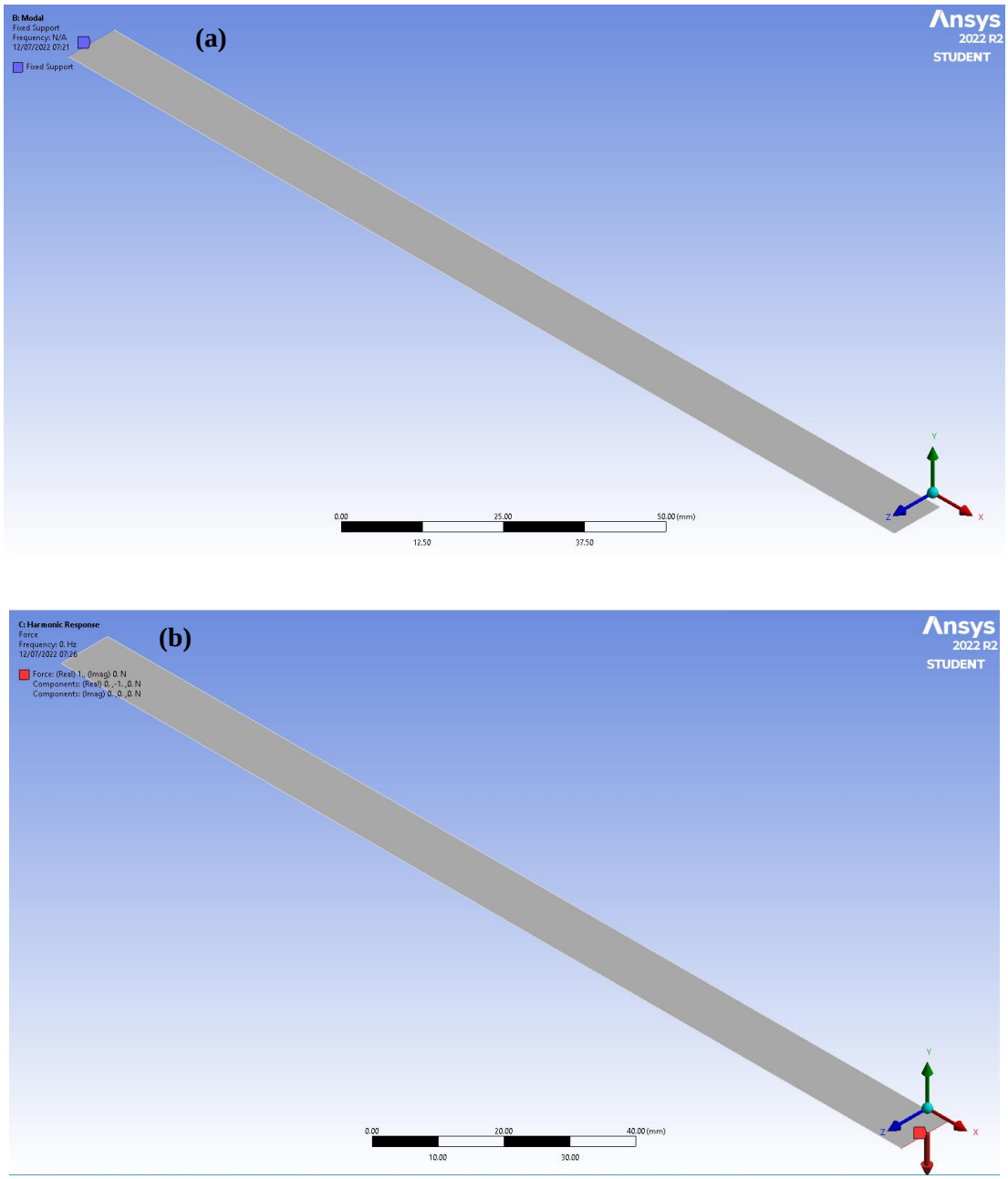

Figure 6.5. Boundary condition **(a)** and force definition **(b)** for the model.

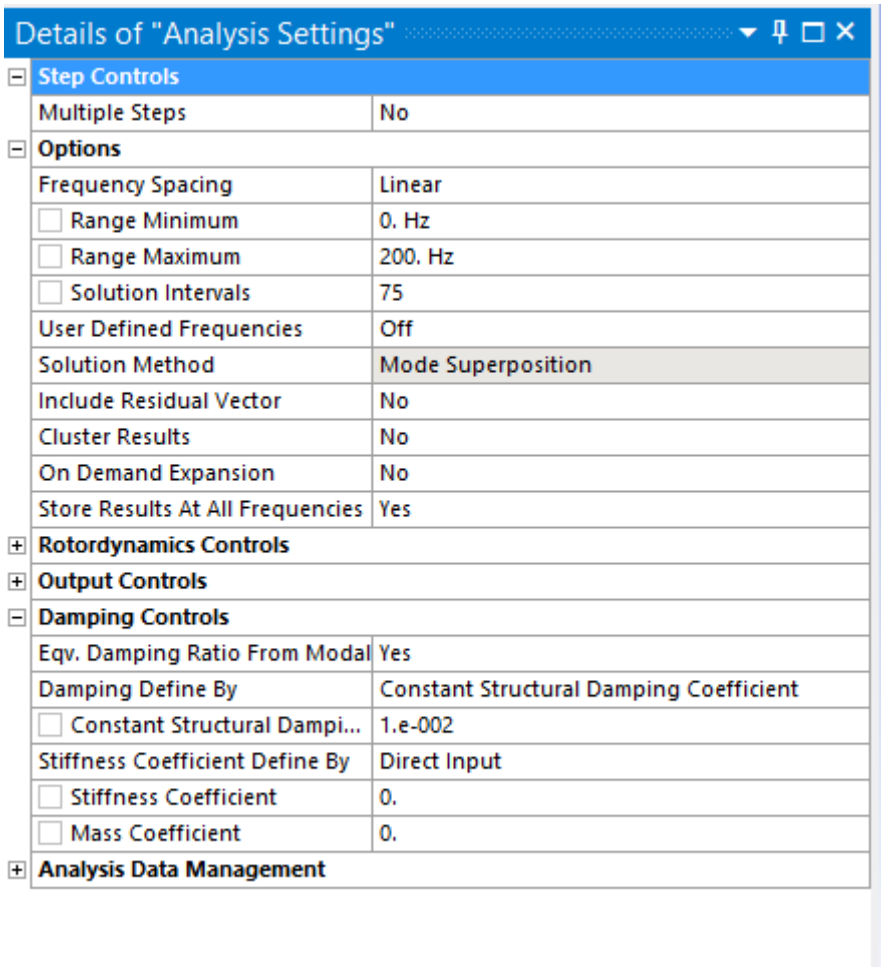

Details of "Analysis Settings"

Step Controls	
Multiple Steps	No
Options	
Frequency Spacing	Linear
Range Minimum	0. Hz
Range Maximum	200. Hz
Solution Intervals	75
User Defined Frequencies	Off
Solution Method	Mode Superposition
Include Residual Vector	No
Cluster Results	No
On Demand Expansion	No
Store Results At All Frequencies	Yes
Rotordynamics Controls	
Output Controls	
Damping Controls	
Eqv. Damping Ratio From Modal	Yes
Damping Define By	Constant Structural Damping Coefficient
Constant Structural Dampi...	1.e-002
Stiffness Coefficient Define By	Direct Input
Stiffness Coefficient	0.
Mass Coefficient	0.
Analysis Data Management	

Figure 6.6. Details of analysis settings for the harmonic analysis.

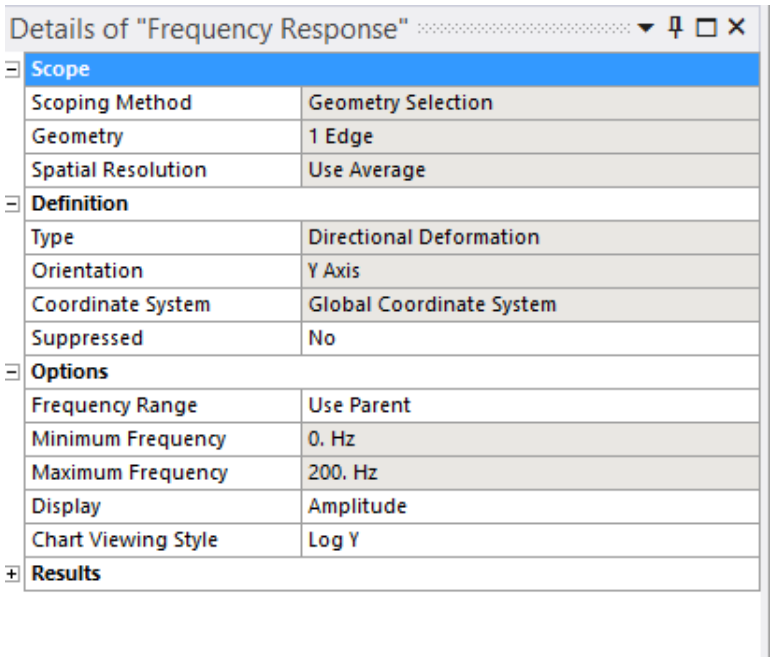

Details of "Frequency Response"

Scope	
Scoping Method	Geometry Selection
Geometry	1 Edge
Spatial Resolution	Use Average
Definition	
Type	Directional Deformation
Orientation	Y Axis
Coordinate System	Global Coordinate System
Suppressed	No
Options	
Frequency Range	Use Parent
Minimum Frequency	0. Hz
Maximum Frequency	200. Hz
Display	Amplitude
Chart Viewing Style	Log Y
Results	

Figure 6.7. Details of frequency response for the harmonic analysis.

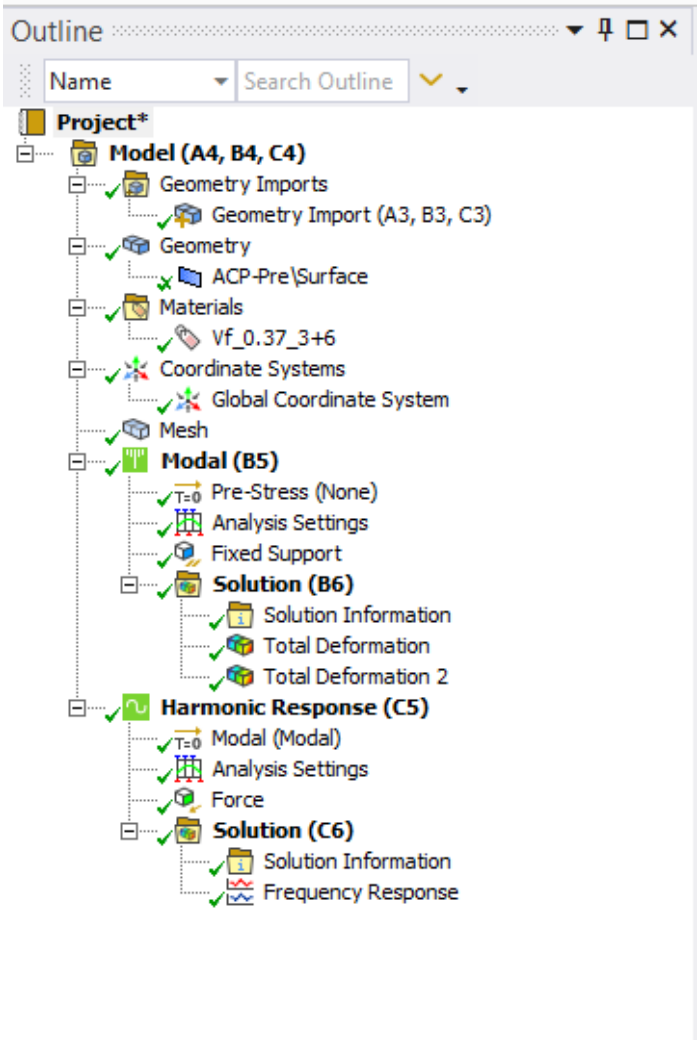

Figure 6.8. Details of the outline of the project.

6.3 RESULTS AND DISCUSSIONS

Using **eq 6.13** [142], the theoretical natural frequencies for the first two modes (associated modes for the simulated frequencies ranging from 0 to 200 Hz) were calculated:

$$f_n = \frac{h\lambda_n{}^2 (E_f)^{\frac{1}{2}}}{2\pi L^2 (12\rho)^{\frac{1}{2}}} \qquad 6.13$$

where E_f is the effective flexural modulus of the composite ($E_{rCFmatComposite}$); ρ, L, and h are the density, free length, and thickness of the composite, respectively; f_n is the natural frequency in Hertz at the nth mode; and λ_n is the corresponding coefficient

of the nth mode [for a cantilevered beam, the first five modes, $\lambda_1 = 1.87510407, \lambda_2 = 4.69409113, \lambda_3 = 7.85475744, \lambda_4 = 10.99554073, \lambda_5 = 14.13716839$] [142].

Table 6.1. Comparison of the theoretical and FEA natural frequencies for the first two modes for all studied parameters

Investigating factors	Composite laminates	Elastic modulus (GPa)	Specific elastic modulus ($\frac{\text{GPa}}{\text{Kg/m}^3}$)	Modes	FEA Natural frequency (Hz)	Theoretical Natural frequency (Hz)	% error
Effect of fiber volume fraction	(0.37Vf) (FEA-L1)	46.093	0.032	1	28.569	28.350	0.772
				2	178.990	177.640	0.760
	(0.30Vf) (FEA-L2)	38.479	0.028	1	26.500	26.300	0.760
				2	166.030	164.790	0.752
	(0.23Vf) (FEA-L3)	30.978	0.023	1	24.148	23.970	0.743
				2	151.290	150.200	0.726

Effect of fiber length combination	(T700+M46J) (3mm+3mm) (FEA-L1)	46.093	0.032	1	28.569	28.350	0.772
				2	178.990	177.640	0.760
	(T700+M46J) (3mm+6mm) (FEA-L4)	46.705	0.033	1	28.759	28.530	0.803
				2	180.180	178.810	0.766
	(T700+M46J) (6mm+3mm) (FEA-L5)	46.686	0.033	1	28.753	28.530	0.782
				2	180.140	178.780	0.761
Effect of rCF and vAF hybridization	(T700+M46J+vAF) (75+25+0) (%) (FEA-L1)	46.093	0.032	1	28.569	28.350	0.772
				2	178.990	177.640	0.760
	(T700+M46J+vAF) (50+25+25) (%) (FEA-L6)	43.344	0.031	1	28.023	27.810	0.766
				2	175.570	174.310	0.723
	(T700+M46J+vAF) (25+25+50) (%) (FEA-L7)	37.394	0.028	1	26.343	26.150	0.738
				2	165.040	163.870	0.714

Percent error (%): $\left(\frac{\text{FEA}-\text{Theoretical}}{\text{Theoretical}}\right) \times 100\%$

The relationship between the natural frequencies and specific elastic modulus (specific stiffness) for various composites is depicted in **Table 6.1**. Increasing the fiber content in composites from 23 percent to 37 percent resulted in an increase in natural frequencies (from 24.148 Hz to 28.569 Hz and 151.290 Hz to 178.990 Hz for modes 1 and 2, respectively) and an increase in the specific stiffness of the composites (that is from 0.023 $\frac{\text{GPa}}{\text{Kg/m}^3}$ to 0.032 $\frac{\text{GPa}}{\text{Kg/m}^3}$). The trend indicates that increasing the fiber content of the composites increases their specific stiffness (see **FEA-L1**, **FEA-L2**, and **FEA-L3**).

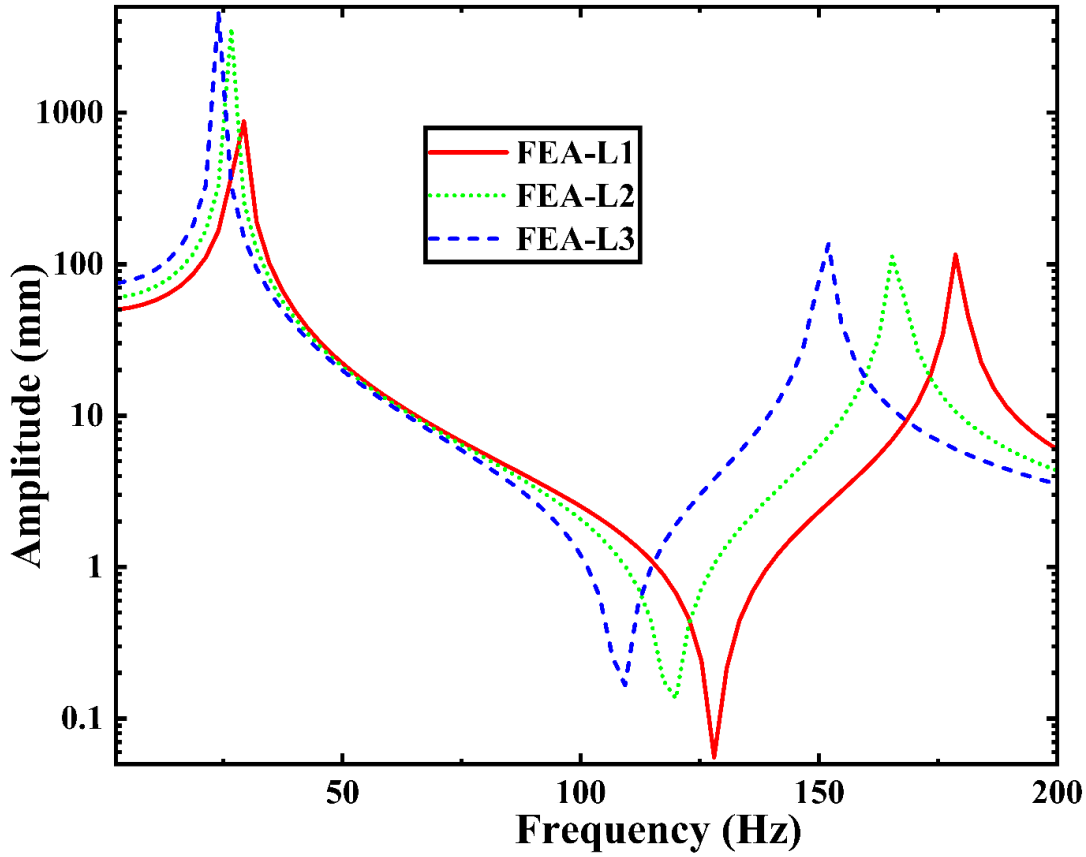

Figure 6.9. Effect of fiber volume fraction.

Regarding **Figure 6.9**, raising the composite's fiber content from 23 percent to 37 percent also increased specific stiffness (**Table 6.1**), which significantly impacted the natural frequencies by shifting the resonance peak location (see **FEA-L1**, **FEA-**

L2, and **FEA-L3**). This also resulted in lower amplitudes for modes 1 and 2, which suggests a high level of damping because increasing damping decreases the amplitude of an amplitude-frequency plot.

Regarding the effect of fiber length combination, also from **Table 6.1**, the combination of 3mm of T700 and 3mm of M46J produced a specific stiffness of 0.032 $\frac{\text{GPa}}{\text{Kg/m}^3}$; increasing the length of the M46J to 6mm while maintaining the length of the T700 at 3mm resulted in an additional increase of 0.033 $\frac{\text{GPa}}{\text{Kg/m}^3}$. This tendency was reflected in the natural frequencies of the corresponding composites: for modes 1 and 2, the natural frequencies climbed from 28.569 Hz to 28.759 Hz and from 178.990 Hz to 180.140 Hz, respectively. An increment in specific stiffness was shown to increase the natural frequencies for the two modes, with an increase in damping behavior. Increasing the fiber content from 23% to 37% is more significant for mode 1 than increasing it from 23% to 37% for mode 2.

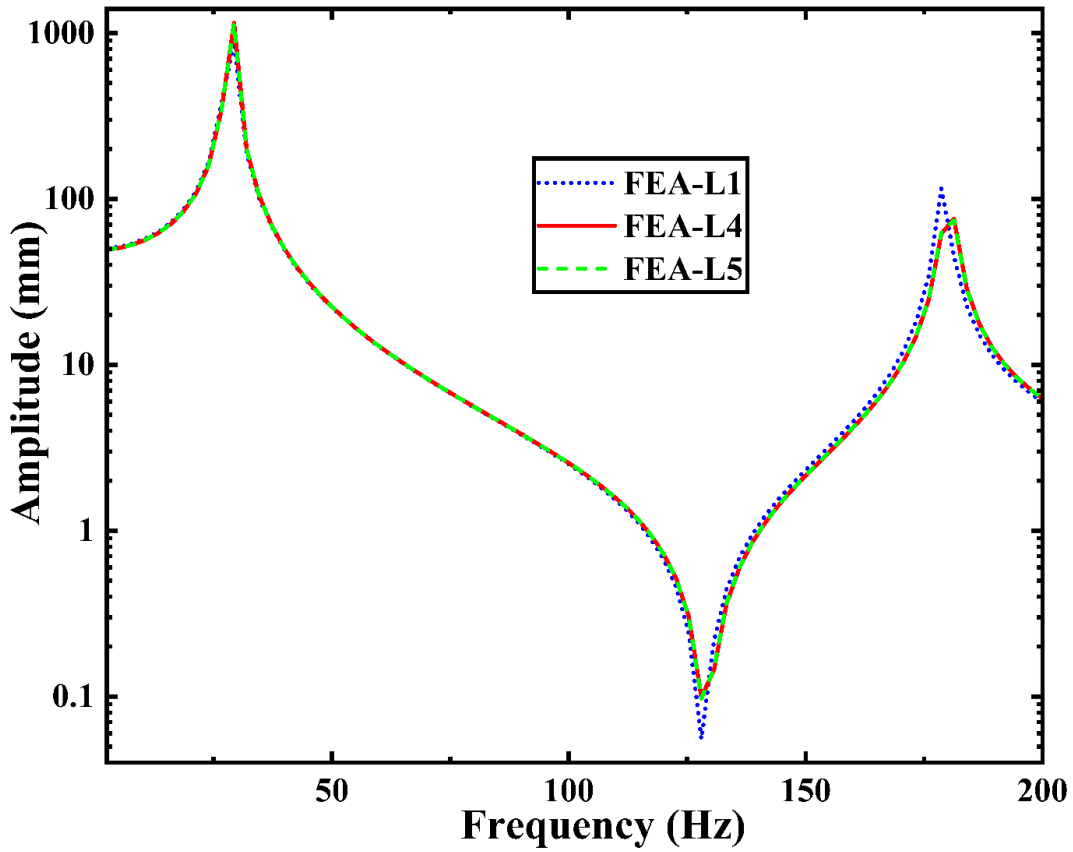

Figure 6.10. Effect of fiber length combination.

Changing the length of the T700 to 6mm and the M46J to 3mm resulted in nearly the same specific stiffness as the **(T700+M46J) (3mm+6mm)**, albeit with a slight reduction in the natural frequencies for modes 1 and 2. **Figure 6.10** depicts a similar pattern of behavior for the amplitude-frequency graph. Regarding the effect of rCF and vAF hybridization, **Table 6.1** demonstrates that the introduction of vAF into the non-woven mats had a negative synergistic effect by lowering the specific stiffness from 0.032 $\frac{\text{GPa}}{\text{Kg/m}^3}$ to 0.028 $\frac{\text{GPa}}{\text{Kg/m}^3}$ and lowering the natural frequencies for all the modes (see **FEA-L1**, **FEA-L6**, and **FEA-L7**).

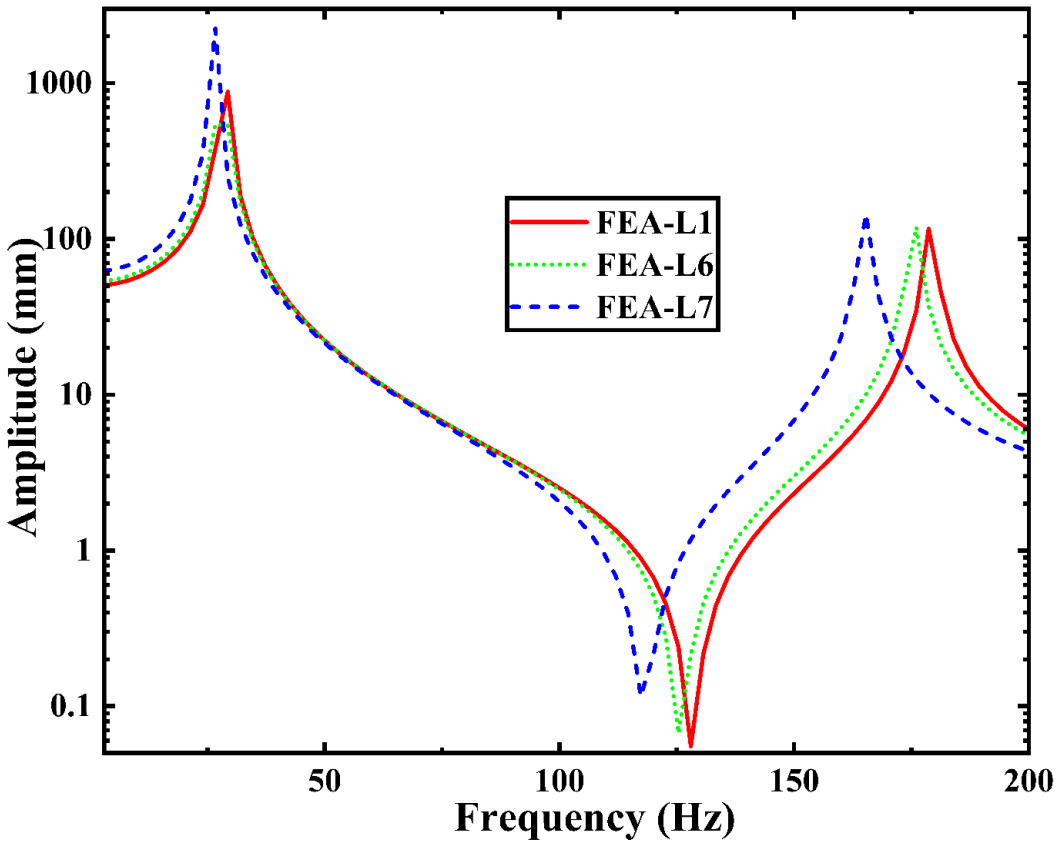

Figure 6.11. Effect of rCF and vAF hybridization.

In addition, **Figure 6.11** demonstrates that the negative synergistic effect is reflected in the peak responses of the amplitude-frequency plots; increased amplitudes are detected, indicating poor damping capabilities (see **FEA-L1**, **FEA-L6**, and **FEA-L7**).

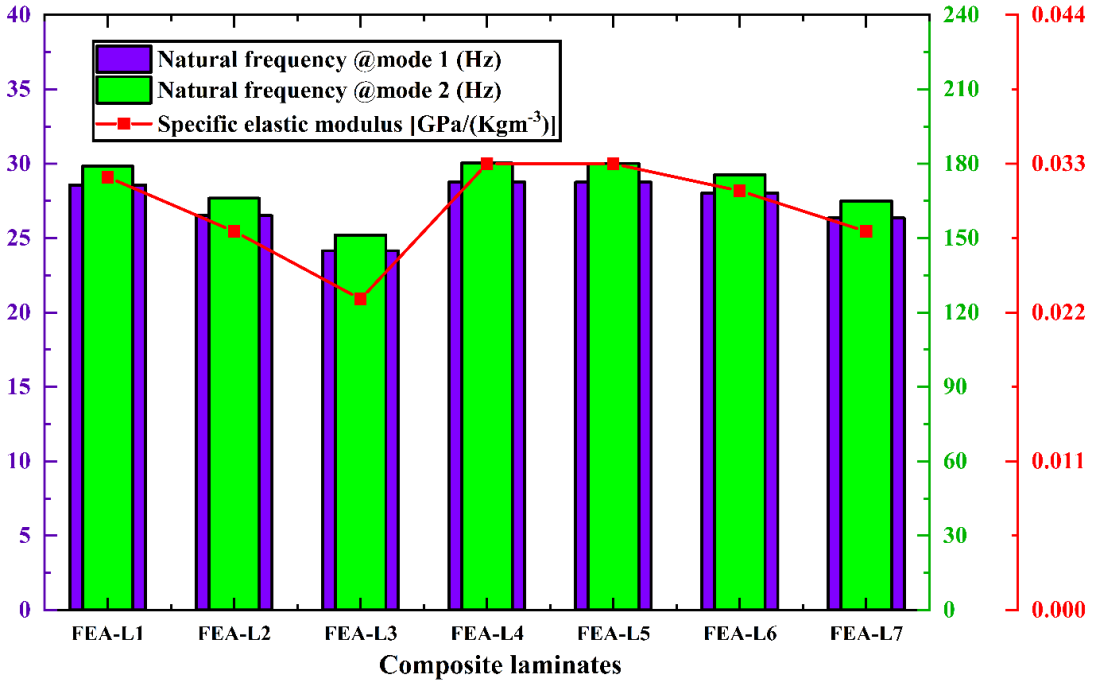

Figure 6.12. Combined effects of specific elastic modulus on the natural frequencies for modes 1 and 2.

Figure 6.12 depicts the combined effects of specific elastic modulus on the natural frequencies for modes 1 and 2. See **FEA-L1**, **FEA-L2**, and **FEA-L3** for the effect of fiber volume fraction; see **FEA-L1**, **FEA-L4**, and **FEA-L5** for the effect of fiber length combination; and see **FEA-L1**, **FEA-L6**, and **FEA-L7** for the effect of rCF and vAF hybridization. The pattern is suggestive of the observations under respective effects, and, for the two modes, the composite laminates' damping capabilities improve with increasing specific stiffness.

The mode shapes for all investigated factors were similar; hence presented are the first mode shape (first pure bending) and second mode shape (second pure bending) for the effect of fiber length combination only; therefore, respectively, **Figure 6.13**, **Figure 6.14**, and **Figure 6.15** depict the two mode shapes for modes 1 and 2 for **FEA-L1 [(T700+M46J) (3mm+3mm)]**, **FEA-L4 [(T700+M46J) (3mm+6mm)**, and **FEA-L5 [(T700+M46J) (6mm+3mm)]**.

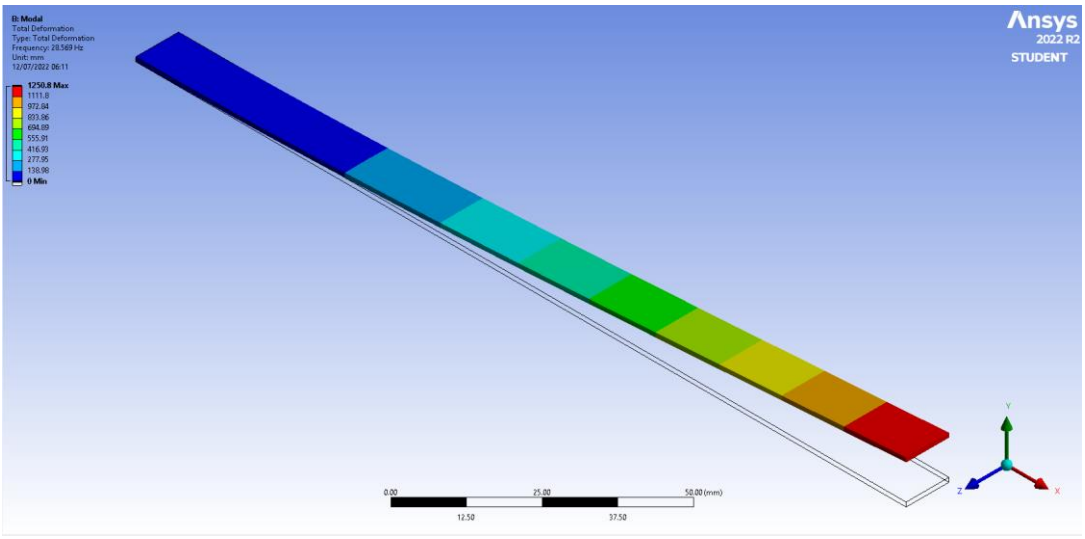

(a) first mode shape (first pure bending)

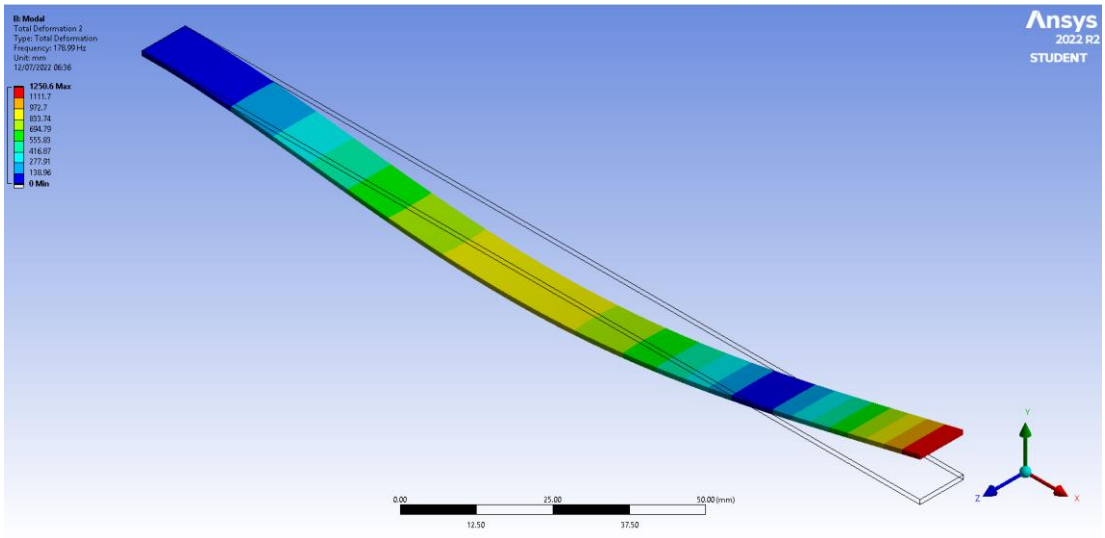

(b) second mode shape (second pure bending)

Figure 6.13. Mode shapes for FEA-L1 [(T700+M46J) (3mm+3mm)].

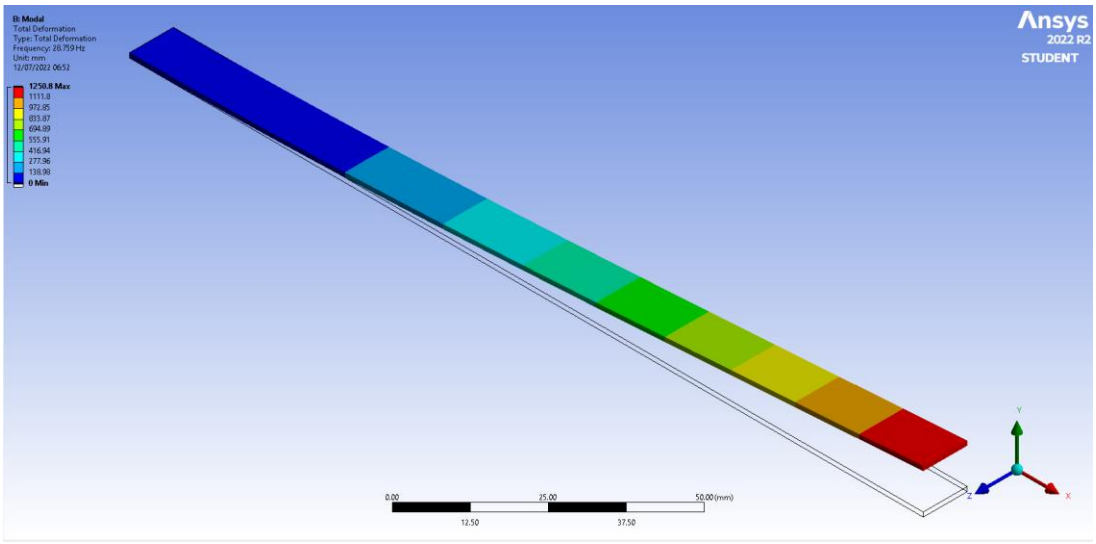

(a) first mode shape (first pure bending)

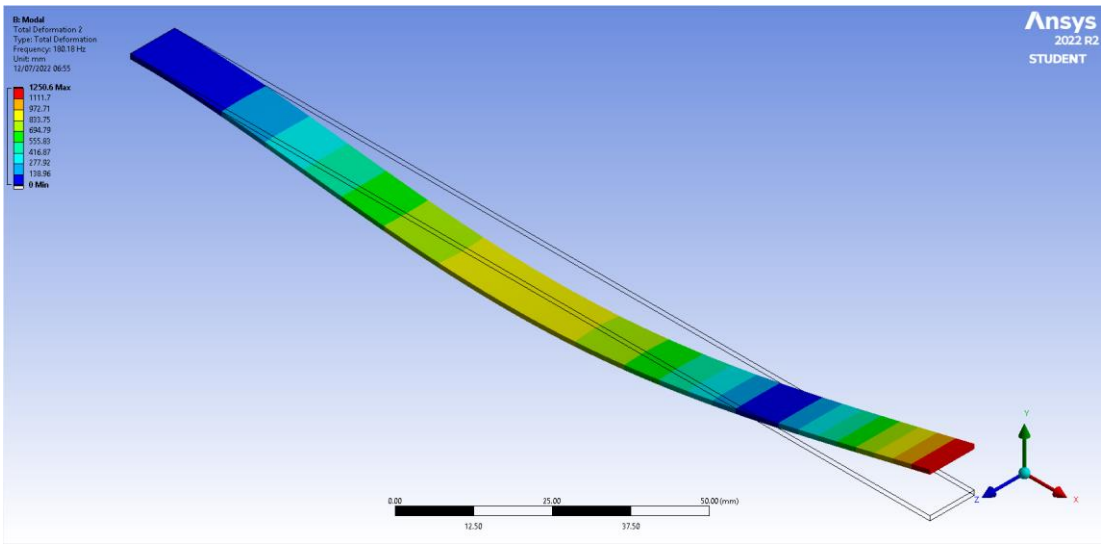

(b) second mode shape (second pure bending)

Figure 6.14. Mode shapes for FEA-L4 [(T700+M46J) (3mm+6mm)].

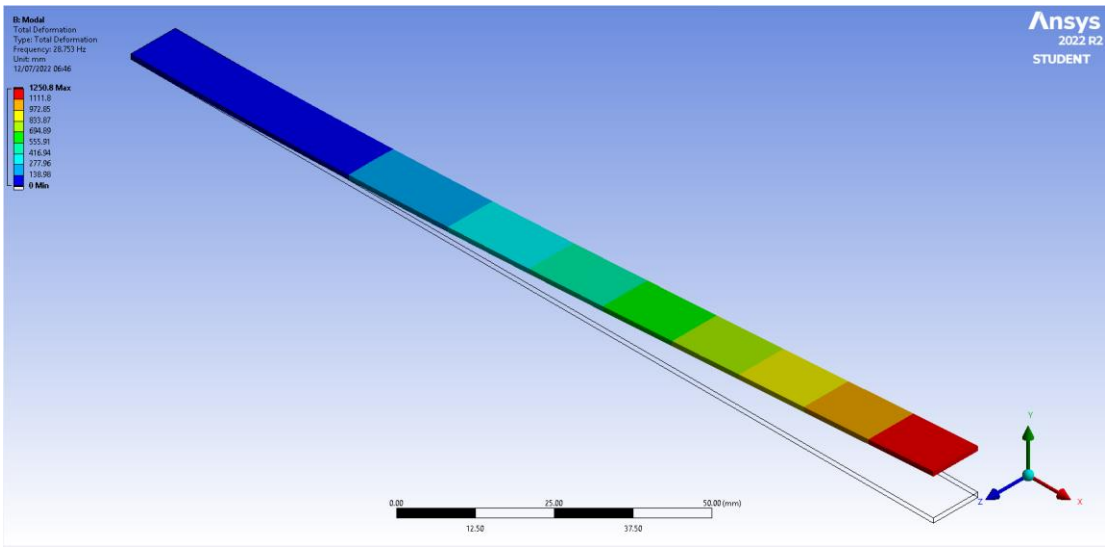

(a) first mode shape (first pure bending)

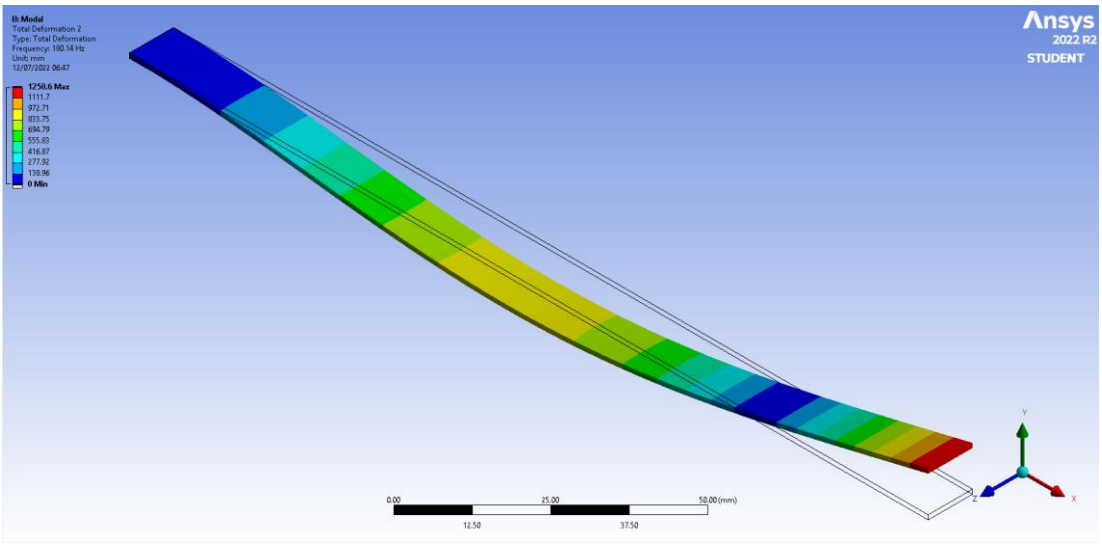

(b) second mode shape (second pure bending)

Figure 6.15. Mode shapes for FEA-L5 [(T700+M46J) (6mm+3mm)].

It is a well-known fact that any structure capable of resonating will generate small forces that can result in massive deformations that can cause induced damage to the structure. Understanding deformation behaviors (mode shapes) is therefore vital when designing structures. By examining the natural frequencies and mode shapes

(vibration characteristics), we can better understand the structure's potential dynamic responses in response to various excitations.

In a dynamic system, damping causes a loss of energy. Damping decreases the harmonic analysis's peak responses (peak responses of the amplitude-frequency plots). All observed patterns are consistent with **eq 6.13**; according to **eq 6.13**, the natural frequency is directly related to the material's stiffness and inversely proportional to its density. This means that, in general, increasing the stiffness will increase the natural frequency (by shifting the frequency to the right on an amplitude-frequency plot), while decreasing the amplitude (lower peaks) indicates a strong damping capacity.

6.4 CONCLUSION

The material properties of the designed composite laminates were predicted using micromechanical models. The dynamic behavior of the composite laminates was examined using free (modal analysis) and forced (harmonic analysis) vibrations. An equation was utilized to calculate the natural frequencies theoretically, and it was discovered that the findings of the theoretical technique for obtaining the natural frequencies coincided very well with those from the ANSYS FEA (modal analysis). The natural frequencies were identified as the resonant peaks of the dynamic response for the forced vibration (harmonic analysis) (amplitude-frequency plot). The results indicate that the composite material **(T700+M46J) (3mm+6mm)** has superior dynamic properties compared to other examined materials. It offers excellent damping capability (smaller peak in the amplitude-frequency plot for the two modes) and relatively high natural frequencies for the two modes. It is lightweight since its specific stiffness is considerably greater than other composite materials. The trend for the various designed composites was identical to that of manufactured laminates

interleaved with nonwoven mats (see **chapter 5**). The larger objective is to simultaneously increase the stiffness and damping of composite laminates destined for structural applications.

7 SUMMARY AND FUTURE WORKS

7.1 SUMMARY

This investigation sought to incorporate recycled carbon fibers into conventional virgin fibers for possible light-weight structural applications such as the trays in the aircraft's cabin, racing bicycle frames, and other suitable applications. Since, for structural applications, stiffness and damping (loss factor) are critical, there was the need to quantify these properties simultaneously. In that regard, it was imperative to escape the Ashby limit for mechanical damping/stiffness trade-off. To escape the limit as far as possible to the right-hand corner (the ideal location) when compared with the control sample, factors such as effects of the sizing agent; the effect of the interleaved rCFs mat's numbers and location/position; the effects of the recycled carbon fibers' lengths and their combinations; and the effect of the recycled carbon fiber's types and their micro-hybridization with short virgin aramid fibers were investigated. **Table 5.7** and **Table 5.8** summarize the comparison between the best composite laminate developed in this project and the best materials developed by other authors: the competitiveness of the developed composite laminate is very encouraging.

The composite laminates with the non-woven mats can be reclaimed regardless of the introduction of the vAFs since from the works of Asmatulu et al. [143], Okajima et al. [144], Yuyan et al. [145], and Chuang et al. [146], vAFs are recyclable. Notwithstanding that no literature was seen at the time of writing wherein mixed fibers (hybridized carbon and aramid fibers) were being recovered, with the pace of recycling technologies, such materials can be inescapably reclaimed soon. As seen in **Figure 5.13**, the objective of the investigations carried out in this paper has been well achieved.

Compared with the control sample, the best laminate was 54.2 % better in the figure of merit.

7.2 CONCLUSIONS

This investigation sought to incorporate recycled carbon fibers and virgin aramid fibers into conventional UD prepreg for possible light-weight structural applications and with emphasis on finding a trade-off between mechanical damping and stiffness performances (a measure for laminates' appropriateness for structural applications). The trade-off was expressed in terms of the figure of merit. The recycled carbon fibers and virgin aramid fiber were converted into non-woven mats and then interleaved with UD prepreg to form laminates via a compression molding process. Extra resin films were provided to aid the full wet-out of the mats. The effects of sizing agent content, the mat's quantity, and their location on the laminates' flexural properties, short beam strength, and dynamic performance were studied experimentally. From the experimental results obtained, the following main conclusions can be drawn:

1. The titanate coupling agent has been shown as an adequate sizing for improving interfacial adhesion of rCF and vAF mats with epoxy matrix, improving flexural properties and short beam strength. A content of 1.5 wt.% was selected for achieving the maximum flexural moduli design criteria.
2. Laminate with a single core layer of sized rCF mat showed better flexural properties and dynamic performance than those with the sized vAF mat. The attained figure of merit was 0.68 GPa, which was 15.2% higher than the control sample.

3. The flexural modulus and dynamic properties depended on the stacking sequence of the added non-woven mats. Inclusion of the mats closer to the skin region (of the UD CFRP) led to a reduction in flexural and storage moduli. The decline increased with mat quantity (increasing the number of mats).
4. On the other hand, compared with the control sample, the best laminate had a figure of merit of 0.91 GPa, which was 54.2% higher. This was achieved by interleaving the UD CFRPs with a non-woven rCF core mat made up of 75% of 3mm T700 rCFs and 25% of 6mm M46J rCFs; the laminate herein is referred to as **Laminate T**.
5. This project's guiding premise was to design nonwoven mats with higher stiffness and high damping meticulously. The non-woven mats were meticulously designed using the concept of hybridization. As stiffness is a fiber-dominated attribute, the interleaving technique was employed to insert the non-woven mats into the UD CFRP (this is done to provide extra fibers). In addition, as damping is primarily a resin-dominated feature, an adequate amount of resin must be introduced into the system. This (introducing a proper amount of resin into the system) was accomplished by sandwiching the non-woven mats between two resin films before their employment as interleaving.
6. Including non-woven mats in the UD CFRP composites substantially enhanced the stiffness and damping properties; the increment in the damping properties might be due to the interfacial friction between the fibers in the matrix resin at a microscale level.

7. Based on experimental and FEA data, the damping capacities of the evaluated composite laminates are positively correlated with the specific stiffness. This project aimed to improve the trade-off between stiffness and damping; as proven in this thesis, it is possible to use rCFs to create a composite laminate for structural applications (also known as structural damping composites).

7.3 FUTURE WORKS

Non-woven mats made of recycled carbon fibers are being produced commercially. Notably is the fiber recycling specialist ELG Carbon Fiber Ltd. (Coseley, U.K.) [147, 148]. Due to the difficulties in making consistent thicknesses of mats using the homemade rig, the effect of the non-woven mats' thicknesses was not carried out in this project (to tackle this problem, many mats were manufactured, their thicknesses taken, and the mats with similar thicknesses were then selected to manufacture the composite laminates used in the investigations carried out in this project). As a result, it is recommended that the non-woven mats should be purchased to investigate the effect of the non-woven mats' thicknesses for further work.

Additionally, further investigations such as mode-I fracture toughness (to study the resistance of the composite laminates to crack initiation and propagation) and compression after impact (CAI) (to define the damage resistance of the composite laminates after an impact event) can be carried out on the best composite laminate (**Laminate T**) in this project to gain further understandings of the developed material.

Moreover, a bolted structure of the best composite laminate (**Laminate T**) in this project can be investigated to understand the progressive damage behavior when used (the developed material) in a structural application.

REFERENCES

[1] S. Zhao, W. Liang, Z. Wang, and H. Lei, “Effect of nano-silica modification on the tensile property of SMA/gf/cf/epoxy super hybrid woven fabric composites,” *Journal of Wuhan University of Technology-Mater. Sci. Ed.*, vol. 32, no. 6, pp. 1293–1300, 2017. https://doi.org/10.1007/s11595-017-1744-1.

[2] S. Rana, and F. R. M. E. de Sousa, in *Advanced composite materials for aerospace engineering: Processing, properties and applications*, Oxford: Woodhead Publishing, 2016, pp. 1–4.

[3] V. Khanna, V. Kumar, and S. A. Bansal,2021 “Aluminium-carbon fibre metal matrix composites: a review” *IOP Conference Series: Materials Science and Engineering*, vol. 1033, pp. 012057, 2021.

[4] D. D. L. Chung, “introduction to carbon fibers,” in *Carbon Fiber Composites*, Boston: Butterworth-Heinemann, 1994, pp. 3.

[5] P. Bajpai, “Introduction,” in *Carbon Fiber*. Amsterdam: Elsevier, 2021, pp. 4.

[6] K. Acatay, “Carbon fibers,” in *Fiber technology for fiber-reinforced composites*. M. Ö. Seydibeyoğlu, A. K. Mohanty, and M. Misra, Eds., Duxford, United Kingdom: Woodhead Publishing, 2017, pp. 123–124.

[7] F. Wang, “Chapter 6 - Carbon Fibers and Their Thermal Transporting Properties,” in *Thermal transport in carbon-based nanomaterials*. G. Zhang, Ed., Amsterdam, Netherlands: Elsevier, 2017, pp. 137–139.

[8] D. He, V. K. Soo, F. Stojcevski, W. Lipiński, L. C. Henderson, P. Compston, and M. Doolan, “The effect of sizing and surface oxidation on the surface properties and

tensile behaviour of recycled carbon fibre: An end-of-life perspective," *Composites Part A: Applied Science and Manufacturing*, vol. 138, p. 106072, 2020. https://doi.org/10.1016/j.compositesa.2020.106072.

[9] S. A. Hadigheh, Y. Wei, and S. Kashi, "Optimization of CFRP composite recycling process based on energy consumption, kinetic behaviour and thermal degradation mechanism of recycled carbon fibre," *Journal of Cleaner Production*, vol. 292, p. 125994, 2021. DOI: 10.1016/j.jclepro.2021.125994.

[10] L. Low. Researchers develop improved recycling process for carbon fibers [Online]. Available: https://phys.org/news/2021-03-recycling-carbon-fibers.html. [Accessed: 19-Jul-2022].

[11] S. Francis. The state of Recycled Carbon Fiber [Online]. Available: https://www.compositesworld.com/articles/the-state-of-recycled-carbon-fiber. [Accessed: 19-Jul-2022].

[12] A. K. Bledzki, H. Seidlitz, K. Goracy, M. Urbaniak, and J. J. Rösch, "Recycling of carbon fiber reinforced composite polymers—review—part 1: Volume of production, Recycling Technologies, legislative aspects," *Polymers*, vol. 13, no. 2, p. 300, 2021. https://doi.org/10.3390/polym13020300.

[13] C. Cherif, O. Diestel, T. Engler, E. Hufnagl, and S. Weiland. "Processing Aspects and Application Examples," in *Textile Materials for Lightweight Constructions-methods - materials – properties*. C. Cherif, Ed., Berlin, Heidelberg: Springer, 2016, pp. 599–661. https://doi.org/10.1007/978-3-662-46341-3_16.

[14] C. C. Chamis, and R. F. Lark, "Hybrid composites - State-of-the-art review: Analysis, design, application and fabrication" in *Proc. AIAA-18-18th Struct. Dyn.*

Mater. Conf., San Diego, CA, U.S.A, 21st-23rd March 1977, pp. 311-331. AIAA-P-77-415.

[15] A. Pegoretti, E. Fabbri, C. Migliaresi, and F. Pilati, "Intraply and interply hybrid composites based on E-glass and poly(vinyl alcohol) woven fabrics: Tensile and impact properties," *Polymer International*, vol. 53, no. 9, pp. 1290–1297, 2004.

[16] D. K. Rajak, P. H. Wagh, and E. Linul, "Manufacturing Technologies of carbon/glass fiber-reinforced polymer composites and their properties: A Review," *Polymers*, vol. 13, no. 21, pp. 3721, 2021.

[17] P. Dharmavarapu, and S. R. M.B.S, "Aramid fibre as potential reinforcement for Polymer Matrix Composites: A Review," *Emergent Materials*, 2021.

[18] S. J. Pickering, Z. Liu, T. A. Turner, and K. H. Wong, "Applications for carbon fibre recovered from Composites," *IOP Conference Series: Materials Science and Engineering*, vol. 139, pp. 012005, 2016.

[19] G. Oliveux, L. O. Dandy, and G. A. Leeke, "Current status of recycling of fibre reinforced polymers: Review of technologies, Reuse and resulting properties," *Progress in Materials Science*, vol. 72, pp. 61–99, 2015.

[20] J. Zhang, V. S. Chevali, H. Wang, and C.-H. Wang, "Current status of carbon fibre and Carbon Fibre Composites Recycling," *Composites Part B: Engineering*, vol. 193, pp. 108053, 2020.

[21] S. Melendi-Espina, C. Morris, T. Turner, and S. Pickering, "Recycling of carbon fibre composites," in *Proc. World Conf. on Carbon (Carbon 2016),* State College, Pennsylvania, USA, 10th - 15th July 2016, pp.1351-1359.

[22] K. Wong, C. Rudd, S. Pickering, and X. L. Liu, “Composites recycling solutions for the aviation industry,” *Science China Technological Sciences*, vol. 60, no. 9, pp. 1291–1300, 2017.

[23] S. Karuppannan Gopalraj and T. Kärki, “A review on the recycling of waste carbon fibre/glass fibre-reinforced composites: Fibre Recovery, properties and life-cycle analysis,” *SN Applied Sciences*, vol. 2, no. 3, 2020.

[24] V. M. Karbhari, “The use of composites in civil structural applications,” in *Durability of composites for civil structural applications*. Cambridge, UK: Woodhead Publishing, 2007, pp. 1–10.

[25] M. K. Chryssanthopoulos, L. Hollaway, and S. S. J. Moy, “Durability of advanced polymer composites in the civil infrastructure,” in *Advanced polymer composites for structural applications in construction: Proceedings of the second international conference,* S. S. J. Moy, Ed., Cambridge, UK: Woodhead Publishing, 2004, pp. 30–42.

[26] B. Wang, S. Ma, S. Yan, and J. Zhu, “Readily recyclable carbon fiber reinforced composites based on degradable thermosets: A Review,” *Green Chemistry*, vol. 21, no. 21, pp. 5781–5796, 2019.

[27] E. Pakdel, S. Kashi, R. Varley, and X. Wang, “Recent progress in recycling carbon fibre reinforced composites and dry carbon fibre wastes,” *Resources, Conservation and Recycling*, vol. 166, pp. 105340, 2021.

[28] D. May, C. Goergen, and K. Friedrich, “Multifunctionality of polymer composites based on recycled carbon fibers: A Review,” *Advanced Industrial and Engineering Polymer Research*, vol. 4, no. 2, pp. 70–81, 2021.

[29] S. Pimenta, S. T. Pinho, P. Robinson, K. H. Wong, and S. J. Pickering, “Mechanical analysis and toughening mechanisms of a multiphase recycled CFRP,” *Composites Science and Technology*, vol. 70, no. 12, pp. 1713–1725, 2010.

[30] J. Wölling, M. Schmieg, F. Manis, and K. Drechsler, “Nonwovens from recycled carbon fibres – comparison of processing technologies,” *Procedia CIRP*, vol. 66, pp. 271–276, 2017.

[31] H. Wei, W. Nagatsuka, H. Lee, I. Ohsawa, K. Sumimoto, Y. Wan, and J. Takahashi, “Mechanical properties of carbon fiber paper reinforced thermoplastics using mixed discontinuous recycled carbon fibers,” *Advanced Composite Materials*, vol. 27, no. 1, pp. 19–34, 2017.

[32] F. Meng, J. McKechnie, T. A. Turner, and S. J. Pickering, “Energy and Environmental Assessment and reuse of fluidised bed recycled carbon fibres,” *Composites Part A: Applied Science and Manufacturing*, vol. 100, pp. 206–214, 2017.

[33] K. H. Wong, T. A. Turner, S. J. Pickering, and N. A. Warrior, “The potential for fibre alignment in the manufacture of polymer composites from recycled carbon fibre,” *SAE International Journal of Aerospace*, vol. 2, no. 1, pp. 225–231, 2009.

[34] N. van de Werken, M. S. Reese, M. R. Taha, and M. Tehrani, “Investigating the effects of fiber surface treatment and alignment on mechanical properties of recycled carbon fiber composites,” *Composites Part A: Applied Science and Manufacturing*, vol. 119, pp. 38–47, 2019.

[35] S. Y. Fu, B. Lauke, and Y.-W. Mai, in *Science and Engineering of Short Fibre Reinforced Polymer Composites*. Cambridge, UK: Woodhead Publishing, 2009, pp. 29.

[36] N. Shah, J. Fehrenbach, and C. A. Ulven, “Hybridization of hemp fiber and recycled-carbon fiber in polypropylene composites,” *Sustainability*, vol. 11, no. 11, pp. 3163, 2019.

[37] B. Tse, X. Yu, H. Gong, and C. Soutis, “Flexural properties of wet-laid hybrid nonwoven recycled carbon and flax fibre composites in poly-lactic acid matrix,” *Aerospace*, vol. 5, no. 4, pp. 120, 2018.

[38] J. Bachmann, M. Wiedemann, and P. Wierach, “Flexural mechanical properties of hybrid epoxy composites reinforced with nonwoven made of flax fibres and recycled carbon fibres,” *Aerospace*, vol. 5, no. 4, pp. 107, 2018.

[39] H. Ebrahimnezhad-Khaljiri, R. Eslami-Farsani, and E. Akbarzadeh, “Effect of interlayer hybridization of carbon, kevlar, and glass fibers with oxidized polyacrylonitrile fibers on the mechanical behaviors of hybrid composites,” *Proceedings of the Institution of Mechanical Engineers, Part C: Journal of Mechanical Engineering Science*, vol. 234, no. 9, pp. 1823–1835, 2019.

[40] N. Ni, Y. Wen, D. He, X. Yi, T. Zhang, and Y. Xu, “High damping and high stiffness CFRP composites with Aramid non-woven Fabric Interlayers,” *Composites Science and Technology*, vol. 117, pp. 92–99, 2015.

[41] D. W. Y. Wong, H. Zhang, E. Bilotti, and T. Peijs, “Interlaminar toughening of woven fabric carbon/epoxy composite laminates using hybrid aramid/phenoxy interleaves,” *Composites Part A: Applied Science and Manufacturing*, vol. 101, pp. 151–159, 2017.

[42] F. Cheng, Y. Hu, B. Yuan, X. Hu, and Z. Huang, “Transverse and longitudinal flexural properties of unidirectional carbon fiber composites interleaved with

hierarchical aramid pulp micro/nano-fibers," *Composites Part B: Engineering*, vol. 188, pp. 107897, 2020.

[43] R. S. Lakes, "High damping composite materials: Effect of structural hierarchy," *Journal of Composite Materials*, vol. 36, no. 3, pp. 287–297, 2002.

[44] N. Ni, Y. Wen, D. He, X. Yi, Z. Zhao, and Y. Xu, "Synchronous improvement of loss factors and storage modulus of structural damping composite with functionalized Polyamide nonwoven fabrics," *Materials & Design*, vol. 94, pp. 377–383, 2016.

[45] T. Jaglinski and R. S. Lakes, "Zn–al-based metal–matrix composites with high stiffness and high viscoelastic damping," *Journal of Composite Materials*, vol. 46, no. 7, pp. 755–763, 2011.

[46] Y. C. Wang, M. Ludwigson, and R. S. Lakes, "Deformation of extreme viscoelastic metals and composites," *Materials Science and Engineering: A*, vol. 370, no. 1-2, pp. 41–49, 2004.

[47] M. F. Ashby, in *Materials selection in mechanical design*. Amsterdam; The Netherlands: Elsevier, 2011, pp. 76–77.

[48] A. P. Unwin, P. J. Hine, I. M. Ward, M. Fujita, E. Tanaka, and A. A. Gusev, "Escaping the Ashby limit for mechanical damping/stiffness trade-off using a constrained high internal friction interfacial layer," *Scientific Reports*, vol. 8, no. 1, 2018.

[49] D. D. L. Chung, "Review: Materials for vibration damping," *Journal of Materials Science*, vol. 36, no. 24, pp. 5733–5737, 2001.

[50] K. P. Menard, in *Dynamic Mechanical Analysis: A practical introduction*. Boca Raton, FL, USA: CRC Press, 2008, pp. 71–76.

[51] J. Meaud, T. Sain, G. M. Hulbert, and A. M. Waas, “Analysis and optimal design of layered composites with high stiffness and high damping,” *International Journal of Solids and Structures*, vol. 50, no. 9, pp. 1342–1353, 2013.

[52] I. C. Finegan and R. F. Gibson, “Recent research on enhancement of damping in polymer composites,” *Composite Structures*, vol. 44, no. 2-3, pp. 89–98, 1999.

[53] A. Treviso, B. Van Genechten, D. Mundo, and M. Tournour, “Damping in composite materials: Properties and models,” *Composites Part B: Engineering*, vol. 78, pp. 144–152, 2015.

[54] Y. Ma, M. Ueda, T. Yokozeki, T. Sugahara, Y. Yang, and H. Hamada, “Investigation of the flexural properties and failure behavior of unidirectional CF/Nylon 6 and CF/Epoxy Composites,” *Open Journal of Composite Materials*, vol. 07, no. 04, pp. 227–249, 2017.

[55] M. Kumar, H. Kumar, Lokeshwaran, Aravindasan, and A. Kumar, “Influence of stacking sequence and thickness on the free vibrational behaviour of carbon/epoxy laminates,” *Materials Today: Proceedings*, vol. 5, no. 2, pp. 7701–7707, 2018.

[56] M. Rajesh, S. P. Singh, and J. Pitchaimani, “Mechanical behavior of woven natural fiber fabric composites: Effect of weaving architecture, intra-ply hybridization and stacking sequence of fabrics,” *Journal of Industrial Textiles*, vol. 47, no. 5, pp. 938–959, 2016.

[57] C. Dong and I. J. Davies, “Effect of stacking sequence on the flexural properties of carbon and glass fibre-reinforced hybrid composites,” *Advanced Composites and Hybrid Materials*, vol. 1, no. 3, pp. 530–540, 2018.

[58] C. Bennet, N. Rajini, J. T. W. Jappes, I. Siva, V. S. Sreenivasan, and S. C. Amico, "Effect of the stacking sequence on vibrational behavior of Sansevieria cylindrica/coconut sheath polyester hybrid composites," *Journal of Reinforced Plastics and Composites*, vol. 34, no. 4, pp. 293–306, 2015.

[59] I. D. G. Ary Subagia, Y. Kim, L. D. Tijing, C. S. Kim, and H. K. Shon, "Effect of stacking sequence on the flexural properties of hybrid composites reinforced with carbon and basalt fibers," *Composites Part B: Engineering*, vol. 58, pp. 251–258, 2014.

[60] T. Wang, B. Song, K. Qiao, C. Ding, and L. Wang, "Influence of the hybrid ratio and stacking sequence on mechanical and damping properties of hybrid composites," *Polymer Composites*, vol. 40, no. 6, pp. 2368–2380, 2018.

[61] T. E. Alberts and H. Xia, "Design and analysis of fiber enhanced viscoelastic damping polymers," *Journal of Vibration and Acoustics*, vol. 117, no. 4, pp. 398–404, 1995.

[62] J.-M. Berthelot and Y. Sefrani, "Damping analysis of unidirectional glass fiber composites with interleaved viscoelastic layers: Experimental investigation and discussion," *Journal of Composite Materials*, vol. 40, no. 21, pp. 1911–1932, 2006.

[63] C. Capela, S. E. Oliveira, J. Pestana, and J. A. M. Ferreira, "Effect of fiber length on the mechanical properties of high dosage carbon reinforced," *Procedia Structural Integrity*, vol. 5, pp. 539–546, 2017.

[64] S. Jlassi, F. Berthet, G. Bernhart, "Investigation of mechanical properties of non-woven second generation composite material elaborated through a mixture of carbon fibers and filament lengths," in *Proc. ECCM18 - 18th Eur. Conf. Compos. Mater.*, Athènes, Greece, Greece, 24th-28th June 2018, 8 pp. hal-01862432.

[65] S. A. Suarez, R. F. Gibson, C. T. Sun, and S. K. Chaturvedi, “The influence of fiber length and fiber orientation on damping and stiffness of polymer composite materials,” *Experimental Mechanics*, vol. 26, no. 2, pp. 175–184, 1986.

[66] G. Pincheira, C. Canales, C. Medina, E. Fernández, and P. Flores, “Influence of aramid fibers on the mechanical behavior of a hybrid carbon–aramid–reinforced epoxy composite,” *Proceedings of the Institution of Mechanical Engineers, Part L: Journal of Materials: Design and Applications*, vol. 232, no. 1, pp. 58–66, 2015.

[67] T. Karthik, R. Rathinamoorthy, and C. P. Karan, in *Nonwovens: Process, structure, properties and applications*. New Delhi, India: Woodhead Publishing India PVT Ltd, 2016, pp. 2.

[68] K. H. Wong, S. J. Pickering, and C. D. Rudd, “Recycled carbon fibre reinforced polymer composite for electromagnetic interference shielding,” *Composites Part A: Applied Science and Manufacturing*, vol. 41, no. 6, pp. 693–702, 2010.

[69] P. Bajpai, in *Pulp and Paper Industry: Microbiological Issues in papermaking*. Amsterdam, The Netherlands: Elsevier, 2016, pp. 4–15.

[70] M. Hendricks, “Consistency Measurement and Control In a Tissue Mill-The Often Neglected Parameter,” in *Proc. PaperCon*, Northern Kentucky Convention Center, Covington, Kentucky, USA, 1st - 4th May 2011, pp. 1878-1893.

[71] R. J. Kerekes, “Rheology of suspensions,” *Nordic Pulp & Paper Research Journal*, vol. 21, no. 5, pp. 598–612, 2006.

[72] H. Cai, Z. Yuan, X. Zhang, S. Jun, H. Zhang, and J. Olson, "The influence of consistency and fibre length on the yield stress of OCC pulp fibre suspensions," *BioResources*, vol. 12, no. 4, pp. 8368-8377, 2017.

[73] P. Huber, J. C. Roux, J.C., E. Mauret, N. Belgacem, and C. Pierre, " Suspension crowding for a general fibre-length distribution: application to flocculation of mixtures of short and long papermaking fibres," *Journal of Pulp and Paper Science*, vol. 29, no. 3, pp. 77-85, 2003.

[74] J. Hämäläinen, T. Hämäläinen, T. Leppänen, H. Niskanen, and J. Sorvari, "Mathematics in paper - from fiber suspension fluid dynamics to solid state paper mechanics," *Journal of Mathematics in Industry*, vol. 4, no. 1, pp. 14, 2014.

[75] F. Lundell, L. D. Söderberg, and P. H. Alfredsson, "Fluid Mechanics of Papermaking," *Annual Review of Fluid Mechanics*, vol. 43, no. 1, pp. 195–217, 2011.

[76] K. H. Wong, "*Use of recycled carbon fibre for electromagnetic interference shielding*," PhD Thesis, Dept. of Mech., Mater. and Manufact. Eng., Univ. of Nottingham, Nottingham, UK, 2006, pp. 4-1 – 4-3.

[77] G. Pritchard, "Coupling agents," in *Plastics additives: An A-Z reference.* G. Pritchard, Ed., Dordrecht, The Netherlands: Springer, 1998, pp. 189.

[78] S. J. Monte. Why Titanates and Zirconates May Be Better Adhesion Promoters Than Silanes [Online]. Available: https://4kenrich.com/wp-content/uploads/2020/05/CAMX-2020-why-titanates-zirconates-are-differeent-than-silanes.pdf. [Accessed: 9-Feb-2022].

[79] N. Menon, F. D. Blum, and L. R. Dharani, "Use of titanate coupling agents in Kevlar–phenolic composites," *Journal of Applied Polymer Science*, vol. 54, no. 1, pp. 113–123, 1994.

[80] N. A. N. Alkadasi, B. D. Sarwade, D. G. Hundiwale, and U. R. Kapadi, "Studies on the effect of titanate coupling agent (2.0%) on the mechanical properties of flyash-

filled polybutadiene rubber," *Journal of Applied Polymer Science*, vol. 93, no. 3, pp. 1293–1298, 2004.

[81] S. Pimenta and S. T. Pinho, "Recycling carbon fibre reinforced polymers for structural applications: Technology Review and market outlook," *Waste Management*, vol. 31, no. 2, pp. 378–392, 2011.

[82] M. M. Nazhad, E. J. Harris, C. T. Dodson, and R. J. Kerekes, "The influence of formation on tensile strength of paper made from mechanical pulps," *Tappi Journal*, vol. 83, no. 12, pp. 63–68, 2000.

[83] M. A. Hubbe and A. A. Koukoulas, "Wet-laid nonwovens manufacture – chemical approaches using synthetic and cellulosic fibers," *BioResources*, vol. 11, no. 2, pp. 5500-5552, 2016.

[84] F. C. Campbell, in *Manufacturing Processes for Advanced Composites*. Amsterdam, The Netherlands: Elsevier, 2007, pp. 399–401.

[85] N. Yang, in *Composite materials engineering*. X.-S. Yi et al., Ed., Singapore, Singapore: Springer, 2018, pp. 13–15. DOI: 10.1007/978-981-10-5690-1_1.

[86] K. N. Shivakumar, R. Panduranga, and M. Sharpe, "Interleaved Polymer Matrix Composites - A Review," in *Proc. 54th AIAA/ASME/ASCE/AHS/ASC Struct., Struct. Dyn., and Mater. Conf.*, Boston, USA, April 2013, pp.1-13.

[87] M. K. Buragohain, in *Composite structures: Design, mechanics, analysis, manufacturing, and testing*, Boca Raton, FL, USA: Taylor & Francis Group, LLC, 2018, pp. 518. DOI: 10.1201/9781315268057.

[88] P. K. Mallick, in *Materials, design and manufacturing for Lightweight Vehicles.* Duxford, UK: Woodhead Publishing, 2010, pp. 227–227.

[89] W. Woigk, K. Masania, F. Stork, A. Heusi, E. Poloni, and A. R. Studart, “Bio-inspired platelet-reinforced polymers with enhanced stiffness and damping behavior,” *ACS Applied Polymer Materials*, vol. 2, no. 8, pp. 3557–3565, 2020.

[90] K. P. Menard, and N. R. Menard, “Dynamic Mechanical Analysis in the Analysis of Polymers and Rubbers,” in *Encyclopedia of Polymer Science and Technology*. New York, NY, USA: Wiley, 2015, pp. 1–5, doi: 10.1002/0471440264.pst102.pub2.

[91] K. P. Menard, in *Dynamic Mechanical Analysis: A practical introduction*. Boca Raton, FL, USA: CRC Press, 1999, pp. 3.

[92] P. Gabbott, in *Principles and applications of thermal analysis*. Oxford, UK: Blackwell, 2008, pp. 131–134.

[93] I. R. Henriques, L. A. Borges, M. F. Costa, B. G. Soares, and D. A. Castello, “Comparisons of complex modulus provided by different DMA,” *Polymer Testing*, vol. 72, pp. 394–406, 2018.

[94] *ASTM D5023-15 Test method for plastics: Dynamic Mechanical Properties: In Flexure (three-point bending)*, ASTM International, West Conshohocken, PA, USA, 2015.

[95] C. Matthews, in *Engineers' data book*. Oxford, USA: Wiley-Blackwell, 2012, pp. 72–75.

[96] *ASTM D790-20 Test methods for flexural properties of unreinforced and reinforced plastics and electrical insulating materials*, ASTM International, West Conshohocken, PA, USA, 2020.

[97] *ASTM D2344 / D2344M-16 Test method for short-beam strength of polymer matrix composite materials and their laminates*, ASTM International, West Conshohocken, PA, USA, 2016.

[98] A. A. Shabana, in *Theory of vibration an introduction*. Cham, Switzerland: Springer International, 2019, pp. 69.

[99] R. N. Jazar, in *Vehicle Dynamics Theory and Application*. Cham, Switzerland: Springer International, 2018, pp. 734.

[100] P. Avitabile, in *Modal Testing: A practitioner's guide*. Hoboken, NJ, USA: Wiley, 2018, pp. 17–18.

[101] *ASTM E756-05 Test method for measuring vibration-damping properties of materials*, ASTM International, West Conshohocken, PA, USA, 2017.

[102] W. T. Thomson, and M. D. Dahleh, in *Theory of vibrations with applications*, Harlow, Essex, UK: Pearson, 2020, pp. 31–33. ISBN-13: 978-0136510680.

[103] Y. C. Wang, M. Ludwigson, and R. S. Lakes, "Deformation of extreme viscoelastic metals and composites," *Materials Science and Engineering: A*, vol. 370, no. 1-2, pp. 41–49, 2004.

[104] *ASTM D3171-15 Standard Test Methods for Constituent Content of Composite Materials*, ASTM International, West Conshohocken, PA, USA,2015. DOI: 10.1520/D3171-15.

[105] N. Abidi, "Introduction to FTIR Microspectroscopy," in *FTIR microspectroscopy: Selected emerging applications*. Cham: Springer International Publishing AG, 2022, pp. 1–11. https://doi.org/10.1007/978-3-030-84426-4_1.

[106] Y. Swolfs, L. Gorbatikh, and I. Verpoest, “Fibre hybridisation in Polymer Composites: A Review,” *Composites Part A: Applied Science and Manufacturing*, vol. 67, pp. 181–200, 2014.

[107] T. J. Singh and S. Samanta, “Characterization of kevlar fiber and its composites: A Review,” *Materials Today: Proceedings*, vol. 2, no. 4-5, pp. 1381–1387, 2015.

[108] S. G. Annapoorani, in *Agro textiles and its applications*, New Delhi: Woodhead Publishing India, 2018, pp. 70–70.

[109] Gibson, in *Cellular solids: Structure and properties*, Cambridge University Press, UK, 1997, pp. 345–345.

[110] B. Zhang, L. Jia, M. Tian, N. Ning, L. Zhang, and W. Wang, “Surface and interface modification of aramid fiber and its reinforcement for Polymer Composites: A Review,” *European Polymer Journal*, vol. 147, pp. 110352, 2021.

[111] N. W. Elshereksi, M. Ghazali, A. Muchtar, and C. H. Azhari, “Review of titanate coupling agents and their application for dental composite fabrication,” *Dental Materials Journal*, vol. 36, no. 5, pp. 539–552, 2017.

[112] S. Bose and P. A. Mahanwar, “Effects of titanate coupling agent on the properties of mica-reinforced nylon-6 composites,” *Polymer Engineering & Science*, vol. 45, no. 11, pp. 1479–1486, 2005.

[113] R. Hagen, L. Salmén, H. Lavebratt, and B. Stenberg, “Comparison of dynamic mechanical measurements and TG determinations with two different instruments,” *Polymer Testing*, vol. 13, no. 2, pp. 113–128, 1994. DOI: 10.1016/0142-9418(94)90020-5.

[114] K. P. Menard, in *Dynamic Mechanical Analysis: A practical introduction*, Boca Raton, FL: CRC Press, 2008, pp. 101–104.

[115] J. C. Qiao, Y. H. Chen, R. Casalini, J. M. Pelletier, and Y. Yao, "Main α relaxation and slow β relaxation processes in a la30ce30al15co25 metallic glass," *Journal of Materials Science & Technology,* vol. 35, no. 6, pp. 982–986, 2019.

[116] S. Ibraheem, and S. Bandyopadhyay, "A review of the structure property research on hybrid-reinforced polymer composites," in *Hybrid polymer composite materials: Structure and Chemistry*, V. K. Thakur, M. K. Thakur, and R. K. Gupta Ed., Duxford, UK: Woodhead Publishing, 2017, pp. 165–165. DOI: 10.1016/B978-0-08-100791-4.00007-0.

[117] J.-M. Berthelot and Y. Sefrani, "Damping analysis of unidirectional glass and Kevlar Fibre Composites," *Composites Science and Technology,* vol. 64, no. 9, pp. 1261–1278, 2004.

[118] F.-J. Wortmann and K. Schulz, "Nonlinear viscoelastic stress relaxation behaviour of aramid fibers," *Makromolekulare Chemie. Macromolecular Symposia,* vol. 50, no. 1, pp. 55–65, 1991.

[119] L. Balis Crema, A. Castellani, and U. Drago, "Damping characteristics of fabric and laminated Kevlar Composites," *Composites,* vol. 20, no. 6, pp. 517, 1989.

[120] M. Z. Rahman, "Mechanical and damping performances of Flax Fibre Composites – a review," *Composites Part C: Open Access*, vol. 4, p. 100081, 2021.

[121] Y. Zhang, R. D. Adams, and L. F. da Silva, "A rapid method of measuring the glass transition temperature using a novel Dynamic Mechanical Analysis Method," *The*

Journal of Adhesion, vol. 89, no. 10, pp. 785–806, 2013. DOI: 10.1080/00218464.2013.763677.

[122] E. J. Bosze, A. Alawar, O. Bertschger, Y.-I. Tsai, and S. R. Nutt, "High-temperature strength and storage modulus in unidirectional hybrid composites," *Composites Science and Technology*, vol. 66, no. 13, pp. 1963–1969, 2006.

[123] N. Constantin, M. Sandu, A. Sandu, and M. Găvan, "Damage identification and mechanical assessment of impacted Sandwich Composites," *Procedia Engineering*, vol. 188, pp. 178–185, 2017.

[124] C. C. Foo, G. B. Chai, and L. K. Seah, "Mechanical properties of Nomex material and Nomex honeycomb structure," *Composite Structures*, vol. 80, no. 4, pp. 588–594, 2007.

[125] M. Brodt and R. S. Lakes, "Composite materials which exhibit high stiffness and high viscoelastic damping," *Journal of Composite Materials*, vol. 29, no. 14, pp. 1823–1833, 1995.

[126] X. Li, and D. Shi, "Short fiber reinforced composite materials mechanical performance analysis," in *Proc. 21st Int Conf. Compos Mater.*, Xi'an, China, August 2017, pp.1-7.

[127] G. Zak, M. Haberer, C. B. Park, and B. Benhabib, "Estimation of average fibre length in short-fibre composites by a two-section method," *Composites Science and Technology*, vol. 60, no. 9, pp. 1763–1772, 2000.

[128] S. Y. Fu, B. L. Zhou, S. H. Li, and G. H. He, "Theoretical study of the stress transfer in single-fibre composites. part I. Perfectly debonded fibre-matrix interface," *Science and Engineering of Composite Materials*, vol. 3, no. 4, pp. 283–289, 1994.

[129] S. Y. Fu, S. H. Li, S. X. Li, G. H. He, and B. L. Zhou, “Theoretical study of the stress transfer in single-fibre composites. part II. partially debonded fibre-matrix interface,” *Science and Engineering of Composite Materials*, vol. 3, no. 3, pp. 145-151, 1994.

[130] Y. Termonia, “Theoretical study of the stress transfer in single Fibre Composites,” *Journal of Materials Science*, vol. 22, no. 2, pp. 504–508, 1987.

[131] M. Bulut, M. Alsaadi, A. Erkliğ, and H. Alrawi, “The effects of S-glass fiber hybridization on vibration-damping behavior of intraply woven carbon/aramid hybrid composites for different lay-up configurations,” *Proceedings of the Institution of Mechanical Engineers, Part C: Journal of Mechanical Engineering Science*, vol. 233, no. 9, pp. 3220–3231, 2018.

[132] A. Rajpurohit, V. Singery, S. Joannès, P. Sanial, L. Laiarinandrasana, “Manufacturing and performance of hybrid fabric reinforcements and their composites,” in *Proc. ECCM18 - 18th Eur. Conf. Compos. Mater.*, Athènes, Greece, 24th-28th June 2018, pp. hal-01958219.

[133] T. Khan, A. Fikri, M. S. Irfan, E. Gunister, and R. Umer, “The effect of hybridization on microstructure and thermo-mechanical properties of composites reinforced with different weaves of glass and carbon fabrics,” *Journal of Composite Materials*, vol. 55, no. 12, pp. 1635–1651, 2020.

[134] E. Suhir, T. X. Yu, and D. S. Steinberg, “Applications of Finite Element Analysis: Attributes and Challenges,” in *Structural Dynamics of electronic and Photonic Systems*. Metin Ozen, Eds., Hoboken, NJ: Wiley, 2011, pp. 331–336. DOI:10.1002/9780470950012.

[135] M. Gupta and K. K. Wang, “Fiber orientation and mechanical properties of short-fiber-reinforced injection-molded composites: Simulated and experimental results,” *Polymer Composites*, vol. 14, no. 5, pp. 367–382, 1993. https://doi.org/10.1002/pc.750140503.

[136] R. Reixach, F. X. Espinach, E. Franco-Marquès, F. Ramirez de Cartagena, N. Pellicer, J. Tresserras, and P. Mutjé, “Modeling of the tensile moduli of mechanical, thermomechanical, and chemi-thermomechanical pulps from Orange Tree pruning,” *Polymer Composites*, vol. 34, no. 11, pp. 1840–1846, 2013. https://doi.org/10.1002/pc.22589.

[137] N. G. Andre, D. Ariawan, and Z. A. Mohd Ishak, “Elastic anisotropy of kenaf fibre and micromechanical modeling of nonwoven kenaf fibre/epoxy composites,” *Journal of Reinforced Plastics and Composites*, vol. 35, no. 19, pp. 1424–1433, 2016. doi:10.1177/0731684416652740.

[138] S. B. Visweswaraiah, M. Selezneva, L. Lessard, and P. Hubert, “Mechanical characterisation and modelling of randomly oriented strand architecture and their hybrids – a general review,” *Journal of Reinforced Plastics and Composites*, vol. 37, no. 8, pp. 548–580, 2018. doi:10.1177/0731684418754360.

[139] M. R. Loos and K. Schulte, “Is it worth the effort to reinforce polymers with carbon nanotubes?,” *Macromolecular Theory and Simulations*, vol. 20, no. 5, pp. 350–362, 2011. https://doi.org/10.1002/mats.201100007.

[140] X. Wang, T. Stapf, H. Jöhri, F. Löhl, and M. Pedrozzi, “Structural Dynamic Modelling and Measurement of SwissFEL Bunch Compressor,” in *9th Mechanical Engineering Design of Synchrotron Radiation Equipment and Instrumentation (MEDSI*

2016), Barcelona, Spain, 11th-16th September 2016, pp. 128-132. https://doi.org/10.18429/JACoW-MEDSI2016-TUCA02.

[141] S. Alam, "Ansys Spaceclaim: Everything to know: Explore the future of engineering: 3D modeling, CAD and more," Explore the Future of Engineering: 3D Modeling, CAD and More - [Online]. Available: https://sunglass.io/ansys-spaceclaim/. [Accessed: 25-Jul-2022].

[142] R. D. Blevins, in *Formulas for natural frequency and mode shape*, New York (NY): Van Nostrand Reinhold Company, 1979, pp. 108.

[143] E. Asmatulu, J. Twomey, and M. Overcash, "Recycling of fiber-reinforced composites and direct structural composite recycling concept," *Journal of Composite Materials*, vol. 48, no. 5, pp. 593–608, 2013.

[144] I. Okajima, H. Okamoto, and T. Sako, "Recycling of Aramid fiber using subcritical and Supercritical Water," *Polymer Degradation and Stability*, vol. 162, pp. 22–28, 2019.

[145] L. Yuyan, L. I. LI, and M. Linghui, "The experimental research on recycling of aramid fibers by solvent method," *Journal of Reinforced Plastics and Composites*, vol. 28, no. 18, pp. 2211–2220, 2008.

[146] Y.-C. Chuang, L. Bao, C.-W. Lou, and J.-H. Lin, "Hybrid-fiber-reinforced composite boards made of recycled aramid fibers: Preparation and puncture properties," *Fibers and Polymers*, vol. 20, no. 2, pp. 398–405, 2019.

[147] A. K. Bledzki, H. Seidlitz, K. Goracy, M. Urbaniak, and J. J. Rösch, "Recycling of carbon fiber reinforced composite polymers—review—part 1: Volume of

production, Recycling Technologies, legislative aspects," *Polymers*, vol. 13, no. 2, pp. 300, 2021.

[148] A. K. Bledzki, H. Seidlitz, J. Krenz, K. Goracy, M. Urbaniak, and J. J. Rösch, "Recycling of carbon fiber reinforced composite polymers—review—part 2: Recovery and application of recycled carbon fibers," *Polymers*, vol. 12, no. 12, pp. 3003, 2020.

PUBLICATIONS DURING PH.D. STUDY

[1] C. Y. Attahu, J. Yang, K. H. Wong, and C. K. Thein, "Flexural and shear strength properties of unidirectional carbon fiber reinforced polymer composite interleaved with recycled carbon fiber and short virgin aramid fiber non-woven mats," *IOP Conference Series: Materials Science and Engineering*, vol. 1225, pp. 012005, 2022. doi:10.1088/1757-899X/1225/1/012005. (**Won best research paper award-first runner-up**)

[2] Attahu CY, Thein CK, Wong KH, Yang J. Enhanced damping and stiffness trade-off of composite laminates interleaved with recycled carbon fiber and short virgin aramid fiber non-woven mats. Compos Struct 2022; 297: 115981. https://doi.org/10.1016/j.compstruct.2022.115981.

APPENDICES

The project's raw data consists of numerous pages, which would blot the dissertation if added; therefore, it has been published on the Mendeley repository. It can be accessed here (with the permission of the dissertation's author):

https://data.mendeley.com/datasets/v2smy6zb79/1